THE UNIVERSITY OF MICHIGAN
COLLEGE OF LITERATURE, SCIENCE, AND THE ARTS
Department of Physics

Technical Report No. 25

PROTON-DEUTERON ELASTIC SCATTERING AT HIGH MOMENTUM TRANSFERS

Ernest Coleman

ORA Project 03106

under contract with:

DEPARTMENT OF THE NAVY
OFFICE OF NAVAL RESEARCH
WASHINGTON, D.C.

CONTRACT NO. Nonr-1224(23)
NR-022-274

administered through:

OFFICE OF RESEARCH ADMINISTRATION ANN ARBOR

July 1966

This report was also a dissertation submitted in partial fulfillment of the requirements for the degree of Doctor of Philosophy in The University of Michigan, 1966.

TABLE OF CONTENTS

TABLE OF CONTENTS (Concluded)

LIST OF TABLES

LIST OF FIGURES

LIST OF FIGURES (Concluded)

ABSTRACT

An experimental and theoretical investigation of proton-deuteron elastic scattering at high momentum transfers is presented. The differential cross sections for backward elastic scattering at incident proton kinetic energies of 1.0, 1.3, and 1.5 GeV have been measured for four-momentum transfer squared (-t) from 2.6 to 5.0 $(GeV/c)^2$, which corresponds to cosine of center-of-mass proton scattering angles ($\cos \theta^*$) from -0.5 to -0.9. A backward peak is observed, and the slope and magnitude of the peak have been determined. At 2.0 GeV for forward elastic differential cross section has been measured for -t from 0.44 to 1.54 $(GeV/c)^2$ or $\cos \theta^*$ from 0.875 to 0.565. A shoulder-like departure from the forward diffraction peak was observed.

The one-nucleon exchange peripheral model has been successful in interpreting the backward peak. Calculations based on modern three-body quantum mechanical formalisms for the three-nucleon system supporting a two-body bound state also suggest the one-nucleon exchange process as the dominant mechanism. The measured forward differential cross section has been explained by the importance of double-scattering of the incident proton at higher momentum transfers. A negative value for the ratio of the real part to the imaginary part of the neutron-proton elastic scattering amplitude at 2.0 GeV is shown to yield maximum agreement with the experimental data.

I. INTRODUCTION

The interaction between two nucleons has long been the fundamental problem in particle physics. The deuteron is the only bound state of the two-nucleon system, and the elastic scattering of protons by deuterons provides an opportunity to examine any theory which proposes to describe the static and dynamical properties of the two-nucleon system. The static properties of the deuteron have been known for many years. The spin of the deuteron was determined by Murphy and Johnston[1] to equal one $\hbar$ unit. The magnetic moment of the deuteron was first measured by Stern and Estermann,[2] who deflected deuterium molecules in an inhomogeneous magnetic field. A more accurate measurement using the nuclear magnetic resonance absorption method was made by Widmett,[3] who reported the ratio of the deuteron magnetic moment to the proton magnetic moment thus yielding $\mu_d = 0.857411 \pm 0.000019$ nuclear magnetons (nuclear magneton = $e\hbar/2mc$ where m is the proton mass and e is the proton charge). The deuteron electric quadrupole moment was postulated and measured by Kellogg, Rabi, and Ramsey[4] who noticed a discrepancy between their measured deuterium radiofrequency magnetic resonance spectrum and theory. The experimentally measured fine structure was much larger than the magnitude predicted by third-order perturbation calculations. Using an improved design of the molecular beam apparatus, Kolsky et al.[5] found the quadrupole moment, $Q = 0.2738\ f^2$ ($f = 10^{-13}$ cm). In order to explain the presence of the electric quadrupole moment Schwinger[6] proposed a tensor contribution to the nuclear force, which gave the deuteron a $^3S_1 + {}^3D_1$ ground state.

In the low energy scattering problem extensive use is made of the effective range theory. This method assumed that the scattering cross section could be expressed in terms of only the S-wave phase shift, and such quantities as the triplet scattering length $a_t = 5.41$ f, the singlet scattering length $a_s = -23.78$ f, and the effective range $r_e = 1.69$ f were determined. However in high energy scattering, the assumptions of the effective range theory are no longer valid. Theories must then be tested by computing the differential cross sections and comparing them with the experimental data. In the 100 MeV to 700 MeV incident proton kinetic energy range, several determinations of the differential cross sections have been made.[7-13] The common characteristic of these measurements was a strong forward peak and a smaller backward peak. No other structure was seen at these energies. Above 700 MeV, proton-deuteron elastic scattering data are very scarce. Bayukov et al.[14] have measured a single point of the differential cross section near 180° at three energies, 0.715 GeV, 1.00 GeV, and 3.66 GeV. Kirillova et al.[15] have determined the differential cross section for angles less than 20° at five energies from 2.0 GeV to 10.0 GeV. In the present experiment the elastic differential cross sections for incident proton kinetic energies of 1.0, 1.3, and 1.5 GeV have been measured for values of four-momentum transfer squared (-t) from 2.6 to 5.0 $(GeV/c)^2$, corresponding to cosine of center-of-mass scattering angles

(cos θ^*) from -0.5 to -0.9. The 2.0 GeV differential cross section was measured in this experiment for -t from 0.44 to 1.54 $(GeV/c)^2$, corresponding to cos θ^* from 0.875 to 0.656. In Chapter II the backward differential cross section is interpreted as a one-nucleon exchange process, and the results are compared with the available experimental data at high energies. Chapter III considers the three-nucleon system within the framework of modern quantum mechanical three-body formalisms. The shoulderlike departure of the 2.0 GeV forward scattering data from the exponential trend of the diffraction peak is analyzed in Chapter IV via multiple scattering processes. In Chapters V through VIII the experimental techniques and results are explained, and a discussion of the conclusions is presented in Chapter IX.

II. ONE-NUCLEON EXCHANGE MODEL

The one-nucleon exchange model was observed by Blankenbecler et al.[16] to peak in the backward direction. However they confined their calculation of elastic neutron-deuteron scattering to forward angles at low energies where phase shift data are available. Perl et al.[17] noted that the one nucleon model could be utilized to analyze pion-nucleon elastic scattering and the reactions $\pi^- + p \to \bar{p} + d$ and $p + d + \pi^+$. The one nucleon exchange diagram for $p + p \to d + \pi^+$ has been analyzed by Heinz et al.[18] and later by Mathews et al.[20] Cook et al.[21] have calculated the diagram for pion-nucleon scattering but were not able to obtain good agreement with experimental data. Bernstein[22] and Nearing[23] have used the one nucleon exchange diagram in attempts to explain intermediate boson production via the reaction $p + p \to d + W^+$.

The one neutron exchange Feynman diagram for proton-deuteron elastic scattering is given in Fig. 1b with the R-matrix element. The initial proton and deuteron have four momenta p_1 and d_1 respectively, whereas the scattered proton and deuteron have four-momenta p_2 and d_2. The exchanged neutron has four-momentum n. The metric is defined such that

$$p_1^2 = p_2^2 = -m^2, \qquad d_1^2 = d_2^2 = -M_d^2$$

for the particles on the mass shell. The Γ_1 and Γ_2 in the R-matrix, with $\bar{\Gamma} = \gamma_4 \Gamma^T \gamma_4$, are the proton-neutron-deuteron vertex functions. The relativistically invariant matrix, M, is defined by

$$R = (2\pi)^4 N_d^2 N_p^2 \delta^4 (d_2 + p_2 - d_1 - p_1) M \left[\left(\frac{1}{2\pi}\right)^{3/2} \right]^4$$

where N_p and N_d are the normalization factors for the proton and deuteron. The differential cross section is then

$$\frac{d\sigma}{d\Omega} = \left(\frac{1}{2\pi}\right) \frac{(mM_d)^2}{U^2} \frac{p_f}{p_i} \frac{1}{6} \sum |M|^2$$

where p_i and p_f are the magmitudes of the initial and final three-momenta in the center-fo-mass (c.m.) system, U is the total c.m. energy and

$$M = u(p_1)^T \bar{\Gamma}_2 \frac{1}{i\not{n} + m + i\epsilon} \Gamma_1 u(p_2)^T .$$

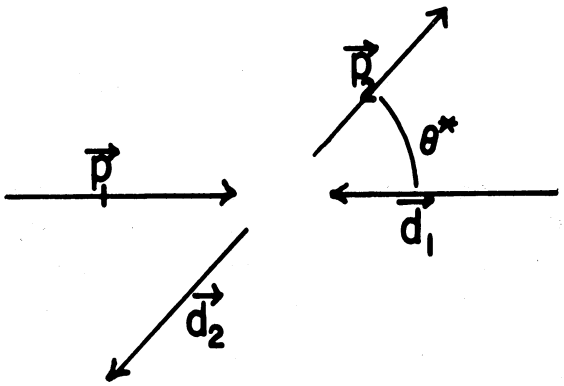

(a)

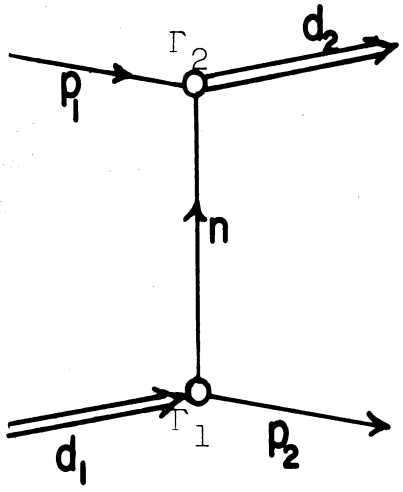

(b)

Fig. 1. (a) Notation for center-of-mass system. (b) One-nucleon exchange Feynman diagram. The R-matrix for this diagram is:

$$R = \left(\frac{-i}{hc}\right)^2 \int d^4n\ (2\pi)^4\ \delta^4(d_2-n-p_1)(2\pi)^4$$
$$\delta^4(p_2+n-d_1)\left[\left(\frac{1}{2\pi}\right)^{\frac{3}{2}}\sqrt{\frac{m}{p_{10}}}\ u(p_1)\right]^T$$
$$\left(\frac{1}{2\pi}\right)^{\frac{3}{2}}\ \bar{\Gamma}_2\ \left(\frac{i}{2\pi}\right)^4\ \left(\frac{1}{i\not{n}+m+i\epsilon}\right)\ \left(\frac{1}{2\pi}\right)^{\frac{3}{2}}$$
$$\Gamma_1\ \left[\left(\frac{1}{2\pi}\right)^{\frac{3}{2}}\sqrt{\frac{m}{p_{20}}}\quad \bar{u}(p_2)\right]^T$$

The summation is taken over all proton and deuteron spin states.

A. PROTON-NEUTRON-DEUTERON VERTEX FUNCTION

The form of the proton-neutron-deuteron vertex function must be known to evaluate the matrix elements. The non-relativistic vertex function has been discussed by Blankenbecler et al.[16] and Goldberger et al.[24] A phenmenological description of the relativistic vertex function has been given by Gourdin et al.[25] The functions of Gourdin et al. were limited by the use of only low energy photodisintegration data to fix the positions of the three poles used to approximate the left-hand cut in the complex κ^2 plane. As a consequence, their relativistic vertex functions are valid for magnitudes of the three-momentum, κ, of the neutron or proton inside the deuteron less than 0.370 GeV/c. This study of the one-nucleon-exchange diagram is concerned with large momentum components of the deuteron from κ = 0.465 GeV/c to κ = 1.025 GeV/c. The expression for κ^2 is shown to be

$$\kappa^2 = \frac{1}{2}\left[M_d^2 - 2M^2 + (n^2 + M^2)\right] + p_1 \cdot d_2 + \left(\frac{p_1 \cdot d_2}{M_d}\right)^2$$

by evaluating $d_2^2 = (n + p_1)^2$ in the rest frame of the deuteron. The vertex function of Blankenbecler, Goldberger, and Halpern[16] will be considered in the following discussion.

The vertex function of Blankenbecler et al. was obtained through the use of dispersion techniques. Although the theory was developed for all angles, they published only the real part of the forward neutron-deuteron elastic scattering amplitude at 9.6 MeV. In addition to the necessary assumptions of unitarity, time symmetry, casualty, linearity and high-energy convergence for the derivation of dispersion relations, the following additional assumptions were made for determination of the vertex function:

(1) The deuteron is treated as a boson.

(2) The discrete neutron pole is the dominant term.

(3) Evaluation of the vertex function and propagator function is required only at the singularity where the intermediate neutron becomes real.

(4) When the S-matrix is expressed as a retarded commutator of the proton fields, the equal-time commutator contribution vanishes identically because the deuteron cannot absorb a single pion and remain bound.

(5) The number of subtractions should be no greater than the number required in nucleon-nucleon scattering.

(6) The discrete contributions to the absorptive part of the amplitude yield the renormalized Born approximation with the residues evaluated at the pole.

When the deuteron D-State is neglected, the vertex function may be expressed by

$$\Gamma = \frac{4\pi N}{m} S_o$$

with

$$S_o = \frac{1}{2\sqrt{2}} \frac{M_d - i\not{\xi}}{M_d} (\gamma \cdot \xi) C$$

where S_o is the deuteron triplet spin function, γ are the Dirac matrices, N is normalization parameter, ξ is the deuteron polarization parameter, and $C = i\gamma_4\gamma_2$ is the charge conjugation matrix with the properties $C^2 = 1$ and $C\gamma_\mu C = -\gamma_\mu$. The D-state may be included by assuming that the D-state has the same momentum dependence near the neutron pole. The deuteron triplet sping function is then expressed by

$$S = (1 + \frac{\rho}{\sqrt{8}} S_{12}) S_o$$

with

$$S_{12} = \left[3 (\sigma^{(1)} \cdot r) (\sigma^{(2)} \cdot r)\right] / r^2 - \sigma^{(1)} \cdot \sigma^{(2)}$$

where S_{12} is the usual tensor operator well known from dipole-dipole interactions and introduced into proton-neutron interactions by Rarita and Schwinger[26] while ρ is the normalization ratio for the D-state admixture. The deuteron D-state has very little influence on the final cross sections, consequently S_o has been taken as the triplet spon function and the D-state wave function has been represented by ρ times the S-state wave function. This has been evidenced by defining the normalization parameter as

$$N = \frac{\alpha}{2\pi (1 + \rho^2) (1 - \alpha r_e)}$$

where $\alpha = \sqrt{mb}$, b is the deuteron binding energy, and r_e is the effective range of the deuteron.

B. VERTEX FORM FACTORS

The expression for the vertex function by Blankenbecler et al. is valid only in the limit where the intermediate neutron becomes real. The vertex functions may be significantly changed as the off-the-mass-shell effects and the high momentum components are taken into account. in applying the one-nucleon-exchange diagram, others [18,22,23] have found it necessary to introduce the Fourier transform of the deuteron wave function as a form factor. The form factor was used to adjust the shape and the magnitude of the cross sections to experimental data. The advantages and disadvantages of various vertex form factors will be discussed. If the vertex function can be written as $\Gamma = HS_o$ where S_o contains all of the spin dependent terms, Chew and Goldberger[27] have shown that

$$H = < \psi(\underline{r}) \mid V(\underline{r}) \mid e^{-i\underline{\kappa}\cdot\underline{r}} >$$

where $\underline{r}$ is the relative coordinate of the neutron and proton, $\psi(r)$ is the deuteron wave function, and $V(\underline{r})$ is the central force nuclear interaction potential. The potential $V(\underline{r})$ may be written as an operator $V(\underline{r}) = \frac{\nabla^2}{m} - b$ via the Schrödinger equation for the deuteron to show that

$$H = -\frac{(\alpha^2 + \kappa^2)}{m} < \psi(\underline{r}) \mid e^{-i\underline{\kappa}\cdot\underline{r}} > .$$

The expression for the vertex function is then

$$\Gamma = -\frac{(\alpha^2 + \kappa^2)}{m} < \psi(\underline{r}) \mid e^{-i\underline{\kappa}\cdot\underline{r}} > S_o$$

or

$$\Gamma = \frac{4\pi N}{m} S_o F(\kappa)$$

with

$$F(\kappa) = \frac{\alpha^2 + \kappa^2}{4\pi N} < \psi(\underline{r}) \mid e^{-i\underline{\kappa}\cdot\underline{r}} > .$$

The vertex function of Blankenbecler, Goldberger and Halpern is valid only in the limit $\kappa^2 = -\alpha^2$ where the neutron and the proton forming the deuteron are on the mass shell. The value of $F(\kappa)$ is 1 at $\kappa^2 = -\alpha^2$.

Two deuteron wave functions have been discussed by Hulthén et al.[28] The first phenomenological wave function is

$$\psi(r) = \frac{N}{r}(e^{-\alpha r} - e^{-\beta r}) .$$

Using this wave function, one obtains

$$F(\kappa) = \frac{\beta^2 - \alpha^2}{\beta^2 + \kappa^2} \quad .$$

This form of $F(\kappa)$ was derived via dispersion techniques by Blankenbecler and Cook.[29] A second Hulthén wave function introduces an infinitely repulsive core of radius r_c to give the wave function the form

$$\psi(\underline{r}) = 0, \qquad r < r_c$$

$$\psi(\underline{r}) = \frac{N}{r} e^{-\alpha r} \left[1 - e^{-\beta (r - r_c)}\right], \quad r \geq r_c \quad .$$

The vertex form factor then becomes

$$F(\kappa) = \frac{\alpha^2 + \kappa^2}{\kappa} e^{-\alpha r_c} \left[\frac{\alpha \sin \kappa r_c + \kappa \cos \kappa r_c}{\alpha^2 + \kappa^2}\right.$$

$$\left. - \frac{(\alpha + \beta) \sin \kappa r_c + \kappa \cos \kappa r_c}{(\alpha + \beta)^2 + \kappa^2}\right] \quad .$$

The constants α and N have been fixed by the binding energy and the asymptotic behavior of the wave function while the value of β, 5.18 α, is chosen to satisfy the normalization

$$4\pi \int_0^\infty dr\, r^2 (1 + \rho^2)\, \psi^2(r) = 1 \quad .$$

In Fig. 2, $F(\kappa)$ is shown for several values of the core radius. As the core radius increases, the minimum of $F(\kappa)$ is shifted toward smaller values of κ.

The Schrödinger equation for the two-nucleon potential was solved numerically by Gartenhaus [30] using Yukawa theory with a cut-off energy for virtual mesons. The Gartenhaus wave function improves upon the Hulthén wave function for small values of $\underline{r}$. Moravcsik[31] has fitted the Gartenhaus numerical wave functions by several analytic forms, the best of which is

$$\psi(\underline{r}) = \frac{N}{r} (e^{-\alpha r} - e^{-dr})(1 - e^{-cr})(1 - e^{-gr})$$

yielding

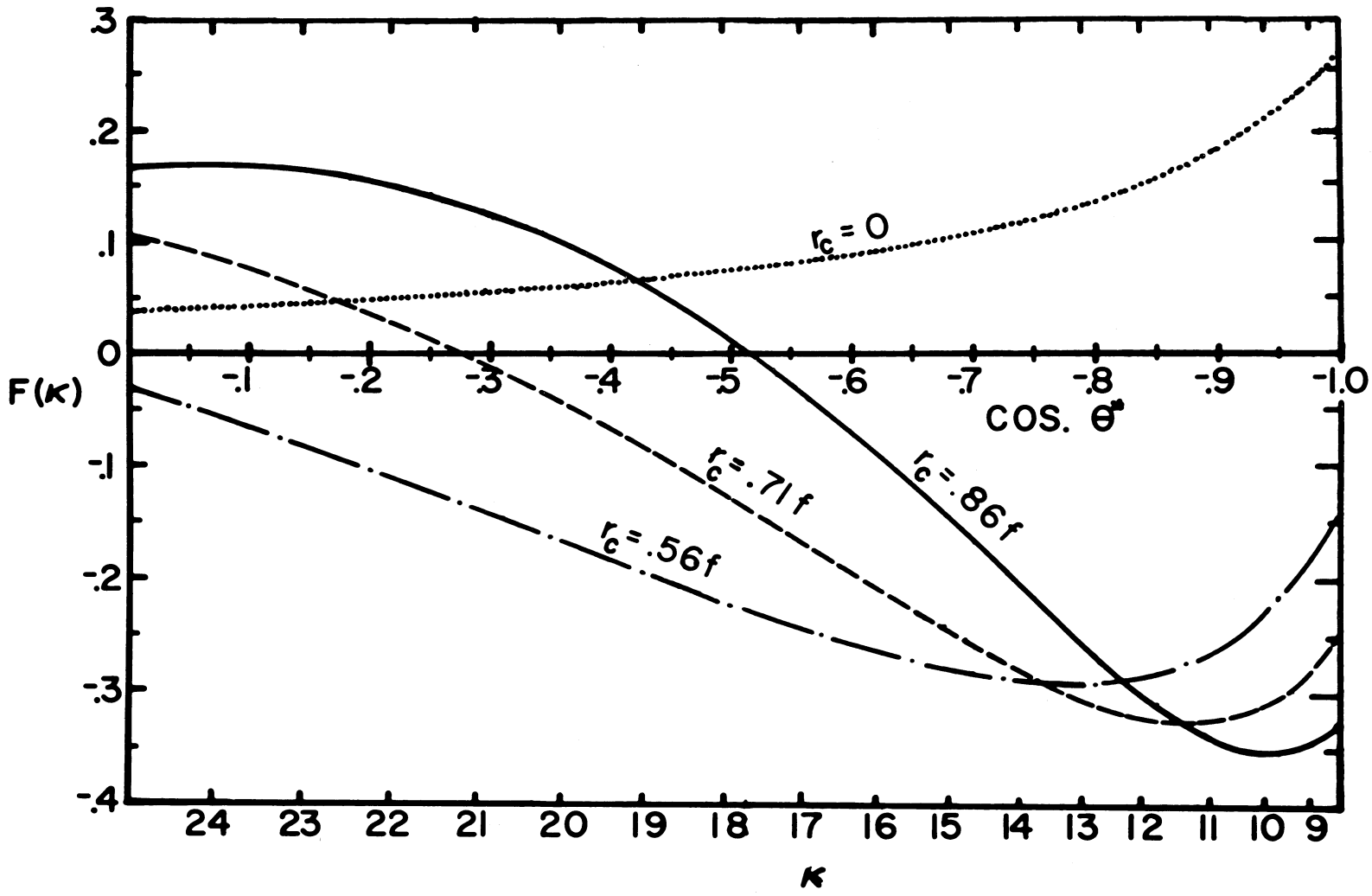

Fig. 2. Form factor from Hulthén wave function with core of various radii.

$$F(\kappa) = (\alpha^2 + \kappa^2)\left[\frac{1}{(\alpha^2 + \kappa^2)} - \frac{1}{(d^2 + \kappa^2)}\right.$$

$$- \frac{1}{(\alpha + c)^2 + \kappa^2} - \frac{1}{(\alpha + g)^2 + \kappa^2}$$

$$+ \frac{1}{(\alpha + c + g)^2 + \kappa^2} + \frac{1}{(c + d)^2 + \kappa^2}$$

$$\left. + \frac{1}{(d + g)^2 + \kappa^2} - \frac{1}{(c + d + g)^2 + \kappa^2}\right]$$

where $c = 6.853\ \alpha$, $d = 8.190\ \alpha$, and $g = 10.776\ \alpha$. In Fig 3, $F(\kappa)$ is shown versus κ for the three above wave functions. The form factor of the Moravcsik fit to the Gartenhaus wave function is observed to display the effects of a repulsive core similar to the phenomenological hard core in the Hulthen wave function.

C. DIFFERENTIAL CROSS SECTIONS

The sum of the matrix element squared given in Section A may now be explicitly obtained by substituting the proton-neutron-deuteron vertex function for Γ and summing over the proton and deuteron spins. The details of the spin summation are given in Appendix A, and are shown to yield

$$\frac{1}{6}\sum\left|M^2\right| = \frac{3}{128}(2mM_d - p_1\cdot d_2)^2 \frac{1}{(mM_d^2)^2} \frac{1}{(n^2 + m^2)^2}$$

$$\cdot K \left(\frac{4\pi N}{m}\right)^4 \left[F(\kappa)\right]^4$$

where

$$K = \left[m^2M_d^2 - m^2\, d_1\cdot d_2 - n^2\, d_1\cdot d_2 - mM_d n\cdot(d_1 + d_2) + 2\, n\cdot d_1\, n\cdot d_2 - M_d^2\, n\cdot n\right]$$

The differential cross section then assumes the form

$$\frac{d\sigma}{d\Omega} = \frac{3\pi^2N^4}{2U^2m^4M_d^2}\left[\frac{2mM_d - p_i\cdot d_2}{n^2 + m^2}\right]\frac{p_f}{p_i} K \left[F(\kappa)\right]^4$$

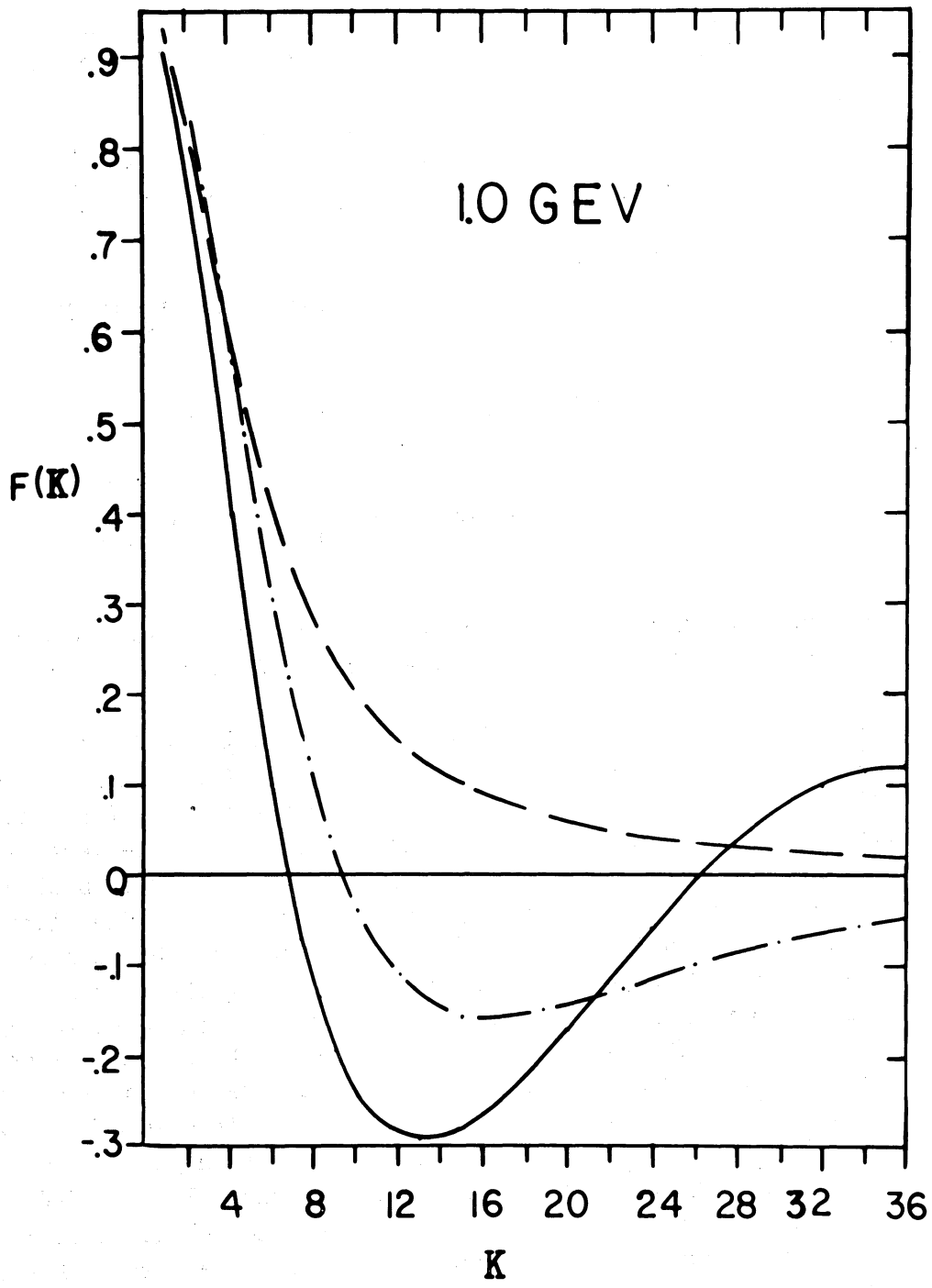

Fig. 3. Form factors for employing various wave functions. (———) Hulthén with hard core; (– – –) Hulthén without core; (–·–·–) Moravcsik analytic fit.

with $\hbar = c = 1$, U is the total center-of-mass energy. If the notation of Fig. 1a is used, the center of mass elastic differential cross section becomes

$$\frac{d\sigma}{d\Omega} = \frac{3\pi^2 N^4}{2U^2 m^4 M_d^2}\left[\frac{2mM_d + U_p U_d + k^2\cos\theta^*}{2U_p U_d - M_d^2 + 2k^2\cos\theta^*}\right]^2 \left[F(\kappa)\right]^4$$

$$\left[2m^2M_d^2 + mM_d^3 + mM_d U^2 - 2mM_d U_p U_d + M_d^4 + M_d^2 U_d^2 - 4M_d^2 U_p U_d\right.$$

$$+ 2U_p^2 U_d^2 + k^2\,(2U_p U_d - mM_d - 2M_d^2)$$

$$\left. + k^2\cos\theta^*\,(2k^2 + 2U_p U_d - 3M_d^2 - 2mM_d)\right]$$

where k is the center-of-mass three-momentum, U_p is the center-of-mass energy of the proton, and U_d is the center-of-mass energy of the deuteron.

The differential cross section is displayed in Fig. 4 for different form factors, $F(\kappa)$. The solid curve assumes $F(\kappa) = 1$, which essentially does not utilize a vertex form factor The unmodified vertex function of Blankenbecler et al. predicts a slope of the backeard peak in satisfactory agreement with the experimental data. The dashed curve shows the differential cross section with the regular Hulthén wave function determining the form factor. The slope of the backward peak becomes much steeper, and the magnitude of the peak is reduced by several orders of magnitude. The effect of using the best Moravcsik analytic fit to the Gartenhaus wave function is evident in the double-dash double-dot (--..) curve The passage of the curve through zero at $\cos\theta^* = -0.957$ is due to the form factor. In Fig. 3, the form factor obtained from the Moravcsik analytic fit is shown to pass through zero in a smooth and well-behaved manner. The point at which it passes through zero happens to be inconvenient for application to differential cross sections below 1.5 GeV incident proton kinetic energy. The results from using the Hulthén hard core wave function are distinguished by the dash-dot (-·-·) curve. The differential cross section is observed to turn over near $\cos\theta^* = -1.0$. The point at which the slope passes through zero is determined by the radius of the hard core as seen from Fig. 2. To obtain maximum agreement between the available experimental data and this expression for the form factor, a radius of at least 0.71 f was necessary. The differential cross sections predicted by the one-nucleon exchange diagram are shown in Figs. 5-10 along with the experimental data. The theoretical curves at all energies have been normalized to the point $\cos\theta^* = -0.875$ at 1.0 GeV incident proton kinetic energy.

For each energy, the unmodified vertex function of Blankenbecler et al. yielded the best fit to the data. The form factor utilizing the Hulthén phenomenological hard core wave function did not fulfill his intended goal of

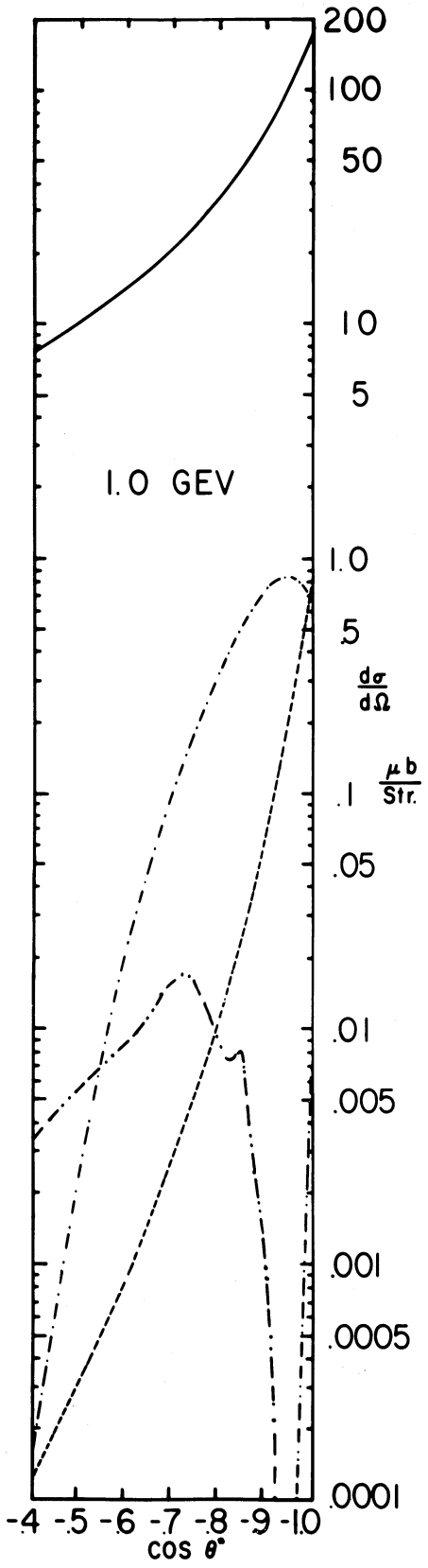

Fig. 4. Unnormalized theoretical differential cross sections at 1.0 GeV. (———) F(r) = 1; (-·-·-) Hulthén with hard core; (– – –) Hulthén without core; (-· ·-) Moravcsik analytic fit.

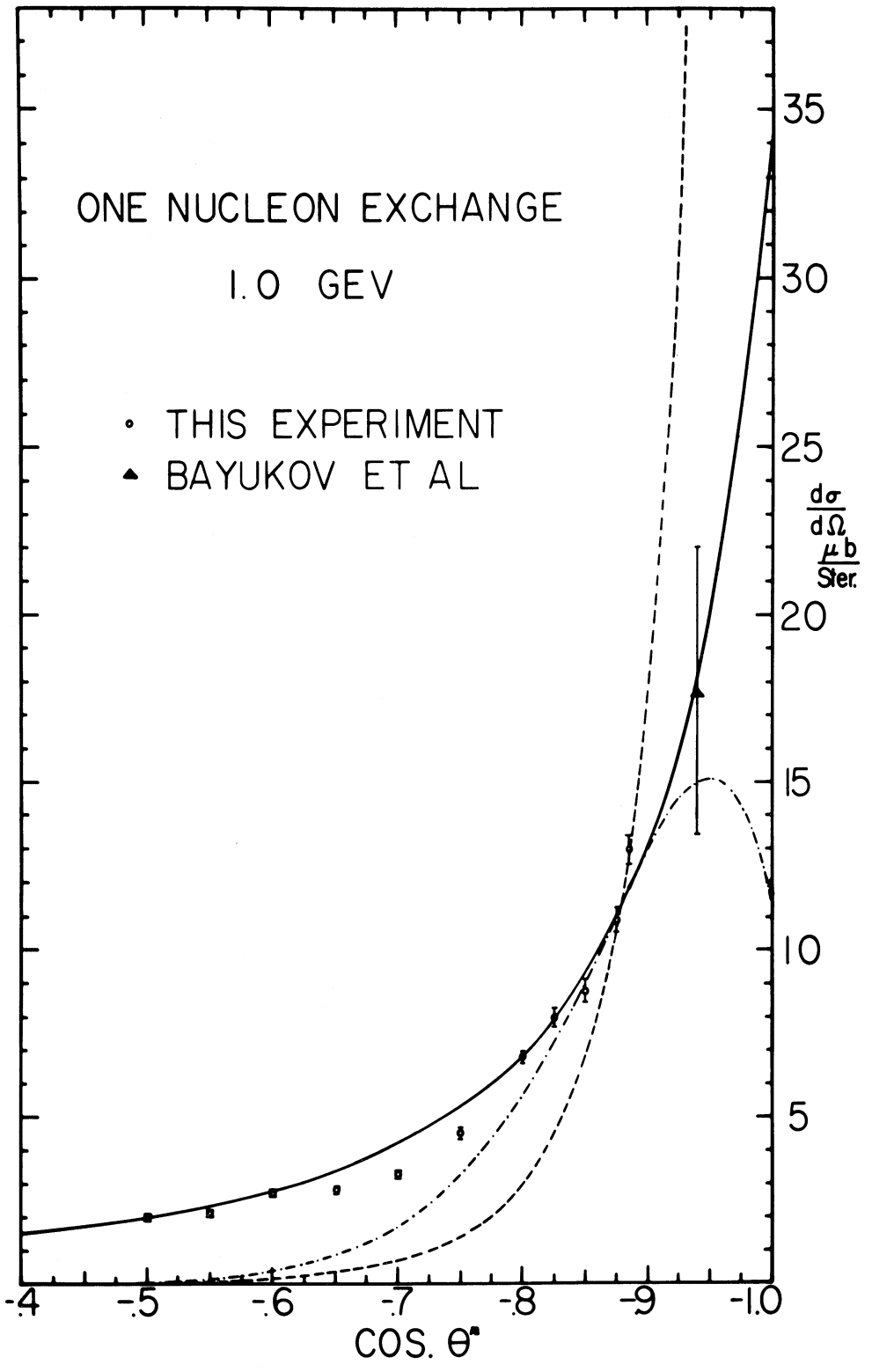

Fig. 5. Theoretical cross sections at 1.0 GeV. (———) $F(\kappa) = 1$; (-·-·-) Hulthén with hard core; (- - -) Hulthén without core.

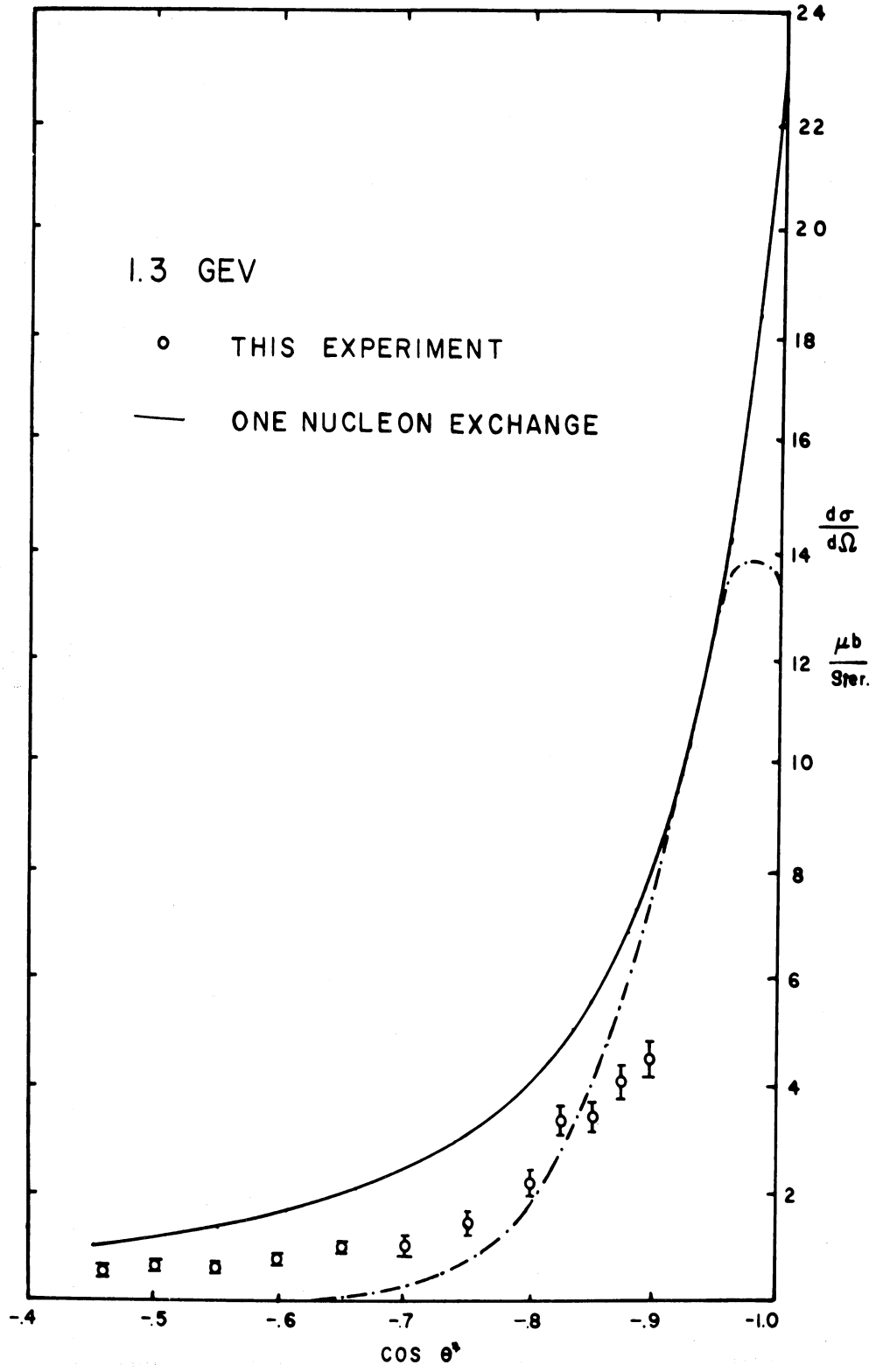

Fig. 6. Theoretical cross sections at 1.3 GeV. (———) $F(\kappa) = 1$; (–·–·–) Hulthén with hard core.

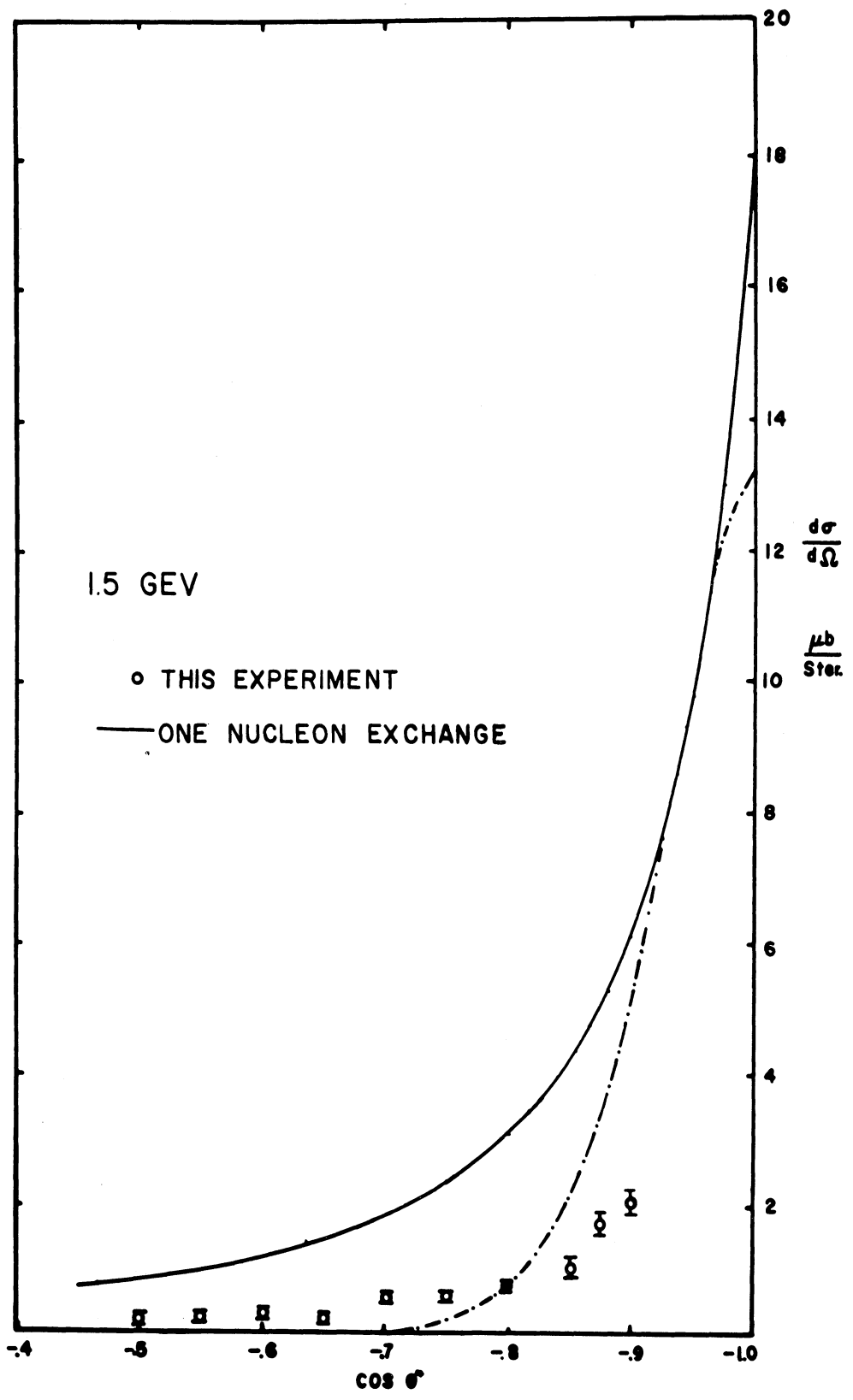

Fig. 7. Theoretical cross sections at 1.5 GeV. (———) $F(\kappa) = 1$; (-.-.-) Hulthén with hard core.

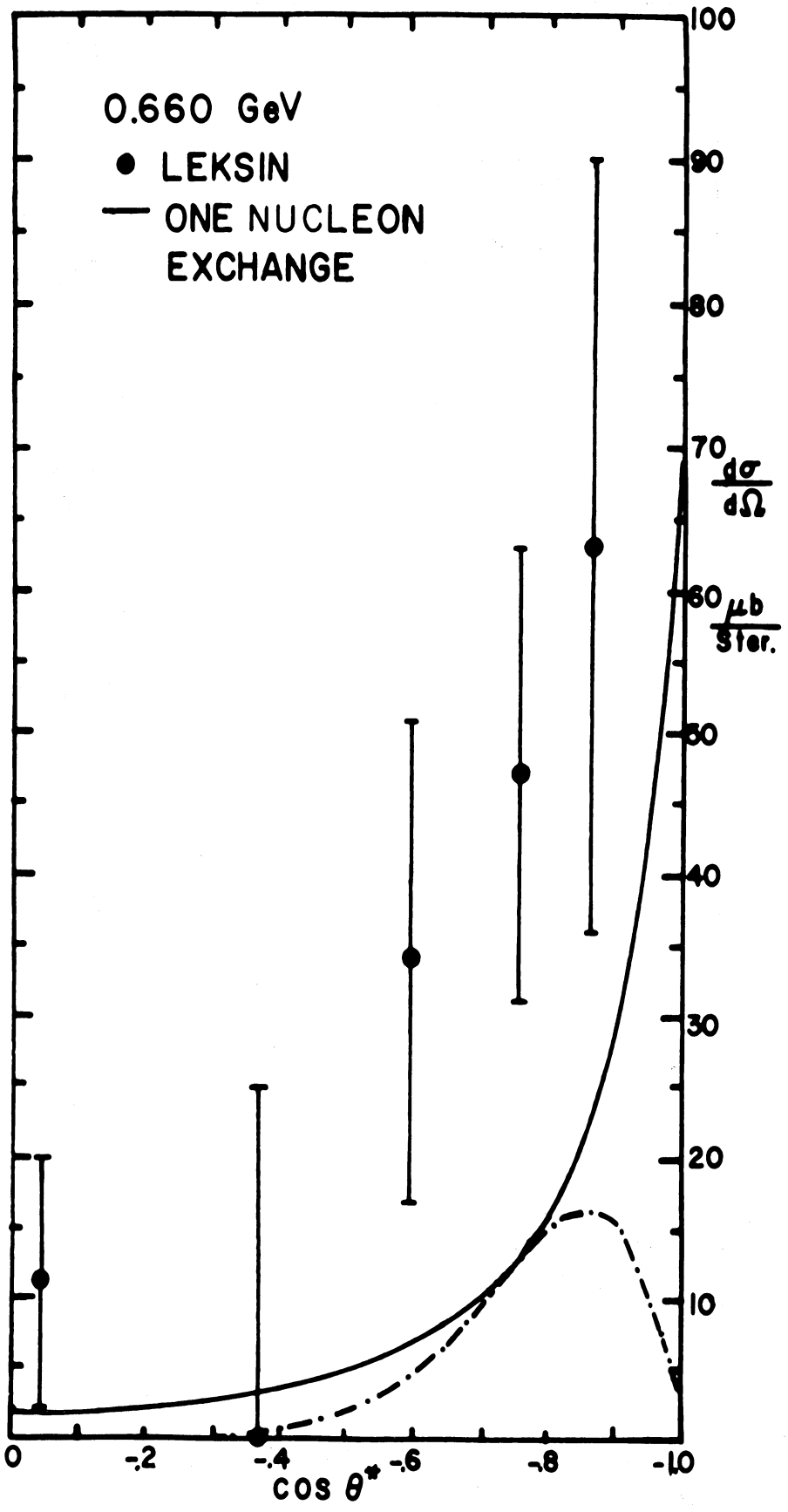

Fig. 8. Theoretical cross sections at 0.660 GeV. (———) $F(\kappa) = 1$; (-·-·-) Hulthén with hard core.

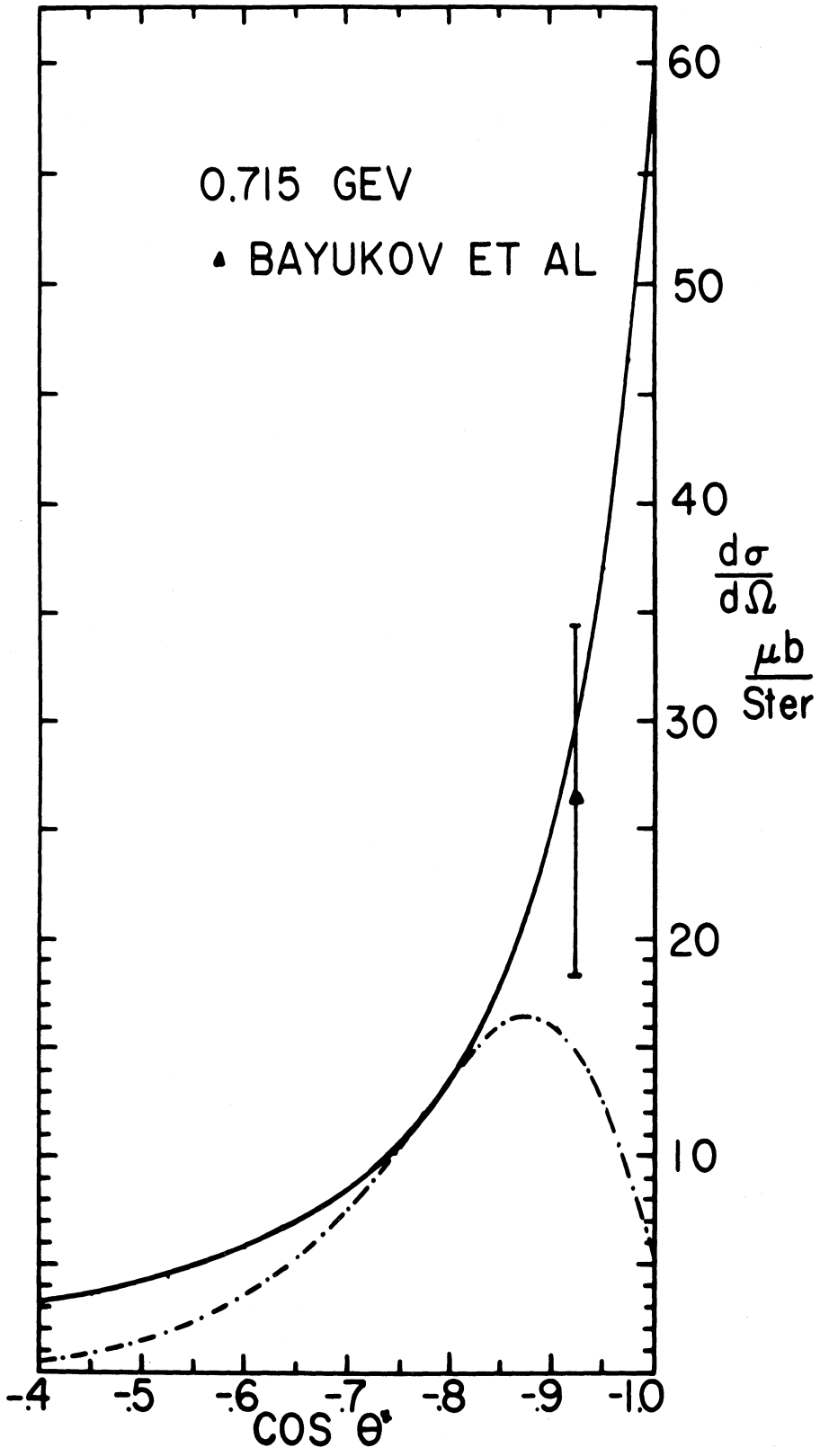

Fig. 9. Theoretical cross sections at 0.715 GeV. (———) $F(\kappa) = 1$; (-·-·-) Hulthén with hard core.

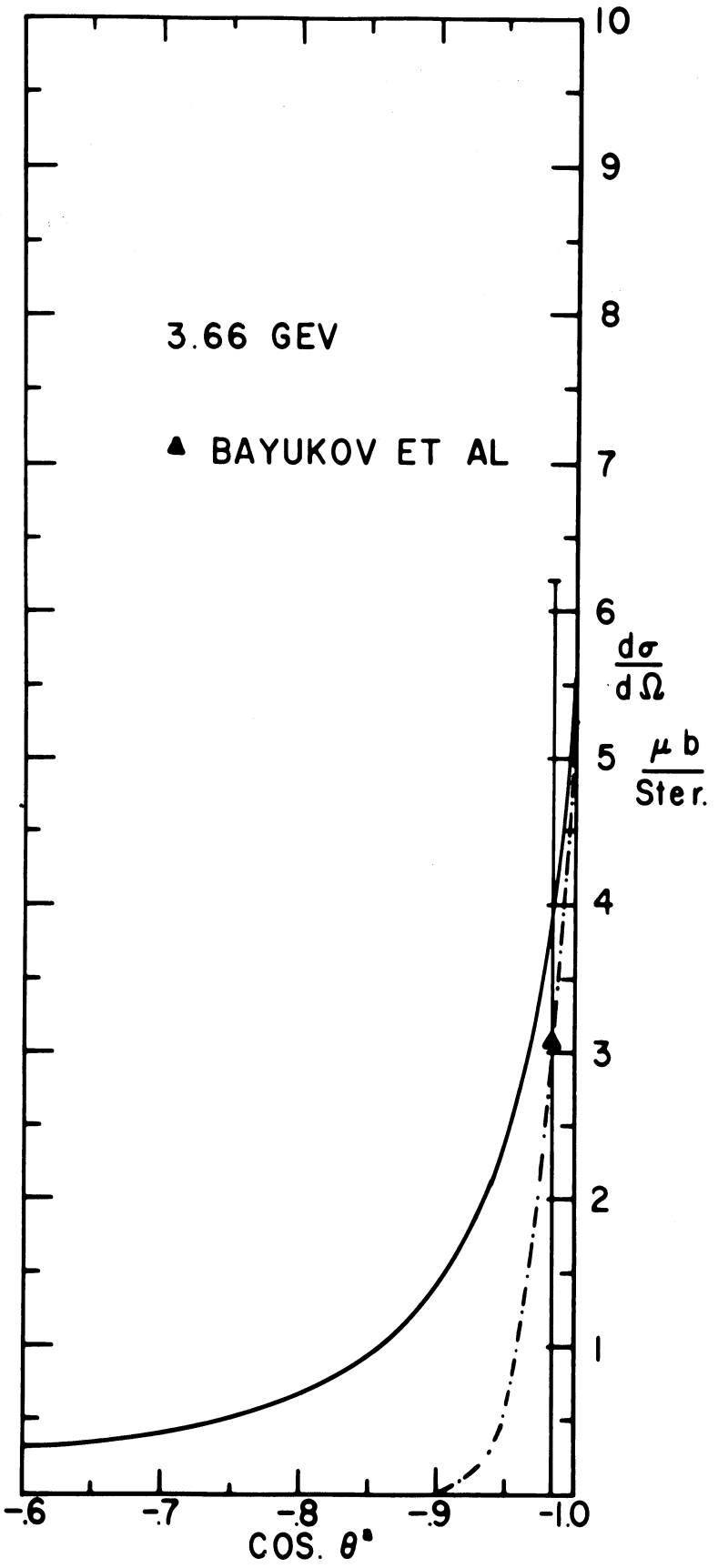

Fig. 10. Theoretical cross section at 3.66 GeV. (———) $F(\kappa) = 1$; (—·—·—) Hulthén with hard core.

accurately representing the high-momentum components of the deuteron at the energies studied here. The regular Hulthén wave function and the Moravcisk fit to the Gartenhaus wave function suggested form factors which show poor agreement with the data. The Moravcsik form factor may, however, show better agreement with the data than the Hulthén hard core form factor at higher energies because before the catastrophic influence of passing through zero the shape of the predicted differential cross section was in good agreement with the experimental slope.

III. THE THREE-NUCLEON SYSTEM

The quantum mechanical three-body scattering problem has recently become tractable through new formalisms. The old methods used various perturbative operations which introduced many phenomenological three-body parameters to fit experimental data and tended to overlook the requirement that the bound states and the scattering states be dictated by the same dynamical relationships. Unlike the two-body problem, a choice of coordinate frames cannot reduce the apparent number of particles in the three-body problem. The six independent momenta in the center-of-mass system and angular momentum considerations complicate the kinematical relationships. The multichannel process for quantum mechanical systems was put on a rigorous mathematical foundation by Jauch.[34] He derived explicit integral representations of the wave operators. However, the appearance of delta functions in the kernel of the Lippman-Schwinger equation [35] made classical iteration methods impractical. Also the homogeneous Lippman-Schwinger equation possessed solutions when bound states existed between pairs of particles which made the problem of satisfying boundary conditions quite difficult. In three-body processes it is possible for two particles to interact while the third particle does not interact. This leads to disconnected graphs which yield integral equations with singular kernels. These equations cannot be solved by the Fredholm method, perturbative methods or any other known form of computation.

The three-body problem was cast into a form solvable through present analytical means by Faddeev.[36] A set of three-body equations was given in which the kernel had no continuous spectrum and for which the homogeneous equation possessed a solution only for bound states of the entire system. The kernels are generalizations of the T matrix and may be determined by working only with pair amplitudes. The coupled integral equations describe all possible processes of the three-particle system without the introduction of free three-body parameters, and the three-body amplitudes obey unitarity on and off the energy shell. The total angular momentum has been separated in the Faddeev equations by Omnes[37] in a manner which preserves the symmetry of the problem with respect to the three particles. The many degrees of freedom in the Faddeev equations make them difficult to solve numerically. This may be resolved by approximating the two-body potential as a sum of separable potentials. Mitra[38] has shown that exact three-body equations are obtained involving only a few coordinates in the intermediate states if the two-body operator is compact. If the parameter of the separable potentials is adjusted suitably, the two-body bound state may be considered in the calculation. The separable potential method is identical in the limit of zero wave function renormalization for the two-body bound state with the quasi-particle method of Amado[39] and Weinberg.[40] This calculation will follow the field theoretic method of Amado because of the physical clarity of his presentation.

The idea of substituting elementary particles for composite systems was rigorously studied by Jauch[34] and by Vaughn, Aaron, and Amado.[41] Jauch pointed out that the distinction between elementary particles and composite fragments is a superficial one from the view of scattering theory. The picture of the composite particle as an elementary particle only breaks down when the internal structure reveals itself in breakup processes. Vaughn, Aaron, and Amado showed that the nonadiabatic behavior of the composite system is overcome by introducing it originally as an elementary particle. Then soluable linear integral equations are derived, whose solutions exactly represent scattering, breakup or stripping reactions. Amado[39] later displayed how these equations could be put into the form of the Lippman-Schwinger equations. Since linear integral equations are derived, off-the-energy shell amplitudes are involved if three-body unitarity is to be satisfied. Remaining on the energy shell requires the solution of nonlinear integral equations. In the following the incident proton will be on the energy shell, and naturally the outgoing proton will be off the energy shell to define the integral equations. Aside from elastic scattering, deuteron breakup into a proton and a neutron will be the only reaction permitted in the following paragraphs. In the energy region considered by this work, deuteron breakup is overwhelmingly the major contribution to the total cross section. Using the notation of Aaron, Amado, and Yam[42] the spin-triplet pair interacts to form a "d" and the spin-singlet pair interacts to form a "φ". The spin-triplet and spin-singlet scattering amplitudes are assumed to have no coupling between them, and they are given nonrelativistically by

$$\langle \vec{k}, d \mid t(E) \mid \vec{k}', d \rangle = \chi_{dd} \langle \vec{k}, d \mid B(E) \mid \vec{k}', d \rangle$$

$$+ \frac{1}{(2\pi)^3} \int d^3p \, \chi_{dd} \langle \vec{k}, d \mid B(E) \mid \vec{p}, d \rangle P_d(p^2;E) \langle \vec{p}, d \mid t(E) \mid \vec{k}', d \rangle$$

$$+ \frac{1}{(2\pi)^3} \int d^3p \, \chi_{d\varphi} \langle \vec{k}, d \mid B(E) \mid \vec{p}, \varphi \rangle P_\varphi(p^2;E) \langle \vec{p}, \varphi \mid t(E) \mid \vec{k}', d \rangle$$

$$\langle \vec{k}, \varphi \mid t(E) \mid \vec{k}', d \rangle = \chi_{\varphi d} \langle \vec{k}, \varphi \mid B(E) \mid \vec{k}', d \rangle$$

$$+ \frac{1}{(2\pi)^3} \int d^3p \, \chi_{\varphi\varphi} \langle \vec{k}, \varphi \mid B(E) \mid \vec{p}, d \rangle P_\varphi(p^2;E) \langle \vec{p}, \varphi \mid t(E) \mid \vec{k}', d \rangle$$

$$+ \frac{1}{(2\pi)^3} \int d^3p \, \chi_{\varphi d} \langle \vec{k}, \varphi \mid B(E) \mid \vec{p}, d \rangle P_d(p^2;E) \langle \vec{p}, d \mid t(E) \mid \vec{k}', d \rangle$$

where $\hbar = 2m = 1$, $B(E)$ is the Born approximation for the exchange of a nucleon between pairs, $P(p^2;E)$ is the full propagator in the intermediate state, and the χ's are the spin and isospin factors. The graphical representation of these equations is given in Fig. 11. The explicit form of the Born terms in the integral equations are

$$\langle \vec{k},d \mid B(E) \mid \vec{k}',d \rangle = \Gamma_d^2 \frac{V_d\left[(\vec{k}+\vec{k}'/2)^2\right] \; V_d\left[(\vec{k}+\vec{k}/2)^2\right]}{E-k^2-k'^2-(\vec{k}+\vec{k}')^2+i\epsilon}$$

$$\langle \vec{k},\varphi \mid B(E) \mid \vec{k}',\varphi \rangle = \Gamma_\varphi^2 \frac{V_\varphi\left[(\vec{k}+\vec{k}'/2)^2\right] \; V_\varphi\left[(\vec{k}+\vec{k}/2)^2\right]}{E-k^2-k'^2-(\vec{k}+\vec{k}')^2+i\epsilon}$$

$$\langle \vec{k},\varphi \mid B(E) \mid \vec{k}',d \rangle = \langle \vec{k}',d \mid B(E) \mid \vec{k},\varphi \rangle$$

$$= \Gamma_\varphi \Gamma_d \frac{V_\varphi\left[(\vec{k}+\vec{k}/2)^2\right] \; V_d\left[(\vec{k}+\vec{k}'/2)^2\right]}{E-k^2-k'^2-(\vec{k}+\vec{k}')^2+i\epsilon}$$

where Γ_d and Γ_φ are the coupling constants to the "d" and "φ" quasiparticles, V_d and V_φ are the vertex form factors. The propagators for the intermediate states have the form

$$P_d(p^2;E) = \left[(\sigma+b)\frac{\Gamma_d^2}{(2\pi)^3}\int d^3n \quad \frac{V_d(n^2) \; V_d(n^2)}{(2n^2+b)^2 \; (\sigma-2n+i\epsilon)}\right]^{-1}$$

$$P_\varphi(p^2;E) = -\left[1+\frac{\Gamma_\varphi^2}{(2\pi)^3}\int d^3n \quad \frac{V_\varphi(n^2) \; V_\varphi(n^2)}{(\sigma-2n+i\epsilon)}\right]^{-1}$$

where $\sigma = E - \frac{3}{2}p^2$ and b is the binding energy of the deuteron. The introduction of separable potentials is evidenced by the appearance of only one vector variable, p, labeling the intermediate states. The form of the vertex form factors must be chosen so that the kernel is square integrable in order to use the Fredholm method of solving these equations. Amado has proven that this condition is satisfied in momentum space by

$$V(\kappa^2) = C/\kappa^{1+\eta}, \quad \eta \geq 0$$

for large κ which corresponds to investigating the potential at small distances in configuration space. Using the momentum representation of the Hulthén wave

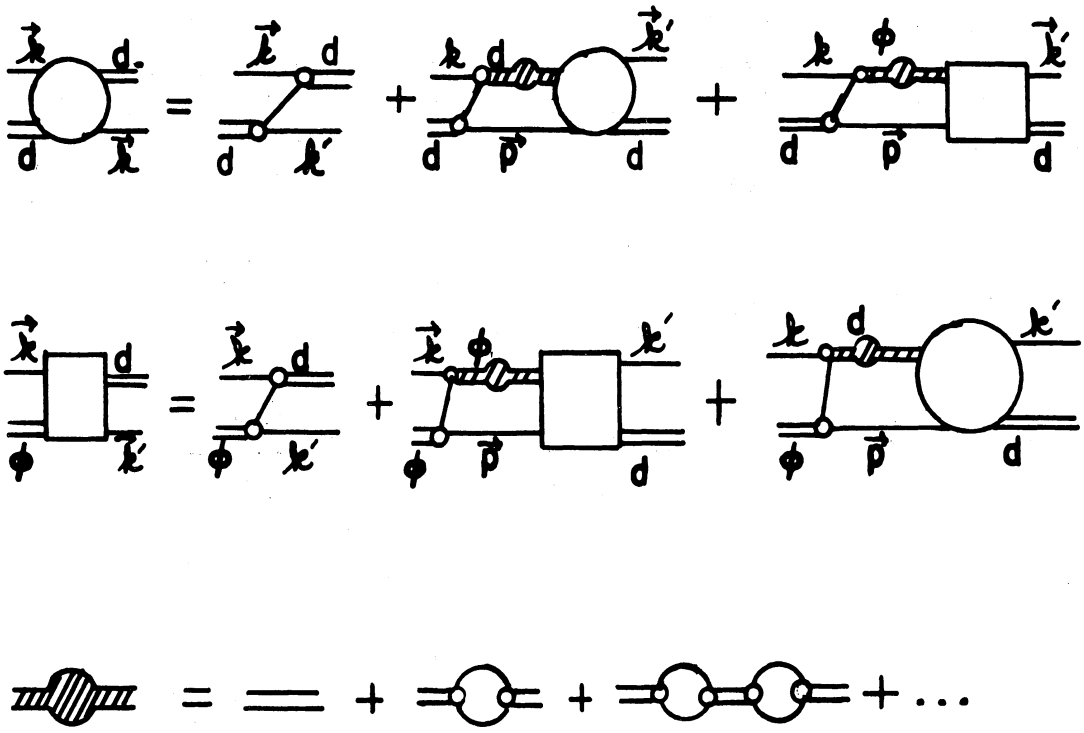

Fig. 11. Diagrams for proton-deuteron scattering. The nucleon is a single line; the double lines are φ for singlet and d for triplet; the small circles are nucleon-nucleon vertices; the rectangles and large circles are three-nucleon amplitudes.

function yields

$$V_d(\kappa^2) = \frac{1}{\kappa^2 + \beta_d} \qquad \text{and} \qquad V_\varphi(\kappa^2) = \frac{1}{\kappa^2 + \beta_\varphi^2}$$

which approximates the left-hand cut in the complex three momentum plane by a pole at $\kappa^2 = -\beta^2$. Only two-body nucleon-nucleon parameters enter the calculations, and in terms of the triplet scattering length a_t, the singlet scattering length a_s and the singlet effective range r_s they are given by

$$\frac{1}{a_t} = \frac{\alpha_d \beta_d (2\beta_d + \alpha_d)}{2(\alpha_d + \beta_d)^2}$$

$$\Gamma_d^2 = 32 \pi \alpha_d \beta_d (\alpha_d + \beta_d)^3$$

$$\Gamma_\varphi^2 = \frac{16 \pi \beta_\varphi^4 a_s}{a_s \beta_\varphi - 2}$$

$$\beta_\varphi = \frac{3}{2r_s}\left[1 + \left(1 - \frac{16 r_s}{9 a_s}\right)^{\frac{1}{2}}\right]$$

where $\alpha_d^2 = b/2$. The integral equations may be solved by the Fredholm inversion method[43] for low energies, but at the energies considered here Yam[44] has shown that the Neumann series for the equations converges. The first term of the expansion is the Born approximation. The unnormalized differential cross section predicted by the Born term is plotted in Fig. 12 both with the Hulthén form factor and with the form factor set equal to one, (i.e., $V(\kappa^2) = 1$). The spin average of the differential cross section when only the Born term is included takes the form

$$\frac{d\sigma}{d\Omega} = \frac{2}{3}\left| \chi_{dd}(\underline{k},d \mid B(E) \mid k',d)\right|^2 + \frac{1}{3}\left| \chi_{\varphi d}(\underline{k},\varphi \mid B(E) \mid \underline{k}',d)\right|^2 .$$

The differential cross sections normalized to the point $\cos\theta^* = -.875$ at 1.0 GeV incident proton kinetic energy are shown in Figs. 13-16 For the first term of the iteration the differential cross section has a slope which is much too steep when the form factor is included. The use of other deuteron wave functions in determining the form factors (see Chapter II) does not improve matters significantly. Further iterations of the equations including the form factor only increases the slope of the backward peak as the amplitude

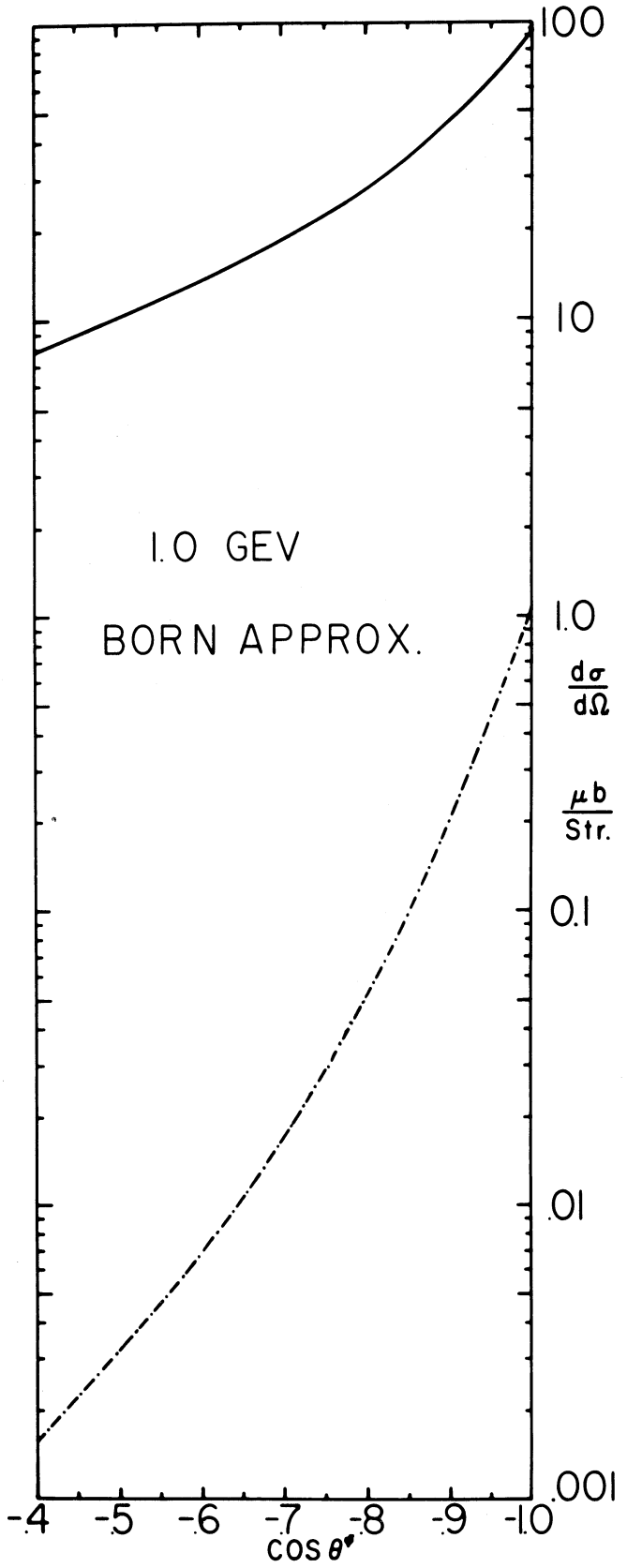

Fig. 12. Unnormalized born terms at 1.0 GeV. (———) $V(\kappa^2) = 1$; (−·−·−) Hulthén form factor.

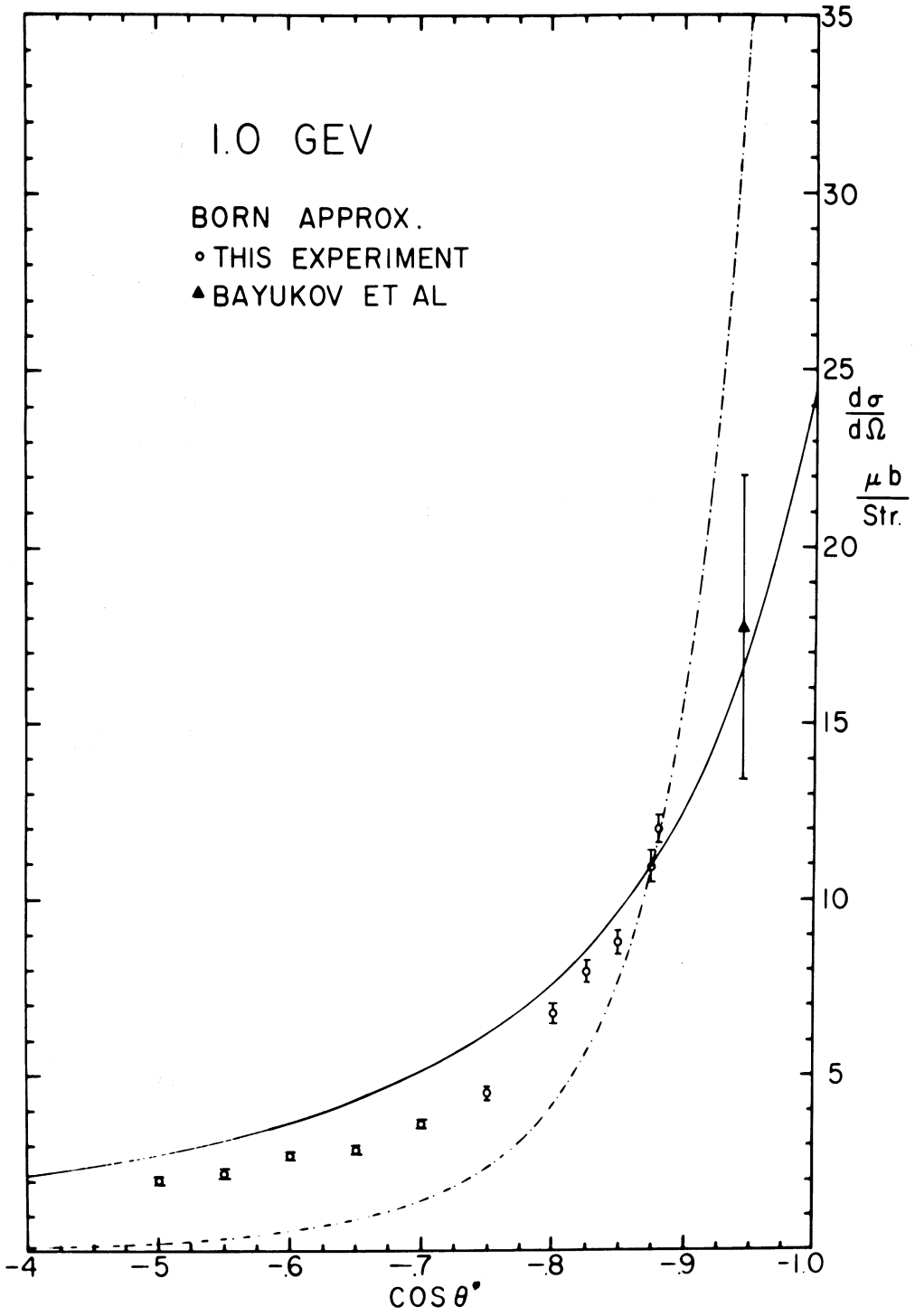

Fig. 13. Contribution of born terms at 1.0 GeV. (———) $V(\kappa^2) = 1$; (-·-·-) Hulthén form factor.

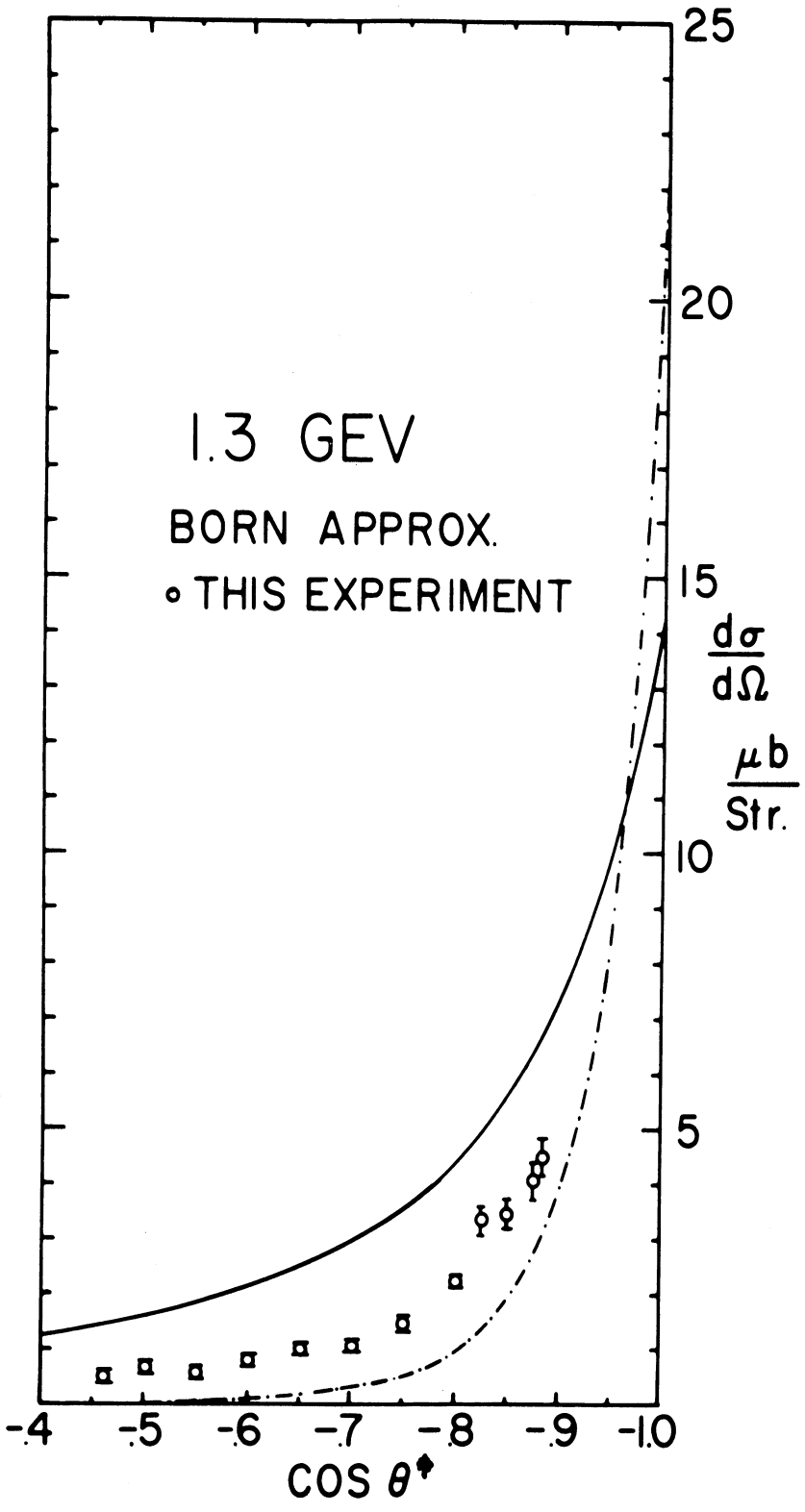

Fig. 14. Contribution of born terms at 1.3 GeV. (———) $V(\kappa^2) = 1$; (-·-·-) Hulthén form factor.

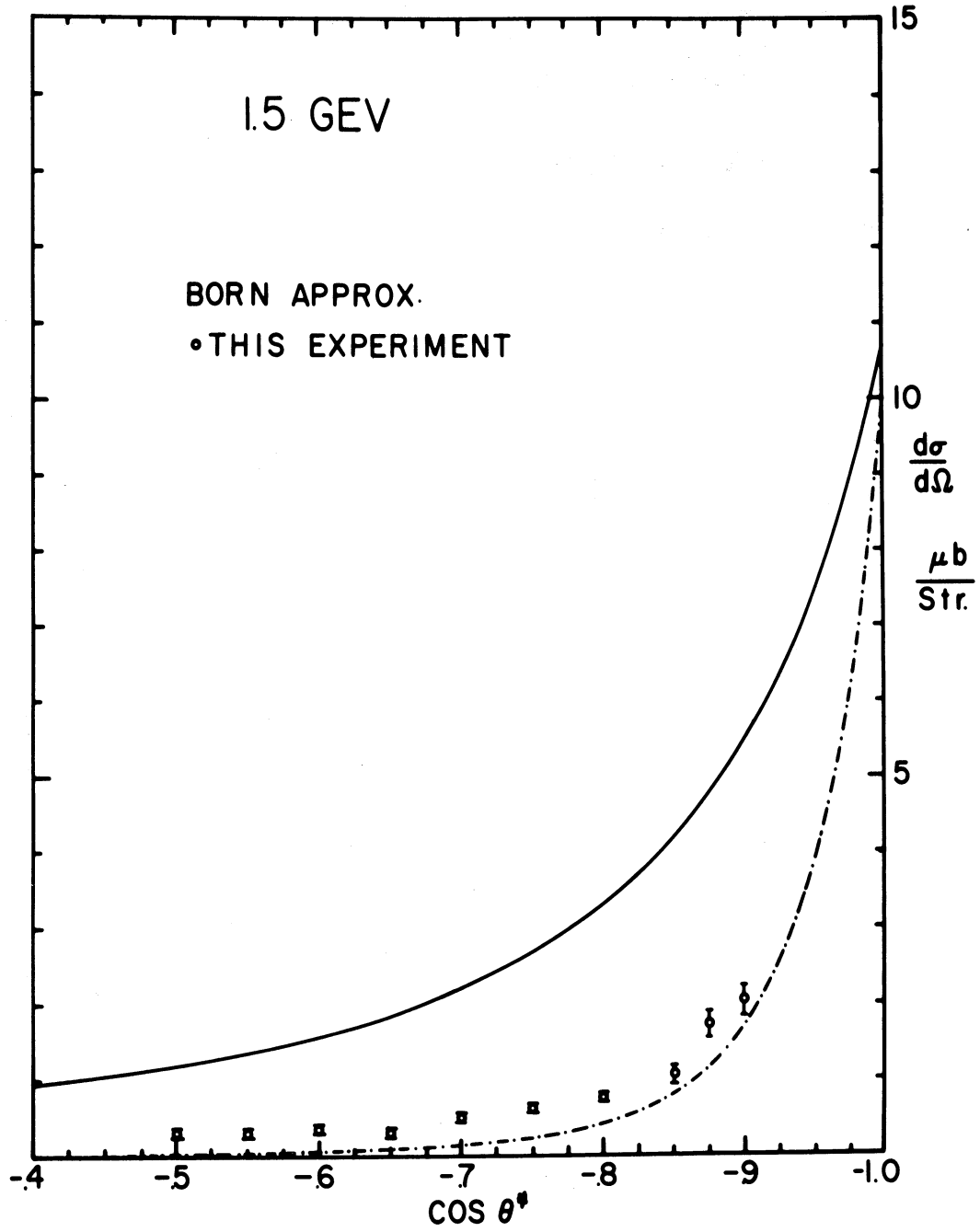

Fig. 15. Contribution of born terms at 1.5 GeV. (———) $V(\kappa^2) = 1$; (-·-·-) Hulthén form factor.

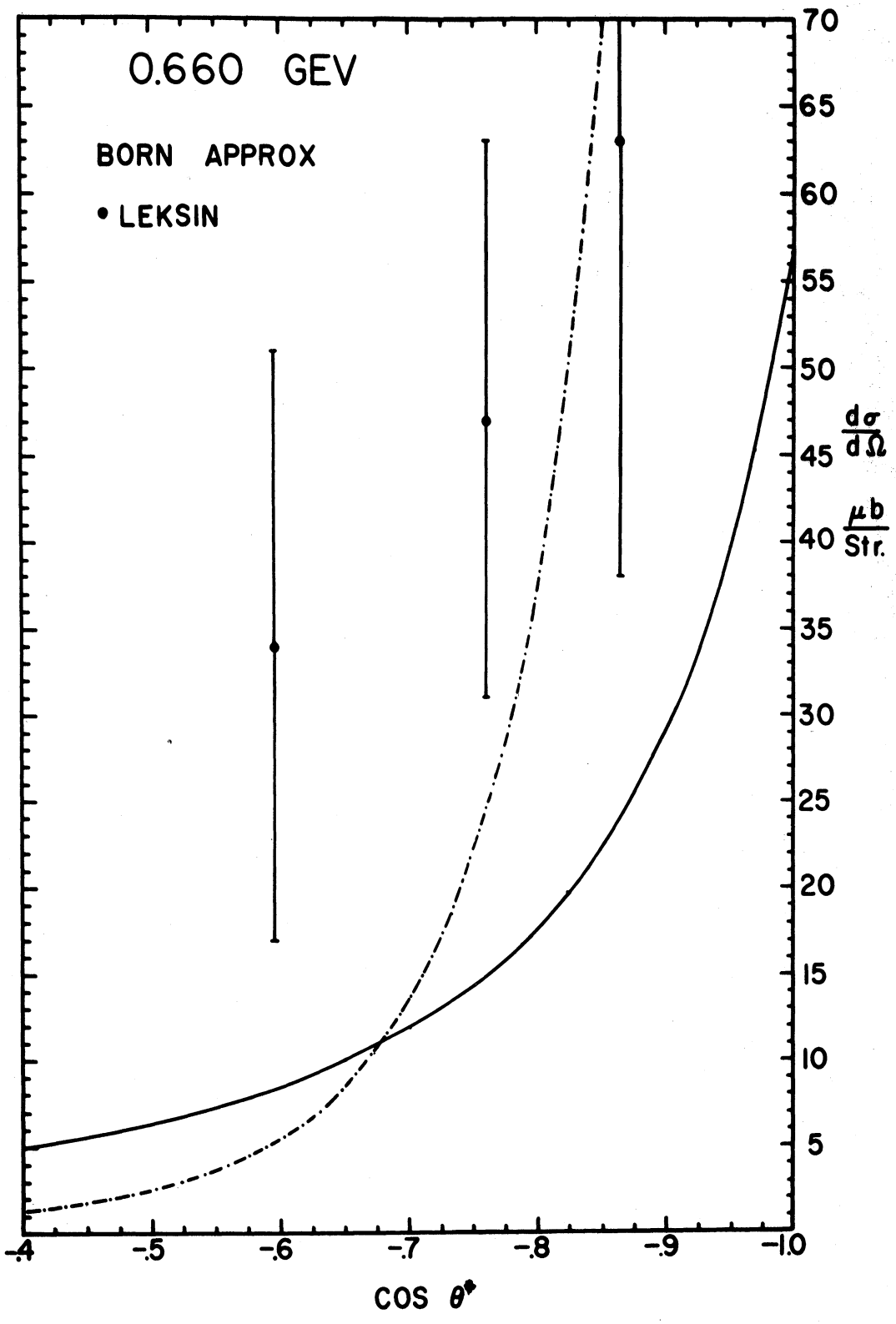

Fig. 16. Contribution of born terms at 0.660 GeV. (———) $V(\kappa^2) = 1$; (-·-·-) Hulthén form factor.

raises in the forward direction to satisfy unitarity. Consequently when the vertex form factors are included, the experimental data is not adequately predicted because the high momentum components of the deuteron are suppressed too greatly. When the form factor equals one, the kernel of the integral equations is not square integrable as mentioned above, and the Fredholm method is not applicable. The Neumann expansion in this calculation depends upon the approximation of the potential by a finite sum of separable potentials, and the factors of the separable potentials are proportional to the bound state form factors.[45] In the three-body system the Neumann expansion differs from the Born expansion because in general the kernel is not a linear function of the two-body coupling constant. When the Hulthén form factors are used, the Neumann series converges for sufficiently high energies for any partial wave. However, when the form factors are set equal to one, the convergence of the Neumann series is not readily proven because the kernel is not known to be compact. The Born series diverges independently of the incident energy of the proton whenever a two-body bound state enters the three-body system.[46] The zeroth iteration, which is the Born approximation, is in closest agreement with the experimental data. The calculations then reduce to the one-nucleon exchange diagram with a non-relativistic propagator In the discussion of Chapter IX, the results of this chapter and Chapter II will be compared.

IV. OFF THE FORWARD DIFFRACTION PEAK

Elastic differential cross sections for scattering of elementary particles at high energies generally have a large peak in the forward direction which has been denoted the diffraction peak. The diffraction peak has been studied for proton-deuteron elastic scattering in the few GeV region by Kirillova et al.,[15] but the analysis was not carried beyond this peak due to the lack of data. The present experiment observed a shoulderlike departure from the strict exponential trend of the differential cross section for four-momentum transfer greater than 0.5 $(GeV/c)^2$ at 2.0 GeV incident proton kinetic energy.[48] Previously, secondary peaks or shoulderlike structures have been noticed in pion-proton elastic scattering, kaon-proton elastic scattering, pion-proton charge exchange scattering, kaon-proton charge exchange scattering, and positive pion-rho elastic scattering.[49-55] However the secondary peak does not appear in proton-proton and proton-neutron elastic scattering.[56] No satisfactory theoretical model for the secondary diffraction peak has been advanced.

The most common method of studying the secondary peak has been via the optical model. As pointed out by Simmons,[57] the position, height, and to some degree the width of the secondary diffraction peak in pion-nucleon scattering may be fitted with the optical model. However, the differential cross section goes to zero as many times as the value of the maximum angular momentum considered. For proton-deuteron elastic scattering at 2.0 GeV incident proton kinetic energy, the model would predict a differential cross section which goes to zero fourteen times since $L_{max} \approx kR \approx 14$. If a diffuse edge is added to the deuteron by assuming small contributions to the differential cross section by values of angular momentum greater than L_{max}, the postion and magnitude of the secondary peak are adversely altered although the number of zeroes may be reduced. Due to the composite nature of the deuteron, other avenues of approach are available which are ostensibly closed when the internal structure of the target particle is unknown. The following methods make use of the known composite structure of the deuteron in an attempt to interpret the behavior of the proton-deuteron elastic differential cross section off the forward diffraction peak.

A. IMPULSE APPROXIMATION

The standard impulse approximation, which neglected multiple scattering effects, gave a reasonable description of proton-deuteron elastic scattering at small angles in the few MeV region.[58,59] The basic assumptions were that the incident proton never interacted strongly with the two components of the deuteron at the same time, and the binding force of the deuteron was negligible during the interaction time. If the incident proton is number 1 and the target proton and neutron are numbers 2 and 3 respectively, let V_2 and V_3 re-

present the two-body interaction of the incident proton with the proton and neutron. Let U be the interaction between the constituents of the deuteron, E be the total energy of the system, and K be the total kinetic energy operator of the system. The total Hamiltonian for the system is then

$$H = K + U + V_2 + V_3$$

$$= H_o + V$$

where $H_o = K + U$ is the unperturbed Hamiltonian. The scattering matrix, T, may be written, as specified by Chew and Goldberger,[60] in the form

$$T = V + VGV$$

with

$$G = \lim_{\epsilon \to 0} \frac{1}{E - H + i\epsilon}$$

Then neglecting multiple scattering, T may be written as

$$T = St_2 + St_3 + \ldots$$

where

$$t_2 = V_2 + V_2 \frac{1}{E - K - V_2 + i\epsilon} V_2$$

$$t_3 = V_3 + V_3 \frac{1}{E - K - V_3 + i\epsilon} V_3$$

and S is the "sticking factor" defined by Chew[63] to be

$$S(q/2) = \int d\vec{r}\, e^{\frac{i\vec{q}\cdot\vec{r}}{2}} \psi^2(r)$$

where q is the three-momentum transfer and $\psi(r)$ is the deuteron wave function. In the two-body problem, the relationship between q and the center-of-mass angle θ_2^* is $q = k_L \sin(\theta_2^*/2)$ where k_L is the momentum of the incident proton when the target proton or neutron is at rest. For the three-body problem the three-momentum transfer remains the same, but the relationship to the three-body center-of-mass scattering angle θ_3^* is then $q = (4/3)\, k_L \sin \theta_3^*/2$. Consequently the scattering angle of the proton-deuteron system is related to

the two nucleon scattering by

$$\sin \frac{\theta_2^*}{2} = \frac{4}{3} \sin \frac{\theta_3^*}{2}$$

which yields the center-of-mass solid angle transformation

$$\frac{d\Omega_2}{d\Omega_3} = \frac{16}{9}$$

The elastic proton-deuteron differential cross section has been expressed by Chew[63] in terms of momentum transfer as

$$\frac{d\sigma}{dq^2} = \left[|f_{np} + f_{pp}|^2 + \frac{2}{3} | f'_{np} + f'_{pp} |^2 \right] S(q/2)$$

where f_{np} and f_{pp} are the spin non-flip amplitudes and f'_{np}, f'_{pp} are the spin flip amplitudes. The relative phase of the proton-proton and neutron-proton amplitudes and the difference in magnitudes of the spin flip and spin non-flip amplitudes are not known at the energies of concern in this work. Neglecting the D-state of the deuteron and only considering the spin dependence required by the Pauli exclusion principle yielded the differential cross section in the form

$$\frac{d\sigma_{pd}}{d\Omega_3} = \frac{16}{9} \left[\frac{d\sigma_{np}}{d\Omega_2} + \frac{3}{4} \frac{d\sigma_{pp}}{d\Omega_2} + \left(\frac{d\sigma_{np}}{d\Omega_2} \frac{d\sigma_{pp}}{d\Omega_2} \right)^{\frac{1}{2}} \cos \Delta \right] S^2 (\theta_3^*)$$

in the center-of-mass system where Δ is the difference between the neutron-proton and proton-proton phase shifts. The $S(\theta_3^*)$ or the corresponding $S(q/2)$ was determined by using the regular Hulthén wave function and the best Moravcsik fit to the Gartenhaus wave function (see Chapter II, Section B). Using the Hulthén wave function yielded the relationship

$$S(q/2) = \frac{8\pi N}{q} \left[\tan^{-1} \frac{q}{4\alpha} + \tan^{-1} \frac{q}{4\beta} - 2\tan^{-1} \frac{q}{2(\alpha + \beta)} \right]$$

whereas the Moravcsik fit to the Gartenhaus wave function yielded

$$S(q/2) = \frac{8\pi N^2}{q}\left[\tan^{-1}\frac{q}{4\alpha} + \tan^{-1}\frac{q}{4\beta} + \tan^{-1}\frac{q}{4\alpha + 4c}\right.$$

$$+ \tan^{-1}\frac{q}{4\alpha + 4g} + \tan^{-1}\frac{q}{4\,(\alpha + c + g)} + \tan^{-1}\frac{q}{4c + 4d}$$

$$+ \tan^{-1}\frac{q}{4d + 4g} + \tan^{-1}\frac{q}{4\,(c + d + g)} - 2\tan^{-1}\frac{q}{2\alpha + 2d}$$

$$-2\tan^{-1}\frac{q}{4\alpha + 2c} - 2\tan^{-1}\frac{q}{4\alpha + 2g} + 4\tan^{-1}\frac{q}{4\alpha + 2c + 2g}$$

$$+ 4\tan^{-1}\frac{q}{2\,(\alpha + c + d)} + 4\tan^{-1}\frac{q}{2\,(\alpha + d + g)} - 8\tan^{-1}\frac{q}{2\,(\alpha + c + d + g)}$$

$$- 2\tan^{-1}\frac{q}{2\,(c + 2d)} - 2\tan^{-1}\frac{q}{2\,(2d + g)} + 4\tan^{-1}\frac{q}{2\,(c + 2d + g)}$$

$$-2\tan^{-1}\frac{q}{2\,(2\alpha + 2c + g)} - 2\tan^{-1}\frac{q}{2\,(\alpha + 2c + d)} + 4\tan^{-1}\frac{q}{2\,(\alpha + 2c + d + g)}$$

$$-2\tan^{-1}\frac{q}{2\,(2\alpha + c + 2g)} - 2\tan^{-1}\frac{q}{2\,(\alpha + d + 2g)} + 4\tan^{-1}\frac{q}{2\,(\alpha + c + d + 2g)}$$

$$\left.-2\tan^{-1}\frac{q}{2\,(\alpha + 2c + d + 2g)} - 2\tan^{-1}\frac{q}{2\,(2c + 2d + g)} - 2\tan^{-1}\frac{q}{2(c + 2d + 2g)}\right]$$

Due to the lack of suitable neutron-proton phase shift data in this region, the phase shift difference has been set equal to zero which implies that the neutron-proton and proton-proton differential cross sections are equal. The predicted proton-deuteron elastic differential cross section at 2.0 GeV incident proton kinetic energy is shown in Fig. 17 using the experimental proton-proton elastic scattering data of Barge[64] and the S(q/2) from the Hulthén wave function. The use of the Moravcsik fit to the Gartenhaus wave function gives essentially the same results. The impusle approximation is in good agreement with the small angle data of Kirillova et al.,[15] but the strict exponential trend of the curve does not reproduce the shoulderlike departure of our data from the diffraction peak. Since there is no evidence of a secondary maximum in either proton-proton or neutron-proton elastic scattering, there is no reason to expect the impulse approximation to predict one in proton-deuteron scattering. However if multiple scattering is allowed, the theoretical curve

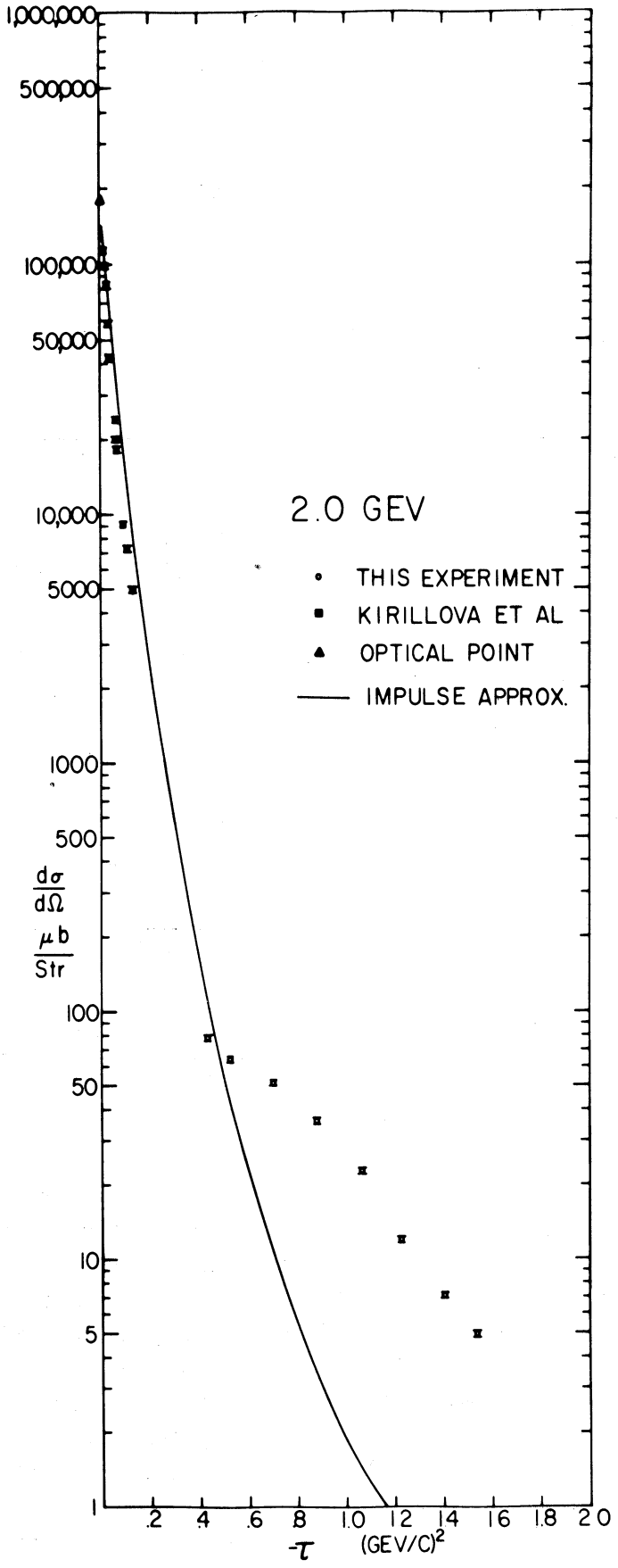

Fig. 17. Prediction of impulse approximation at 2.0 GeV. Differential cross section in center-of-mass system.

may tend to follow the experimental data more closely.

B. MULTIPLE SCATTERING PROCESSES

The effect of binding and multiple scattering processes may be studied as corrections to the impulse approximation as has been shown by Everett.[65] For small momentum transfers, Chew and Wick[62] have estimated that single scattering dominates when the condition

$$\frac{\lambda\!\!\!^{-}}{\bar{R}^2}\left(\frac{\sigma}{4\pi}\right)\frac{1}{2} \ll 1$$

is satisfied where $\bar{R}$ is the average internucleon distance, $\lambda\!\!\!^{-}$ is the wavelength of the incident proton divided by 2π, and σ is the total cross section. At 2.0 GeV the left side of the inequality equals 0.049, and as seen in Section A the single scattering processes indeed dominate on the diffraction peak. However, for larger momentum transfers around -1.0 $(\mathrm{GeV/c})^2$ the inclusion of multiple scattering may have a more noticeable effect than expected from the above inequality. An analysis of multiple scattering in the collision of particles with deuterons using a generalized form of diffraction theory has been advanced by Franco and Glauber.[66] This work follows the method of Franco and Glauber because of the simple physical interpretation of the scattering effects as they appear in the terms of differential cross sections.

Near the forward direction, the scattering amplitude at high energies may be written as

$$f(\vec{k}',\vec{k}) = \frac{ik}{2\pi}\int \exp i\,(\vec{k}-\vec{k}')\cdot\vec{u}\left[1-\exp\left(i\chi\,(\vec{u})\right)\right]\,d\vec{u}$$

where $\vec{u}$ is the impact-parameter perpendicular to the direction of the beam and $\chi\,(\vec{u})$ is the phase shift. For a target particle consisting of a total of A nucleons with positions $r_1,\ldots,r_A$, the wave of the incident particle will undergo a total phase shift $\chi_{tot}\,(\vec{u},\vec{r}_1,\ldots,\vec{r}_A)$. If the incident particle interacted only via two-body interactions with the target nucleons, the total phase shift would be the sum of the individual phase shifts. If $\vec{s}$ is the projection of the postión coordinates on a plane perpendicular to the incident beam the total phase shift may be expressed by

$$\chi_{tot}\,(\vec{u},\vec{r}_1,\ldots,\vec{r}_A) = \sum_{j=1}^{A} x_j\,(\vec{u}-\vec{s}_j).$$

For the deuteron, let $\vec{r}_n$ and $\vec{r}_p$ be the coordinates of the neutron and proton prespectively. Then the relative internal coordinate is $\vec{r} = \vec{r}_p - \vec{r}_n$. The total phase shift is

$$\chi_{tot} = \chi_n \left(\vec{u} - \frac{1}{2}\vec{s}\right) + \chi_p \left(\vec{u} + \frac{1}{2}\vec{s}\right)$$

with $\vec{s}$ now the projection of r. Let the function

$$\Gamma_{tot} (\vec{u}, \vec{s}) = 1 - \exp \left[i\chi_{tot} (\vec{u}, \vec{s}) \right]$$

be introduced for abbreviation purposes. Since the comparison of the proton-deuteron scattering amplitude with the proton-proton and neutron-proton scattering amplitudes would require two center-of-mass systems, the following calculations refer to the laboratory system for convenience in notation. The scattering amplitude is then the matrix element between the initial state $|i>$ to the final state $|f>$, which is

$$F_{fi} (\vec{k}', \vec{k}) = \frac{ik}{2\pi} \int \exp \left[i (\vec{k} - \vec{k}') \cdot \vec{u} \right] < f \mid \Gamma_{tot} (\vec{u}, \vec{s}) \mid i > d\vec{u} .$$

the contributions from single scattering and double scattering are considered here, and the appropriate diagram of the calculated processes is shown in Fig. 18. Tertiary and higher order scattering processes involve at least one or more backward scatterings and have a negligible effect on forward proton-deuteron elastic scattering. If we let the momentum transfer be represented by $\hbar\vec{q} = \hbar (\vec{k} - \vec{k})$ and let the energy transfer to the target particle be negligible for forward scattering, the elastic scattering amplitude assumes the form

$$F_{ii} (\vec{q}) = \frac{ik}{2\pi} \int \exp (i\vec{q} \cdot \vec{u}) \, d\vec{u} \int \psi_i^* (\vec{r}) \, \Gamma_{tot} (\vec{u}, \vec{s}) \, \psi_i (\vec{r}) \, d\vec{r} .$$

The scattering contributions of the individual nucleons may be separated by defining

$$\Gamma_n = 1 - \exp \left[i\chi_n (\vec{u}) \right] \text{ and } \Gamma_p = 1 - \exp \left[i\chi_p (\vec{u}) \right]$$

to obtain the identity

$$\Gamma_{tot} = \Gamma_n \left(\vec{u} - \frac{1}{2}\vec{s}\right) + \Gamma_p \left(\vec{u} + \frac{1}{2}\vec{s}\right) - \Gamma_n \left(\vec{u} - \frac{1}{2}\vec{s}\right) \Gamma_p \left(\vec{u} + \frac{1}{2}\vec{s}\right) .$$

Then substituting this expression in the above equation and shifting the origin in the $\vec{u}$ plane yields

$$F_{ii} (\vec{q}) = \frac{ik}{2\pi} \int \exp \left(\frac{i\vec{q}\cdot\vec{s}}{2}\right) \psi_i^2 (\vec{r}) d\vec{r} \int \exp (i\vec{q}\cdot\vec{u}) \, \Gamma_n (\vec{u}) \, d\vec{u}$$

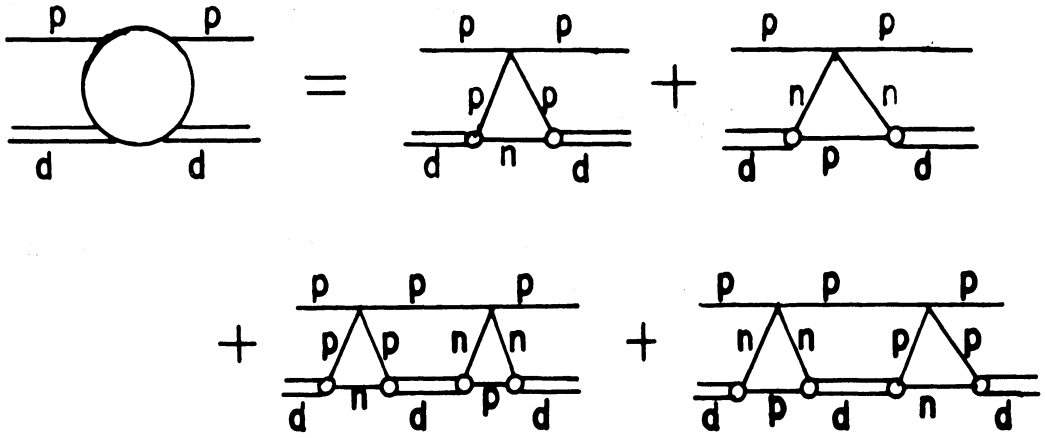

Fig. 18. Diagrams for single and double scattering. The impulse approximation only considers the first two graphs on the right hand side. The influence of all four graphs on the differential cross section is considered in the calculations of Section B.

$$+ \frac{ik}{2\pi} \int \exp\left(\frac{-i\vec{q}\cdot\vec{s}}{2}\right) \psi_i^2 (\vec{r})\, d\vec{r} \int \exp (i\vec{q}\cdot\vec{u})\, \Gamma_p (\vec{u})\, d\vec{u}$$

$$- \frac{ik}{2\pi} \int \psi_i^2 (\vec{r})\, d\vec{r} \int \exp (i\vec{q}\cdot\vec{u}) \Gamma_n (\vec{u} - \tfrac{1}{2}\vec{s})\, \Gamma_p (\vec{u} + \tfrac{1}{2}\vec{s})\, d\vec{u}$$

Using the expression for the sticking factor defined in Section A and noting that $\Gamma(u)$ is the Fourier transform of $f(q)$, that is

$$\Gamma (u) = \frac{1}{2\pi ik} \int \exp (-\vec{q}\cdot\vec{u})\, f (q)\, d\vec{q} \quad ,$$

the elastic scattering amplitude takes the form

$$F_{ii} (q) = S(\tfrac{1}{2}\vec{q})\, f_p (\vec{q}) + S(-\tfrac{1}{2}\vec{q})\, f_n (\vec{q})$$

$$+ \frac{i}{2\pi k} \int S(\vec{q}')\, f_p (\tfrac{1}{2}\vec{q} + \vec{q}')\, f_n (\tfrac{1}{2}\vec{q} - \vec{q}')\, d\vec{q}'$$

The elastic differential cross section is the square of F_{ii} (q) and may be written as

$$\frac{d\sigma}{d\Omega} = S^2 (\tfrac{1}{2}\vec{q}) \left[|f_p (\vec{q})|^2 + |f_n (\vec{q})|^2 + 2\, \mathrm{Re}\ f_p (\vec{q}) f_n^* (\vec{q}) \right]$$

$$- \frac{1}{\pi k} S(\tfrac{1}{2}\vec{q})\, \mathrm{Im} \left[|f_n^* (\vec{q}) + f_p^* (\vec{q})| \int S(\vec{q}')\, f_n (\tfrac{1}{2}\vec{q} + \vec{q}') \right.$$

$$\left. f_p (\tfrac{1}{2}\vec{q} - \vec{q}')\, d\vec{q}' \right]$$

$$+ \frac{1}{(2\pi k)^2} \left| \int S(\vec{q}')\, f_n (\tfrac{1}{2}\vec{q} + \vec{q}')\, f_p (\tfrac{1}{2}\vec{q} - \vec{q}')\, d\vec{q}' \right|^2$$

The contributions from single and double scattering appear explicitly in the above equation. The first term corresponds to the scattering by a free proton and by a free neutron and the interference of the two wave amplitudes respectively. The second term corresponds to the interference between the double-scattering amplitude and the neutron single-scattering amplitude plus the interference between the double-scattering amplitude and the proton single-scattering amplitude. The third term corresponds to solely double-scattering.

For application of the differential cross section formula, expressions must be found for the scattering amplitudes $f_p(\vec{q})$ and $f_n(\vec{q})$. The amplitudes have been assumed to be of the Gaussian form in the momentum transfer and are represented by

$$f_p(\vec{q}) = (i + \alpha_p)(k\alpha_p/4\pi) \exp(-A_p q^2/2)$$

$$f_n(\vec{q}) = (i + \alpha_n)(k\alpha_n/4\pi) \exp(-A_n q^2/2)$$

where σ_p is total proton-proton cross section, σ_n is total proton-neutron cross section, α_p is the ratio of the real to the imaginary part of the proton-proton scattering amplitude, α_n is the ratio of the real to the imaginary part of the proton-neutron scattering amplitude, A_p is the slope of the proton-proton elastic differential cross section, and A_n is the slope of the proton-neutron elastic differential cross section. Substituting these expressions for the amplitudes into the differential cross section yields

$$\frac{d\sigma}{d\Omega} = S^2 \left(\frac{1}{2} q\right) \left(\frac{k}{4\pi}\right)^2 \left[(1 + \alpha_n^2)\, \sigma_n^2\, e^{-A_n q^2} + (1 + \alpha_p^2)\, \sigma_p^2\, e^{-A_p q^2} + 2(1 + \alpha_n \alpha_p)\, \sigma_n \sigma_p\, e^{-\frac{1}{2}(A_n + A_p) q^2} \right]$$

$$- \frac{k^2 \sigma_n \sigma_p}{\pi (4\pi)^3}\, e^{-(A_n + A_p) q^2/8} \left[(1 + \alpha_n^2)\sigma_n e^{-\frac{1}{2} A_n q^2} + (1 + \alpha_p^2)\sigma_p e^{-\frac{1}{2} A_p q^2} \right]$$

$$\int S(\vec{q}')\, e^{-\frac{1}{2}(A_p - A_n)\vec{q}\cdot\vec{q}'}\, e^{-\frac{1}{2}(A_n + A_p)\vec{q}'^2}\, d\vec{q}'$$

$$+ \frac{k^2 \sigma_n^2 \sigma_p^2}{(2\pi)^2 (4\pi)^4} (1 + \alpha_n^2 + \alpha_p^2 + \alpha_n^2 + \alpha_p^2)\, e^{-\frac{1}{2}(A_n + A_p) q^2}$$

$$\left| \int S(\vec{q}')\, e^{-\frac{1}{2}(A_p - A_n)\, q\cdot q'}\, e^{-\frac{1}{2}(A_n + A_p) q'^2}\, d\vec{q}' \right|^2$$

Although the α_p and α_n may not be equal as reported by Kirillova et al.,[15] the slopes of the differential corss sections have about the same values as recently measured by Kreisler et al.[56] Letting $A_n = A_p = A$ simplifies the equation to

$$\frac{d\sigma}{d\Omega} = S^2\left(\frac{1}{2}q\right)\left(\frac{k}{4\pi}\right)^2 e^{-Aq^2}\left[(1+\alpha_n^2)\sigma_n^2 + (1+\alpha_p^2)\sigma_p^2 + 2(1+\alpha_n\alpha_p)\sigma_n\sigma_p\right]$$

$$- \frac{k^2\sigma_n\sigma_p}{\pi(4\pi)^3} e^{-3Aq^2/4}\left[(1+\alpha_n^2)\sigma_n + (1+\alpha_p^2)\sigma_p\right]\int S(q')e^{-Aq'^2}\,dq'$$

$$+ \frac{k^2\sigma_n^2\sigma_p^2}{(2\pi)^2(4\pi)^4}(1+\alpha_n^2+\alpha_p^2+\alpha_n^2+\alpha_p^2)\, e^{-\frac{1}{2}Aq^2}\left|\int S(q')e^{-Aq'^2}\,dq'\right|^2$$

It is interesting to note the magnitude of the error in the α_n determined by Kirillova et al., who found $\alpha_n = 0.2 \pm 0.4$ and $\alpha_p = -0.12 \pm 0.07$. The values of α_n and α_p determine the relative phase between the single and double scattering amplitudes, and the effect of varying α_n to the minimum experimental value is shown in Fig. 19. A theoretical evaluation of the real part of the proton-proton forward scattering amplitude has been published by Söding.[82] By using dispersion relations with the integration in the unphysical region replaced by the ρ meson and ω meson poles, Söding obtained $\alpha_p = -0.27$ for 2.0 GeV incident proton kinetic energy. The real part of the proton-neutron forward scattering amplitude has been determined by Carter and Bugg, who fitted the low energy contribution from the unphysical region with only the ρ pole.[83] Carter and Bugg found $\alpha_n = -0.50$ at 2.0 GeV. The dip in the differential cross section is much less pronounced when the α_n and α_p assume the more negative values of the theoretical predictions as evidenced in Fig. 19. Using the $S(q/2)$ determined by the Moravcsik analytic fit to the Gartenhaus wave function and the predicted values of α_n and α_p, the theoretical differential cross section is displayed in Fig. 20. The theoretical curve is in good agreement with the experimental data in slope and magnitude except at the dip caused by the interference terms. There are no free parameters in the formulation since all quantities are set by nucleon-nucleon data. The valley at $|t| = 0.38\ (\mathrm{GeV/c})^2$ has no apparent justification, but perhaps it can be eliminated by selecting amplitudes which represent the scattering at higher momentum transfers better than the Gaussian amplitude.

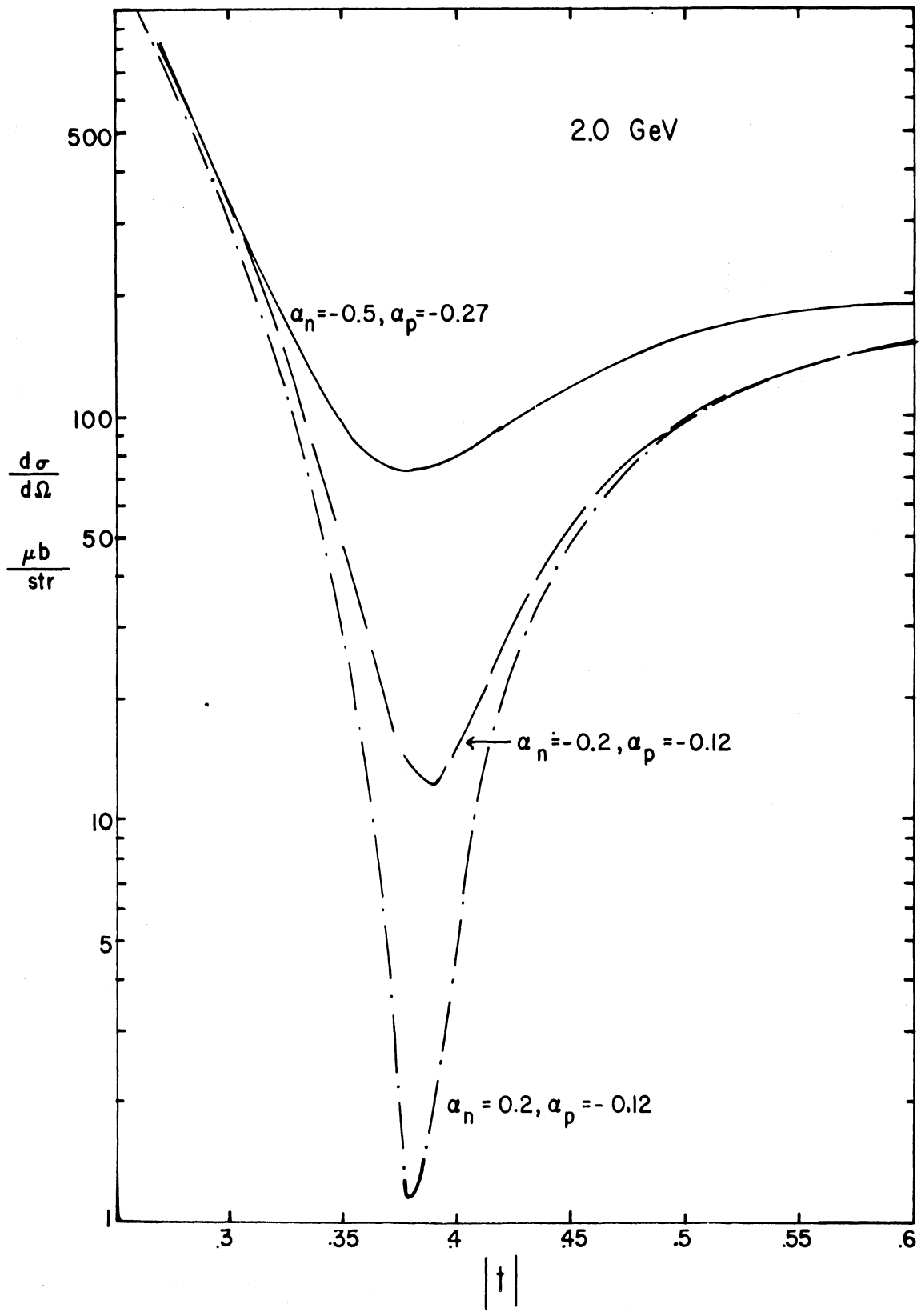

Fig. 19. Effect of the real parts of the nucleon-nucleon scattering amplitudes on the proton-deuteron differential cross section.

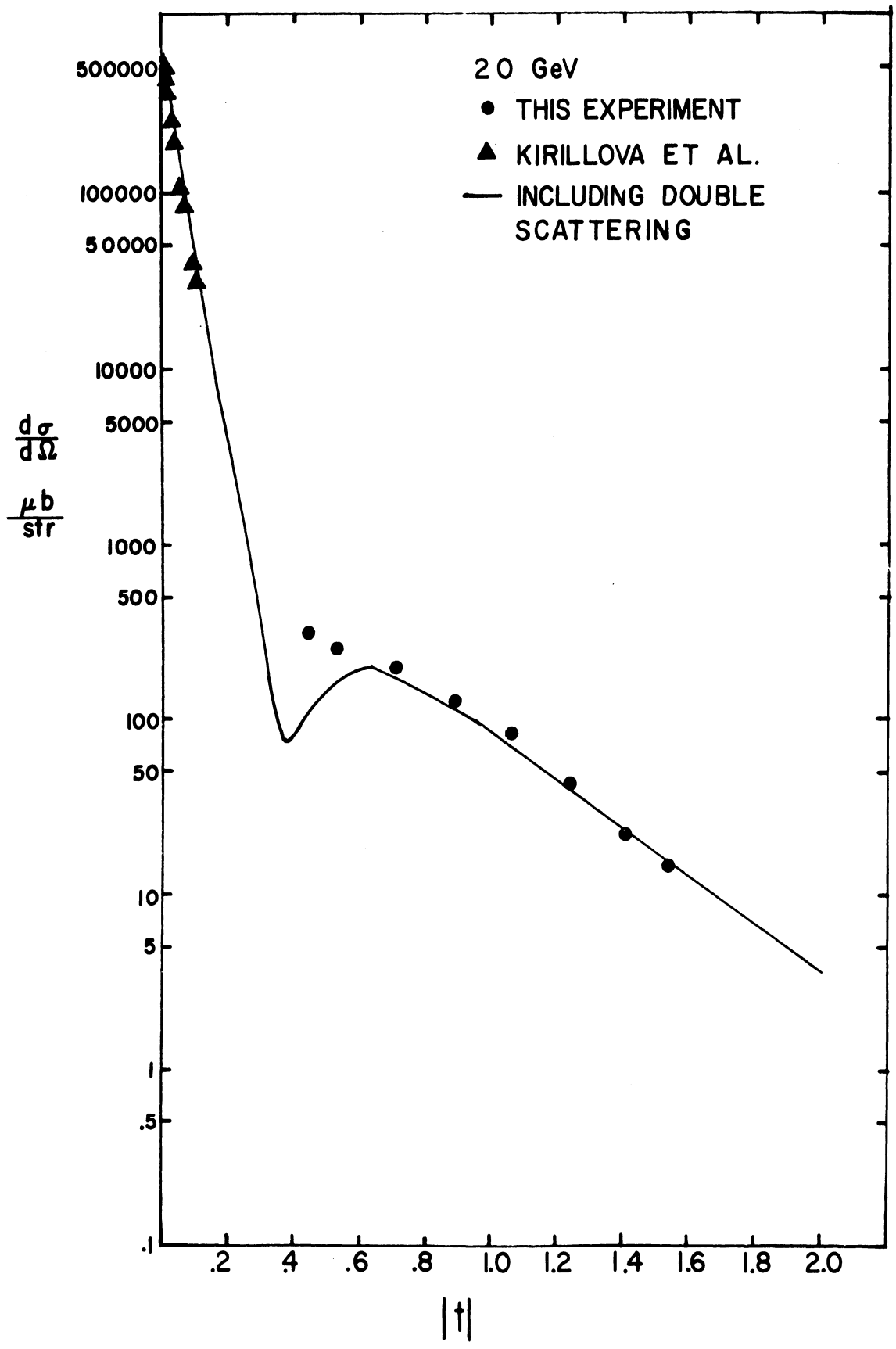

Fig. 20. Theoretical differential cross section in the laboratory system when single- and double-scattering interactions are included.

V. EXPERIMENTAL PROCEDURES

The differential cross sections were measured for backward proton-deuteron elastic scattering at 1.0, 1.3, and 1.5 GeV incident proton kinetic energies and for forward scattering at 2.0 GeV. Protons at the desired energies were obtained from the external beam 2A of the Cosmotron at Brookhaven National Laboratory. The beam was analyzed by a system of three bending magnets and three quadrupoles and focused on a three-inch-long liquid deuterium target. The primary difficulty in determining the differential cross sections at high momentum transfers is that the magnitude of the high momentum transfer portions of the differential cross section is several thousand times smaller than the forward peak. The background from the deuteron breakup processes, which yield many protons available to trigger the counters for each deuteron of elastic scattering processes, is quite large at the energies considered in this experiment. The problem of the immense background was overcome by detecting both of the scattered particles instead of only one as is the case of most proton-deuteron elastic scattering experiments and in addition by performing momentum separation and time-of-flight analysis on one of the scattered particles. By this procedure the chance events were effectively reduced to less than 10% of the desired events.

A. BEAM

The beam was pulsed at 30 pulses per minute yielding 8×10^7 to 1×10^9 protons per pulse for convenient rates of accidentals. The kinetic energy of the protons was determined by two methods. The first method was to measure the frequency, f, and orbital path length, L, of the internal beam. If the proton rest mass equals M, the kinetic energy is known to be

$$T = M\left[\frac{1}{(1 - Lf)^2} - 1\right]$$

where $c = 1$.

The second method consisted in measuring the Cosmotron magnetic field, B, and the radius of the circulating beam, R, which determine the kinetic energy through the relationship

$$T = (M^2 + e^2B^2R^2)^{1/2} - M$$

where e is the proton charge.

Bennett has found the Cosmotron to have an inherent energy spread of 2 MeV.[67] The two deuteron telescopes also provided a check on the beam energy (see Section D). These methods determined the beam energy to within 1%.

B. BEAM OPTICS

The components of the beam optical system are shown in Fig. 21. The currents in the components H200 to H205 were determined by a beam-design computer program to first order. The fine tuning of the magnets were empirically made by exposing Polaroid film simultaneously at the target position and a beam line counter position. The final current values with their energy dependence is given in Table I. The bending magnet H200 served two purposes. The angle at which the beam leaves the Cosmotron ring depends upon the beam energy. H200 allowed one to compensate for the energy dependence of the exit angle by regulating its magnetic field. A collimator was placed in the gap of H200 to provide additional control of the beam spot size. As seen in Table II, the pole faces restricted the spot size vertically to 1-1/2 in. The collimator allowed one to simultaneously satisfy conditions of small spot size and small angular divergence for the beam.

Three quadrupoles focused the beam at the target. Q201 and Q203 focused the beam horizontally while Q202 provided vertical focusing. The currents in these quadrupoles were adjusted to restrict the beam to a maximum angular divergence of 3-1/2 mrad and a maximum spot size of 1-1/2 in. at the target.

The bending magnets H204 and H205 guided the beam along the axis defined by the center of the target and the center of the C counter. Bending magnet H206 (Fig. 22) provided momentum analysis of the scattered deuterons at incident proton kinetic energies of 1.0, 1.3, and 1.5 GeV and of the scattered proton at 2.0 GeV. This magnet will be discussed with greater detail in Section D.

C. LIQUID DEUTERIUM TARGET

The proton beam passed through at .010 in. mylar window to reach the vacuum chamber enclosing the target. The target was connected by a gravity fill line to an overhead reservoir, which maintained liquid deuterium at a temperature of 20.7° $\pm$ 0.2°K. Liquid deuterium at this temperature has a density of .1697 $\pm$ .0002 g/cc. A .010 in. mylar cylinder with mylar domes on the end constituted the target. The cylinder was 3.00 in. in diameter and with the domes had an overall length of 3.00 in. in the median plane. For thermal insulation, the target cylinder was wrapped with 20 layers of .00025 in. NRC Super Insulation (aluminzed mylar) in addition to evacuating the surrounding chamber. The reservoir was wrapped with 120 layers of the NRC insulation. The scattered particles passed through a .014 in. U-shaped window in emerging from the vacuum chamber.

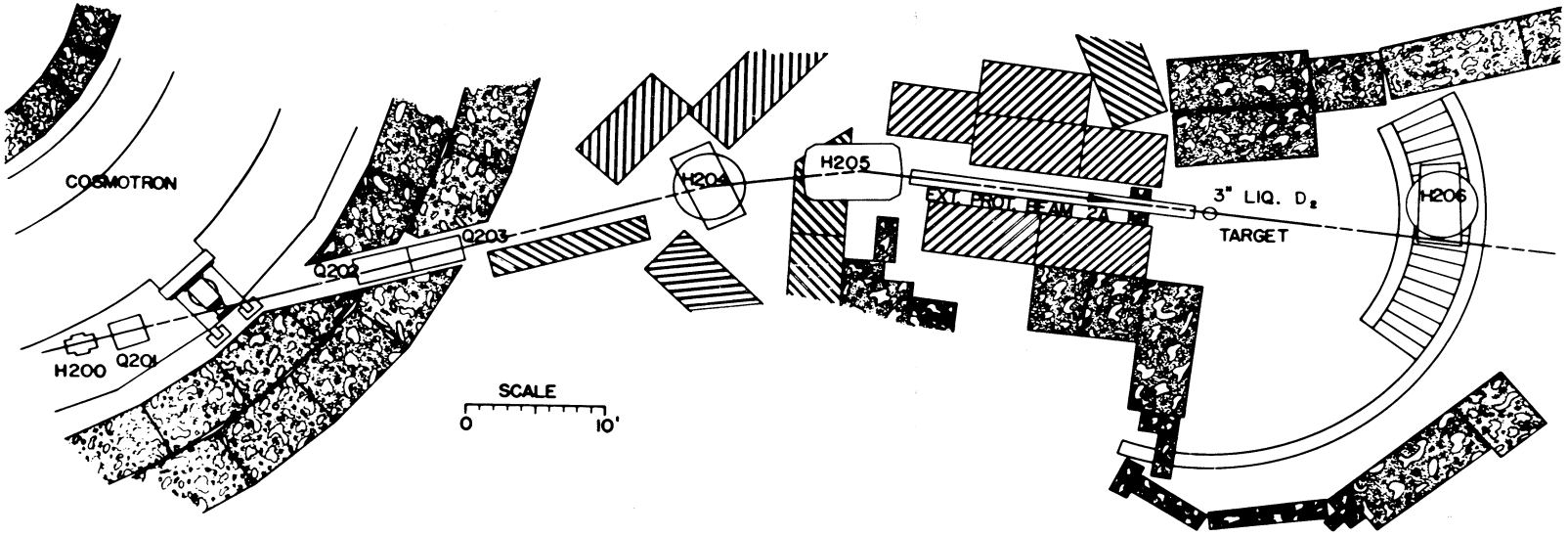

Fig. 21. The beam layout.

TABLE I

MAGNET CURRENTS (AMPS)

Magnet	T_p 1.0 GeV	1.3 GeV	1.5 GeV	2.0 GeV
H200	70	55	50	28
Q201	116	137	146	200
Q202	290	335	365	477
Q203	240	275	300	375
H204	168	235	244	364
H205	745	846	989	1272

TABLE II

MAGNETIC CHARACTERISTICS

Magnet	Size	Max. Current (amps)	Max. Mag. Flux Density (k Gauss)
H200	1.5"x6"x12"	250	11.4
Q201	8"x16"	1000	11.5
Q202	8"x32"	1000	11.5
Q203	18"x32"	1000	11.5
H204	18"x36"	800	22.7
H205	12"x60"	1820	17.6

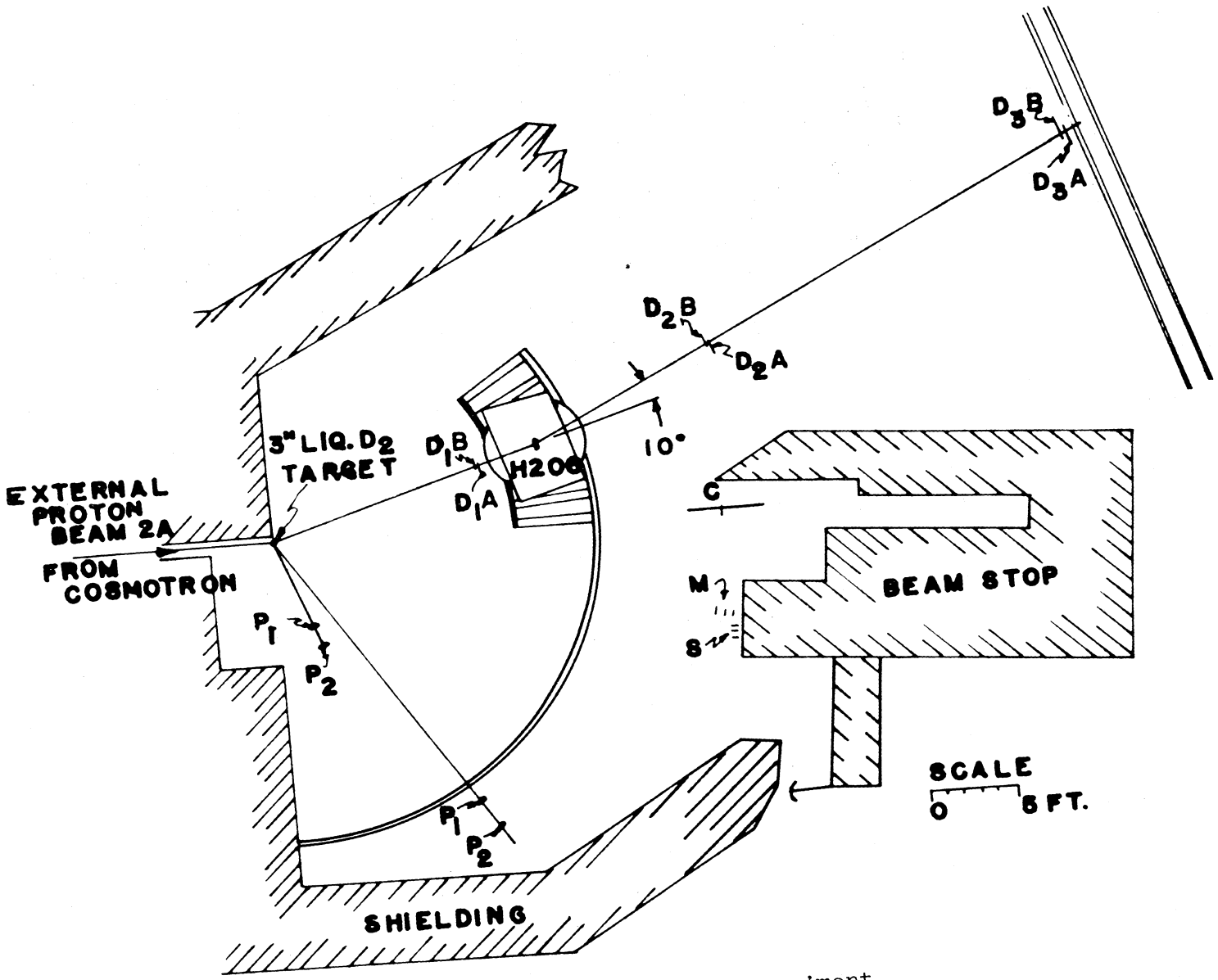

Fig. 22. Plan view of experiment.

D. DETERMINATION OF SCATTERING ANGLES

The kinematical relationships for proton-deuteron elastic scattering were determined by an IBM 7090 computing program to less than .01% uncertainty. The center of the target and the center of the pivot for detection telescopes was determined; then a zero degree beam line was constructed. A theodolite was centered on top of the pivot post to determine the polar angles of both scattered particles. A second theodolite was used to record the height of the center of the target at convenient locations on the shielding walls. These reference points were then utilized to position the centers of the scintillation counters at beam height.

The first counter of the P telescope (Fig. 22) determined the solid angle of acceptance. In backward scattering of the incident proton, the shorter arm determined the polar angle of the scattered proton. The angle between this telescope and the beam line was varied by rotating the I-beam, which was connected to the pivot under the theodolite and rolled on a leveled steel platform. The longer arm determined the polar angle of the scattered deuteron in foward scattering of the incident proton collisions. This arm was varied by rolling the I-beam along a circular rail located 19 ft from the target. The P1 and P2 were aligned along the center of the I-beam using the theodolite mounted over the pivot post. The center of the P1 was set with the theodolite to the polar angle specified by the kinematic tables mentioned above.

The deuteron (proton) in backward (forward) scattering of the incident proton was detected by two overlapping telescopes consisting of three counters each. These counters constituted the D telescopes and were referred to as D1A, D2A, D3A, and D1B, D2B, D3B. The D1 and D2 counters were supported by a motorized carriage, which also supported a bending magnet H206 between them. H206 deflected the particles passing through D1 by $\pm 10°$ to provide momentum separation of the desired elastically scattered particles from quasi-elastic events and reaction products. The 18 in. x 36 in. H206 attained a maximum current of 1000 amps, which was equivalent to a magnetic flux density of 15.3 k gauss with a 10-1/2 in. gap. This was sufficient to separate the desired particle up to 2.4 GeV/c momentum. The relationship between the current in H206 and the cosine of the center-of-mass scattering angle of the incident proton ($\cos \theta^*$) is given in Fig. 23. In addition to H206, the DA and DB channels further increased the momentum resolution by requiring symmetry between the channels. The 40-foot flight path between the D1 and D3 counters provided a time-of-flight criteron which the scattered particle was required to satisfy. The angle of the D1 counters was conveniently adjusted by moving the motorized carriage until the center of the overlapping portion was aligned with the vertical cross hair of the theodolite. The overlap of the D telescopes was determined from multiple Coulomb scattering in the target, and, and any previous counters. The angle, momentum selection, and time-of-flight restriction of the D channel together with the angle of the P channel provided a kinematical check upon the incident beam energy. The angle limitations of the differential cross sections measured in the backward direction were dic-

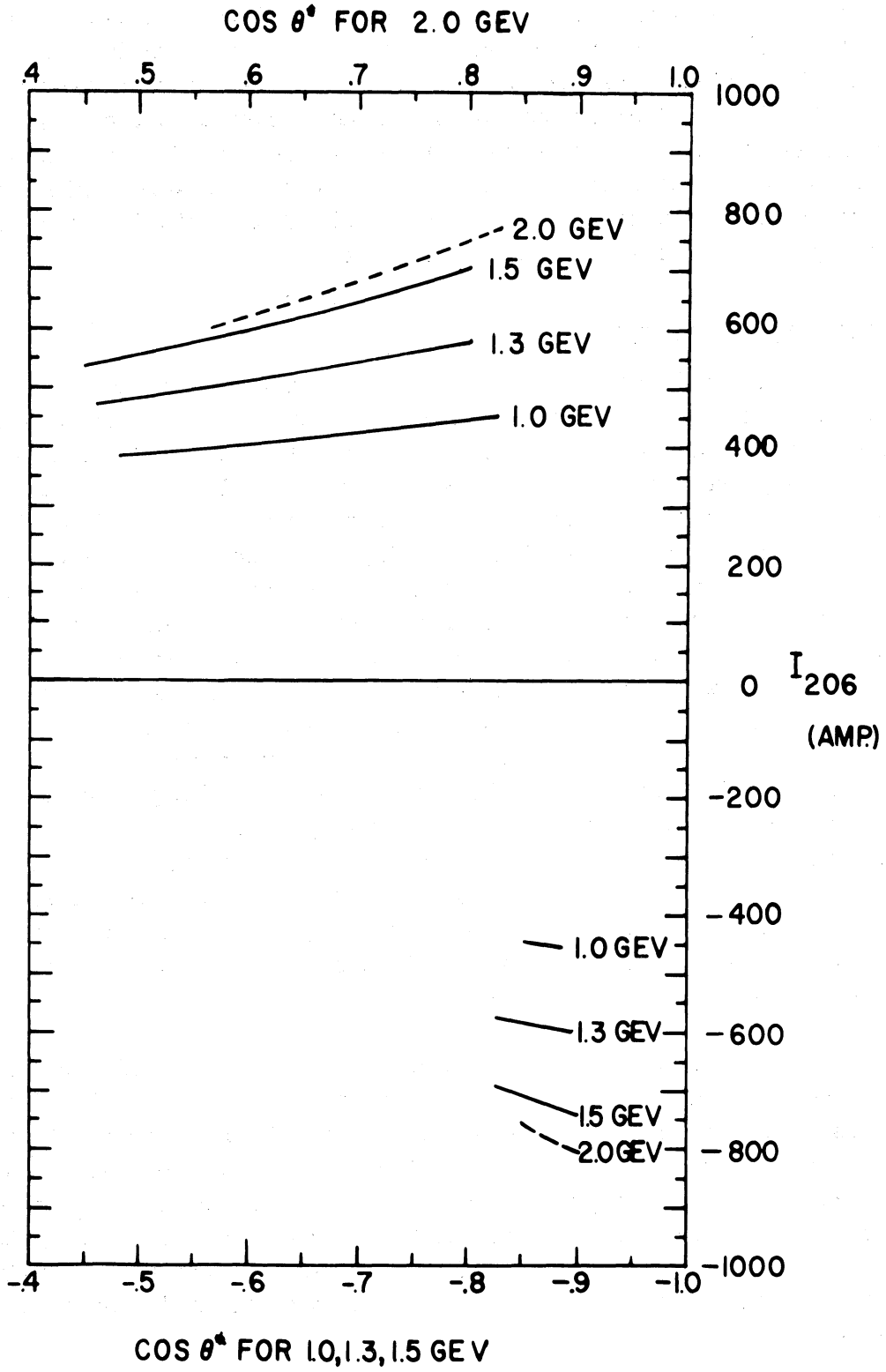

Fig. 23. Current in bending magnet H206 vs. cos θ* at various energies.

tated by the positions of the shielding walls in the experimental area. In the laboratory system, the D1 counter was limited to a maximum angle of 28° from the beam line and the P1 counter was limited to a maximum angle of 122° from the beam line. The forward differential cross section measurements were limited by the requirement that both scattered particles reach the final counters within the 8 ns time resolution (see Section E) and with less than 10% accidental event counting statistics. At very forward angles the energy loss of the recoil deuteron during traversal of the scintillation counters was too great to satisfy the above criteria.

E. DETECTION OF EVENTS

The elastically scattered protons and deuterons were detected by scintillation counters using fast electronic circuitry. The positions of the counters are displayed in Fig. 22. The scintillation material of the counters had a polystyrene base and was commercially available. Except for the M monitor counters, the light from the scintillator was transported to RCA 6810 photomultiplier tubes by Plexiglas light pipes. The scintillator of the M monitor counters was connected directly to the photomultiplier tubes with R-313 epoxy to decrease the small inefficiency introduced by light pipes. The size of the scintillator for each counter in shown in Table III. Each of the counters was checked by a beta source before and after the experiment to ascertain whether the counters remained uniformly sensitive over the area of the scintillator. Several times during the experiment, the counters were thoroughly examined for leaks. The counter supply voltage versus counting rate showed a plateau, and each counter was operated on its plateau, while determining the time delay between incidence of a particle and its output pulse using a light pulser. The D3 counters had a photomultiplier tube on each end of the scintillator to reduce the signal to noise ratio and to decrease the characteristic timing variation caused by particles incident at different portions of the scintillator.

The signature of an event was a coincidence between P1P2 and D1A, D2A, D3A, or between P1P2 and D1B, D2B, D3B or both within 8 ns. Delay cables were inserted bewteen the counters and the coincidence circuits to compensate for the unequal flight times required for the desired particles to reach each counter. The proper lengths of delay cable were determined by considering the time necessary to reach each counter after passing through the successive intervening media. These values were checked by filling the target with liquid hydrogen and measuring a known point in the proton-proton differential cross section.

Standard commercial modules were used for the electronic logic circuitry. A block diagram of the logic circuitry is given in Fig. 24. The details of each block unit are described by Sugarman et al.[68] The duration of a beam pulse (called the beam spill) was typically 200 ms long with very little structure. A gating circuit prevented the recording of events whenever an anomalously large flux density occurred via a trigger pulse from the C counter. Pulses from each channel were split to provide scaler records of

TABLE III

COUNTER DIMENSIONS

Counter	Width x Height x Thickness
P1	3.5" x 5" x 1/8"
	2.5" x 3" x 1/8"
	2.0" x 1" x 1/8"
P2	5" x 7" x 1/2"
	4" x 2" x 1/2"
D1A	5.5" x 8" x 1/2"
D1B	5.5" x 8" x 1/2"
D2A	13" x 19" x 3/8"
D2B	13" x 19" x 3/8"
D3A	17" x 30" x 1/2"
D3B	17" x 30" x 1/2"
C	8" diameter x 1/2"
M1	1" x 1" x 1/4"
M2	1" x 1" x 1/4"
M3	1" x 1" x 1/4"
S	1.5" x 1.5" x 3/8"

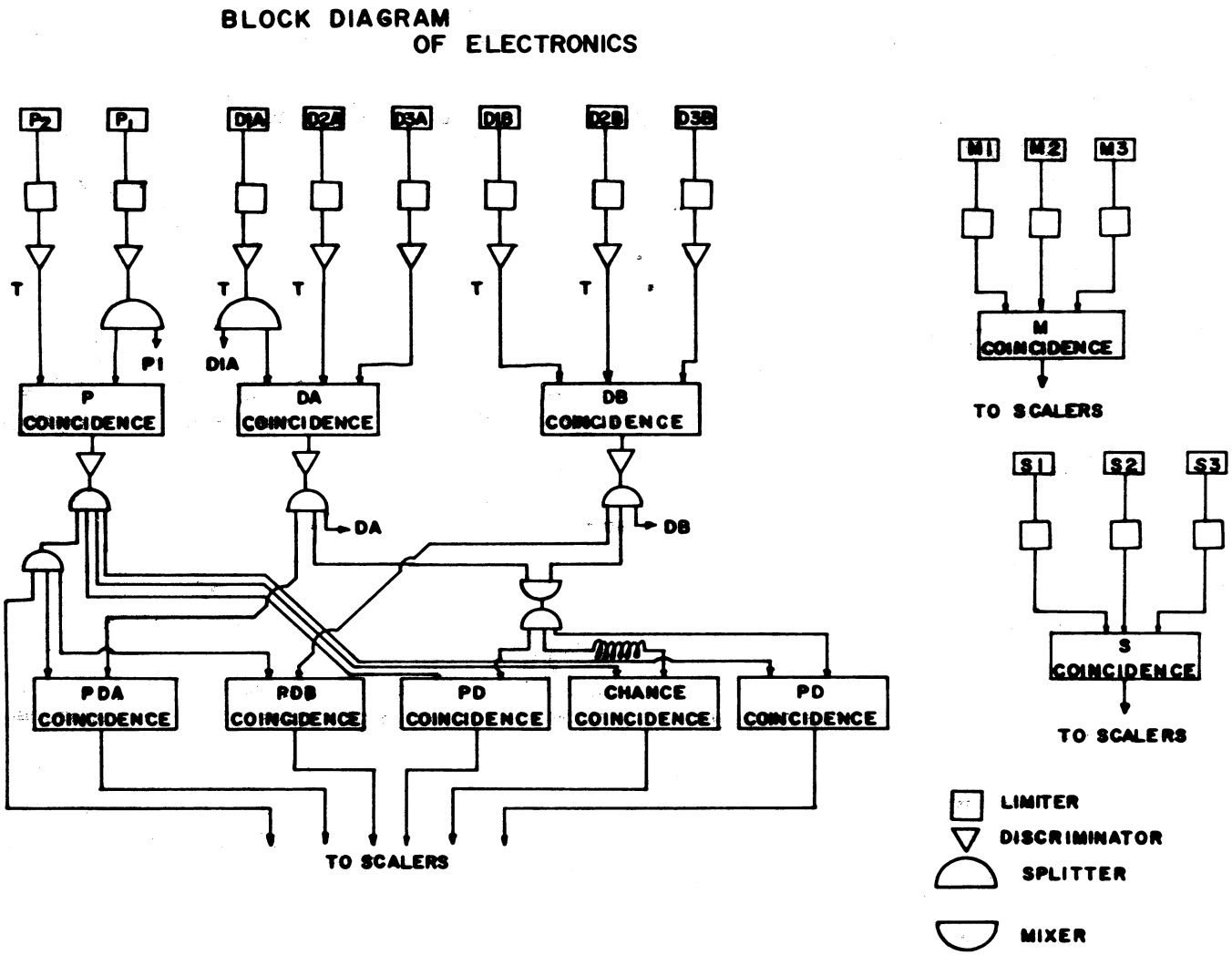

Fig. 24. Electronic logic circuitry. Variable delay cables inserted at positions marked by T.

the P channel, the D channels and their combinations. Accidentals were continuously monitored by delaying a portion of the pulse from the D channels by 50 ns with respect to the desired time for a real event. The clipping lines were selected to give a time resolution of 8 ns for an elastic event. This was slightly larger than the time spread expected due to straggling of the particles before reaching the final counters. The chance coincidence were held to less than 10% of the actual events by regulating the beam intensity. Two scalers were used to record the events to provide evidence of any malfunction within the scalers.

The measurement of a single point in the differential cross section proceeded in the following manner. The P telescope and the H206 magnet carriage supporting the D1 and D2 counters were positioned using the theodolite. The D3 counters were positioned at the desired place on the parallel I-beams. During this time, the target was being filled with liquid deuterium. The delay cables were selected and connected for this kinematical setting. The target was then bombarded until the desired number of events were recorded and printed out from the scalers. The reading of the M monitor scaler depended upon the contents of the target. The reading of the S scaler had a negligible dependence on the target contents because less than 2% of the beam interacted with the target and the S telescope monitored the beam particles scattered by the C counter in the beam line. The target was emptied, and the target was again bombarded until the S scaler indicated that an equal number of protons had passed through the target. The procedure was then repeated for the next point. Several times during the measurement of the differential cross section at a given energy, polyethylene foils were irradiated for normalization purposes.

VI. NORMALIZATION OF CROSS SECTIONS

The M and S telescope were employed to normalize the differential cross sections. The half life of C^{11}, 20.5 minutes, makes the reaction C^{12} (p,pn) C^{11} convenient to study with this apparatus. A beam of 1-5 x 10^9 particles per pulse irradiated a 4 mil polyethylene foil mounted on the downstream end of the target. The decay rate of the C^{11} atom was then measured in a NaI well-counter by detecting the gamma rays produced by pair annihilation of the emitted positron. The rate of producing C^{11} atom in the foil may be expressed by

$$\frac{dN_{11}}{dt} = \frac{\sigma\varphi N\rho}{M}$$

where σ = cross section for C^{11} formation, φ = flux of protons/sec. through foil, N = Avogadro's number, ρ = density of foil in g/cm^2, M = molecular weight of polyethylene $(CH_2)_n$, N_{11} = number of C^{11} atoms.

These C^{11} atoms are lost in two principal ways during irradiation of the foil. Some of the molecules containing C^{11} are scattered out of the foil. This process is termed "hot atom" loss, and has been measured by Cumming et al.[69] The fraction of C^{11} atoms scattered from the foil, a, reduces the rate of producing C^{11} atoms in the foil to

$$\frac{dN_{11}}{dt} = (1 - a)\frac{\sigma\varphi N\rho}{M}$$

According to Cumming et al.,[75] a 4 mil foil has a value of a = .142.

During irradiation some of the C^{11} atoms are lost by decaying. The radioactive decay law gives this as

$$\frac{dN_{11}}{dt} = - KN_{11}(t)$$

where K is the decay constant. Hence the rate of C^{11} accumulation in the foil is

$$\frac{dN_{11}}{dt} = (1 - a)\frac{\sigma\varphi N\rho}{M} - KN_{11}$$

with the boundary condition that $N_{11} = 0$ at $t = 0$; the equation is easily solved to yield,

$$N_{11} = (1 - a) \frac{\sigma\varphi N\rho}{M} (1 - e^{-Kt}) \qquad (1)$$

The foils were irradiated for 1-minute, 2-minute, and 3-minute periods. Let the irradiation period be called t_1. After termination of irradiation, the number of C^{11} atoms in the foil is

$$N_{11} = N_{11}(t_1)\, e^{-K(t - t_1)}$$

where $t > t_1$.

The number of C^{11} decays, D, were counted with the NaI well-counter in one minute intervals. Denoting the initial time of an interval by t_i and the termination by t_f, the number of decays may be expressed by

$$D = -\int_{t_i}^{t_f} KN(t)E\, dt = N_{11}(t_1)\, e^{Kt_1} E(e^{-Kt_i} - e^{-Kt_f}) \qquad (2)$$

where E is the efficiency of the well counter. The total flux, F, is the quantity desired. The $N_{11}(t_1)$ is given in Equation (1) by setting $t = t_1$. Thus substituting into Equation (2) with $\varphi = F/t$, one obtains

$$D = \frac{E(1 - a)\sigma N\rho}{KMt_1} F\, e^{Kt_1}(1 - e^{-Kt_1})(e^{-Kt_i} - e^{-Kt_f})$$

or

$$F = \frac{KMt_1 D\, e^{-Kt_1}}{E(1 - a)\sigma N\rho(1 - e^{-Kt_1})(e^{-Kt_i} - e^{-Kt_f})}$$

The total cross section of the reaction $C^{12}(p,pn)C^{11}$, σ, has been measured at several energies. In Table IV the values of σ are tabulated from 1 to 28 GeV incident protons. The values in our energy range were interpolated from the data of Poskanzer *et al.* and Cumming *et al.* Since the half life of C^{11} is known, the decay constant, K, equals 0.564×10^{-3} sec^{-1}.

The monitor counters were calibrated by using F/M and F/S as standard radios for target full and target empty runs respectively, where M is the number of coincidences in the M monitor and S is the number of coincidences in the S monitor during irradiation of the foil by F protons. The statistical error in D and the error in determination of well-counter efficiency made the value of F uncertain by $\pm$ 8%. Three or more foils were irradiated for each energy, and the normalizations always agreed within 4%.

TABLE IV

CROSS SECTION FOR $C^{12}(p,pn)C^{11}$

T_p	σ(mb)	Reference
1.0	26.6 ± 1.3	70
2.0	26.2 ± 0.9	71
3.0	26.8 ± 1.0	71
3.0	29.5 ± 1.6	72
4.5	27.4 ± 1.4	72
6.0	29.5 ± 1.6	72
9.0	26.2 ± 1.5	73
28.0	25.9 ± 1.2	74

VII. DATA CORRECTIONS

A. NUCLEAR ABSORPTION

While traversing the target, counters and air, a small percentage of the scattered protons and deuterons were lost due to nuclear interactions. The fraction of particles lost during passage through a single medium may be calculated from

$$\frac{S_1}{S_o} = \frac{1}{\ell_1}\int_{o}^{\ell_1} e^{-\mu x}\, dx \quad , \mu = \frac{\sigma N \rho}{M}$$

where S_o = number of incident particles,

S_1 = number of surviving particles, ℓ_1 = path length in medium

N = Avogadro's number, ρ = density of medium

M = molecular weight, σ = total cross section

Losses for a series of F media may then be expressed by

$$\frac{S_f}{S_o} = \frac{1}{\ell_1 \ell_2 \ldots \ell_f} \int_{o}^{\ell_f} \ldots \int_{o}^{\ell_1} e^{-\mu_f x_f} \ldots e^{-\mu_1 x_1}\, dx_1 \ldots dx_f$$

The integrals may easily be performed to yield

$$\frac{S_f}{S_o} = - \prod_{i=i}^{f} \left(\frac{1 - e^{-\mu_i \ell_i}}{\mu_i \ell_i} \right)$$

A recorded event is characterized by both the scattered proton and its corresponding deuteron completely traversing their respective telescopes. The probability of proton surviving nuclear interaction is stochastically independent of the probability that a deuteron survives. The probability of two stochastically independent processes occurring equals the product of their individual probabilities. Therefore the probability of both scattered particles surviving nuclear interaction, P, equals

$$P = \prod_{k=1}^{f}\left(\frac{1 - e^{-\mu_k \ell_k}}{\mu_k \ell_k}\right) \qquad \prod_{j=1}^{m}\left(\frac{1 - e^{-\mu_j \ell_j}}{\mu_j \ell_j}\right)$$

The μ_k and μ_j in the above formula must be determined. The values for N, ρ and M may be found in standard tables. A first approximation to the total cross sections, σ, would be the geometrical cross section. A geometrical consideration only yields $\sigma = \pi (r_o A^{1/3})^2$ where A equals the mass number and r_o is the Bohr radius.

In the energy range investigated here, the deBroglie wavelength is sufficiently small to allow one to consider the nuclear scattering as occurring between the incident proton or deuteron and individual nucleons of the nucleus. The cross sections for proton-nucleon and deuteron-nucleon collisions are known over the desired range.[76] The energy dependence of the cross sections has been taken into account although the percentage of particles surviving changes only as much as 0.5% for the P-telescope and 2% for D-telescope in the energy range considered. The cross sections on materials with $A > 1$ can then be approximated by $\sigma_{DA} = \sigma_{DN} A^{2/3}$ for deuterons and $\sigma_{PN} A^{2/3}$ for protons. The resulting formulae for μ_k and μ_j are thus

$$\mu_k = \frac{N\rho_k}{M_k} \sigma_{pN} A_k^{2/3} \qquad \text{for deuterons}$$

and

$$\mu_j = \frac{N\rho_j}{M_j} \sigma_{pN} A_j^{2/3} \qquad \text{for protons.}$$

The effect of nuclear absorption was tested by placing a slab of lucite .25 in. thick before the P1 counter. The differential cross section at several points was measured with and without the lucite slab and no statistically significant difference was observed. Using the above formula, the percentage of protons surviving nuclear absorption without the slab was shown to be greater than the survival with the slab by magnitudes varying from .30% to .50% which was well below our counting statistical error.

B. COUNTER EFFICIENCY AND DEAD TIME

The P1, P2, and D1 counters were essentially 100% efficient. However the larger size of the D2 and D3 counters introduced a slight inefficiency. The two photomultiplier tubes on the D3 counters served to reduce the inefficiencies of these counters significantly. Although the efficiencies of the D2 and D3 counters were not measured directly, they have been estimated to be 99% $\pm$ 1% efficient.

The counter dead time is the time between the incidence of a particle in

the scintillator and the time that the subsequent electronics has recovered sufficiently to record the incidence of another particle on the scintillator of the counter. The dead time in a given pulse depends upon the length of the beam spill, the number of particles incident per pulse, and the time resolution of the electronic logic. In this experiment, the beam spill was typically 150 ms, and the singles rate on a given counter was usually less than 8×10^4 counts per pulse. Since the time resolution of the logic circuitry was 8 ns, the counter dead time was less than 1%. If one considers the nonuniform structure of the beam spill, more of the true coincidences may be lost because the losses increase in proportion to the counting rate. The singles counting rates of each counter were not monitored continuously because they changed with each pulse. Consequently the correction for anomalies in the beam spill are only approximated. The uncertainties in the counter dead time have been included in the systematic error corrections to the data.

C. BEAM ATTENUATION

The number of protons in the beam is not constant because many of the protons interact while transversing the target. Since the downstream end of the target is exposed to only a fraction of the initial beam intensity, N, the total target is exposed to an effective beam intensity N_e. The initial and effective beam intensities are related by

$$N_e = \frac{N}{L}\int_0^L e^{-\rho\sigma x}\, dx$$

where L equals the target length, ρ equals the density of deuterons in liquid deuterium, and σ equals the total proton-deuteron cross section. The point $x = 0$ corresponds to the upstream end of the target. The effective beam intensity was 0.6% less than the initial beam intensity.

D. ANGULAR UNCERTAINTY

The finite width of the P1 counter, w, and the length of the target, L, introduce an error in the polar angle, θ. The particles from the target entering the P1 counter may have angles as large as $\theta + \Delta\theta_p$ or as small as $\theta - \Delta\theta_n$ where

$$\Delta\theta_p = \tan^{-1}\left[\frac{w + L \sin\theta}{2r - L\cos\theta}\right]$$

$$\Delta\theta_n = \tan^{-1}\left[\frac{w + L \sin\theta}{2r + L\cos\theta}\right]$$

with r equal to the distance between the counter and the target.

Transforming the $\Delta\theta_p$ and $\Delta\theta_n$ into the center-of-mass frame, one obtains the expression

$$\Delta\theta^*_{p,n} = \frac{\left[2\gamma \ \frac{1}{\gamma^2} \ \tan^2\frac{\theta}{2} + 1\right]}{\tan^2\frac{\theta}{2} + 1} \qquad (\Delta\theta_{p,n})$$

using $\Delta\theta^*_{p,n} = \frac{\partial\theta^*}{\partial\theta} \quad (\Delta\theta_{p,n})$

The values of cos θ^*, θ^*, $\Delta\theta^*_p$, and $\Delta\theta^*_n$ are given in Table V for the various angles and counter distances used in this experiment.

E. MULTIPLE COULOMB SCATTERING

The sizes of the counters were designed to eliminate loss of events due to multiple Coulomb scattering. This requirement was checked during the experimental run by substituting a smaller P1 counter for the original P1 defining counter at given points. No significant difference was measured between using the designed subtended solid angle and the smaller solid angle, which would confine the corresponding particles in the D-channel to a smaller portion of the D counters and thus minimize the losses. This technique could not be applied to determine the Coulomb scattering losses sustained by the P1 counter itself. To a first approximation the number of particles scattered out of the line of coincidence with the P telescope is equal to those scattered into the telescope. Due to the energy of the particles and the distances involved, less than 1% of the coincidences are estimated to have been lost through multiple Coulomb scattering.

F. ACCIDENTAL AND BACKGROUND COINCIDENCES

Independent particles in the deuteron and proton channels may produce pulses which would be recorded as an event if they occurred within a short time interval. These chance coincidences were continuously monitored by recording the coincidences between the P and D channels when they were 50 ns out of time. The length of this delay cable was varied over a range of 30ns with no appreciable difference in the percentage of accidentals for a given run. The percentage of chance events was always kept below 10% by adjusting the beam intensity. In determining the number of good events, the number of chance events was subtracted which resulted in a larger statistical error to compensate for the presence of undesireable coincidences.

For each point of the differential cross sections, the measurement was made for a full target and an empty target. The S monitor counters provided

TABLE V

UNCERTAINTY IN SCATTERING ANGLES

Cos θ^*	$\theta^{*\circ}$	$\Delta\theta_p^{*\circ}$	$\Delta\theta_n^{*\circ}$
T_p=1.0 GeV			
-.885	152.25	3.03	3.07
-.875	151.04	3.07	3.11
-.850	148.21	3.33	3.37
-.825	145.59	3.61	3.65
-.800	143.13	4.20	4.24
-.750	138.59	4.31	4.34
-.700	134.43	3.84	3.85
-.650	130.54	3.66	3.66
-.600	126.87	3.69	3.69
-.550	123.37	3.34	3.32
-.500	120.00	3.15	3.13
T_p=2.0 GeV			
.565	55.60	1.41	1.39
.600	53.13	1.40	1.38
.650	49.46	1.37	1.36
.700	45.57	1.35	1.33
.750	41.41	1.32	1.31
.800	36.87	1.29	1.28
.825	24.41	1.28	1.26
.850	31.79	1.26	1.24
.875	28.95	1.24	1.22

TABLE V. CONT'D

Cos θ*	θ*°	$\Delta\theta^{*\circ}_p$	$\Delta\theta^{*\circ}_n$
T_p=1.3 GeV			
-.895	153.51	3.16	3.21
-.875	151.04	3.45	3.50
-.850	148.21	3.79	3.84
-.825	145.59	4.15	4.19
-.800	143.13	4.54	4.59
-.750	138.59	4.34	4.36
-.700	134.43	4.13	4.14
-.650	130.54	3.92	3.92
-.600	126.87	3.73	3.72
-.550	123.37	3.37	3.35
-.500	120.00	3.38	3.36
-.460	117.39	3.18	3.16
T_p=1.5 GeV			
-.900	154.16	3.14	3.19
-.875	151.04	3.46	3.51
-.850	148.21	3.56	3.60
-.825	145.59	3.89	3.93
-.800	143.13	4.24	4.28
-.750	138.59	4.36	4.38
-.700	134.43	4.16	4.16
-.650	130.54	3.95	3.95
-.600	126.87	3.75	3.74
-.550	123.37	3.39	3.38
-.500	120.00	3.20	3.18
-.450	116.74	3.21	3.18

the means to determine when the amount of incident beam for the empty target equalled that for the full target. The average percentage of recorded target empty events to target full events for all runs was 1.3%. Of these target empty events, a .1% contribution was made by the residual deuterium vapor present in the target when the liquid deuterium was removed. The full target does not contain the vapor, consequently this contribution was not subtracted from the true coincidences. The resultant 1.2% background were caused primarily by interaction with the carbon atoms of the mylar surrounding the target. The number of events for each point of the differential cross section was corrected for background events by subtracting 1.2% as quasi-coincidences to yield a net corrected number of PD coincidences.

VIII. RESULTS OF EXPERIMENT

The differential cross section at a given angle was calculated by the formula

$$\frac{d\sigma}{d\Omega} = \frac{Y}{\rho L \frac{F}{M} MJ(\Delta\Omega)} \quad abcdgh$$

where $Y = (E - E_a)_{\text{full tgt.}} - (E - E_a)_{\text{empty}}$

E = number of events

E_a = number of accidental events

ρ = density of liquid deuterium in deuterons/cc.

L = length of deuterium target

$\frac{F}{M}$ = normalization factor for M monitor

M = number of coincidences in M monitor

J = Jacobian transforming solid angle from laboratory to c.m. system

$\Delta\Omega$ = solid angle subtended by P1 counter

a = correction for nuclear absorption

b = correction for counter efficiency

c = correction for counter dead time

d = correction for multiple Coulomb scattering

g = correction for beam attenuation

h = correction for background events

The results are shown in Tables VI and VII and Figs. 25-26. The error bars are those due to counting statistics and range from 3% to 10%. The total error from nonstatistical sources is 10% of which 8% is due to normalization error and 2% is due to the error in the Jacobian introduced by the uncertainty in beam energy.

TABLE VI

BACKWARD PROTON-DEUTERON ELASTIC SCATTERING

$d\sigma/d\Omega$ c.m. $\mu b/ster$

Cos θ^*	1.0 GeV	1.3 GeV	1.5 GeV
-.900			2.05 ± .21
-.895		4.50 ± .33	
-.885	12.99 ± .42		
-.875	10.93 ± .36	4.07 ± .35	1.73 ± .17
-.850	8.80 ± .29	3.47 ± .26	1.06 ± .12
-.825	7.99 ± .26	3.39 ± .23	
-.800	6.82 ± .22	2.22 ± .11	0.76 ± .08
-.750	4.52 ± .15	1.49 ± .15	0.63 ± .06
-.700	3.30 ± .11	1.08 ± .11	0.49 ± .04
-.650	2.84 ± .09	1.00 ± .10	0.30 ± .03
-.600	2.70 ± .12	0.80 ± .08	0.34 ± .03
-.550	2.15 ± .13	0.56 ± .06	0.29 ± .03
-.500	1.99 ± .09	0.66 ± .06	0.29 ± .03
-.460		0.50 ± .05	

TABLE VII

FORWARD PROTON-DEUTERON ELASTIC SCATTERING

Cos θ^*	-t	$\frac{d\sigma}{d\Omega}$ c.m. at 2.0 GeV
.875	.4422	78.09 ± 2.52
.850	.5306	64.65 ± 1.94
.800	.7075	51.55 ± 1.55
.750	.8843	36.42 ± 1.09
.700	1.0612	22.79 ± 0.68
.650	1.2381	12.18 ± 0.37
.600	1.4149	7.11 ± 0.21
.565	1.5387	4.97 ± 0.15

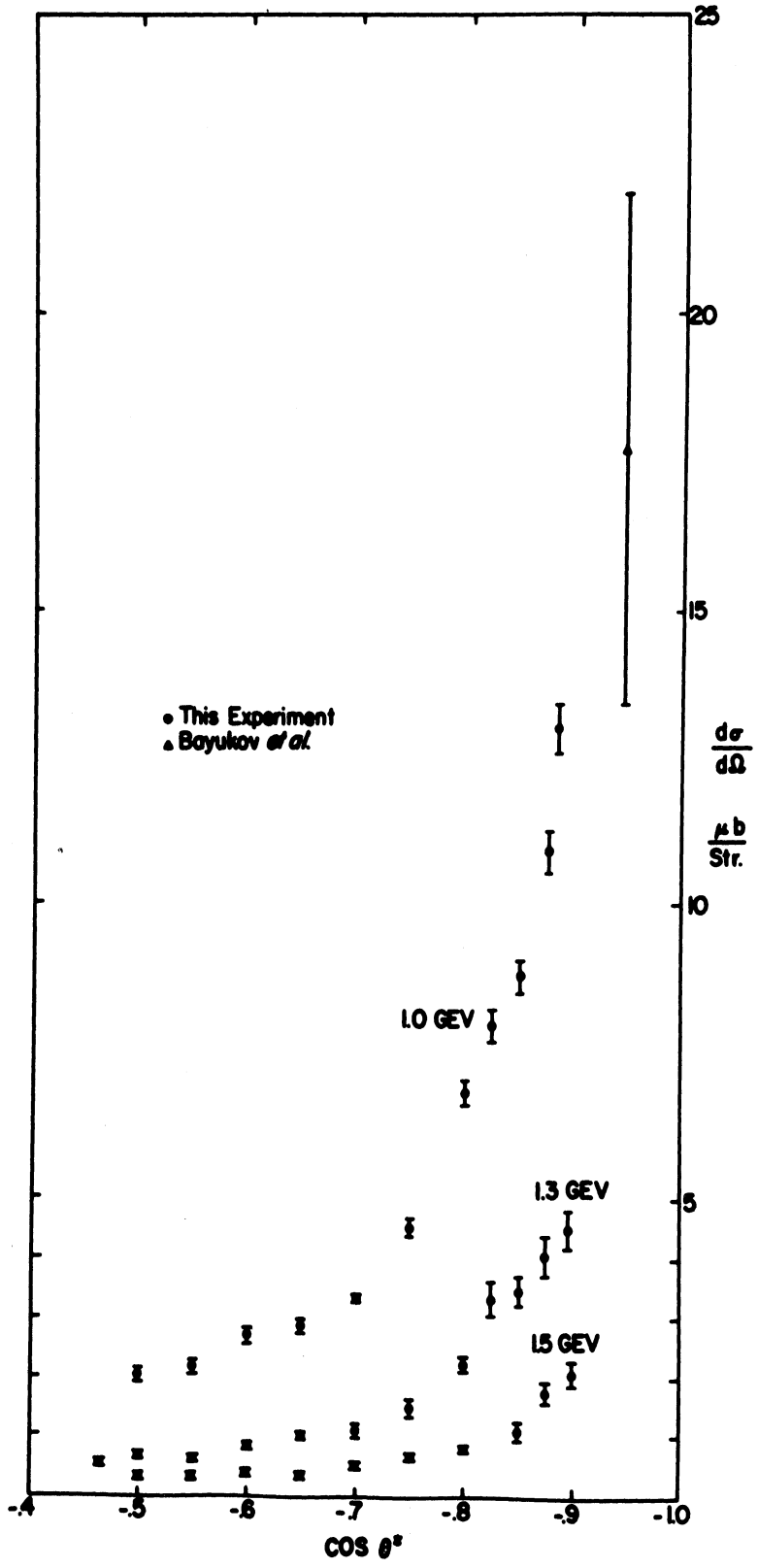

Fig. 25. Experimental differential cross sections at 1.0, 1.3, and 1.5 GeV in the center-of-mass system.

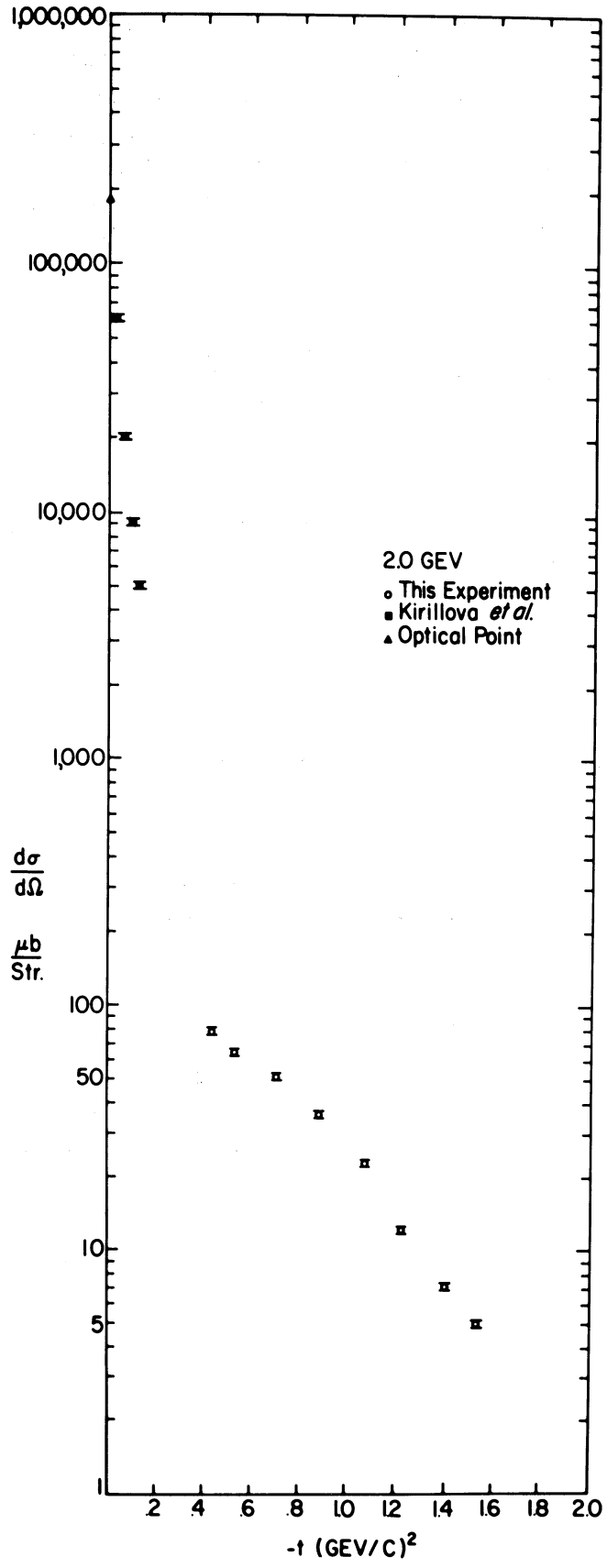

Fig. 26. Experimental differential cross sections at 2.0 GeV in the center-of-mass system.

The curve in Fig. 25 appear approximately exponential in character. In low four momentum work many found it convenient to express differential cross sections as exponentials in four momentum transfer. In Fig. 27 the backward differential cross sections have been plotted as an exponential to a polynomial in τ, where τ equals the four-momentum transfer minus the four-momentum transfer at 180°. A chi-square test of the powers of tau up to the fourth power specified a quadratic as the best fit. The differential cross sections were then written as

$$\frac{d\sigma}{d\tau} = e^{(a + b\tau + c\tau^2)} \quad \frac{\mu b}{(GeV/c)^2}$$

where the values of a, b, and c were determined by a least square procedure and are displayed in Table VIII.

TABLE VIII

COEFFICIENTS IN EXPONENTIAL FIT

T_p (GeV)	a	b $(GeV/c)^{-2}$	c $(GeV/c)^{-4}$
1.0	-4.97	6.48	-3.54
1.3	-3.58	4.47	-1.49
1.5	-2.66	4.68	-1.82

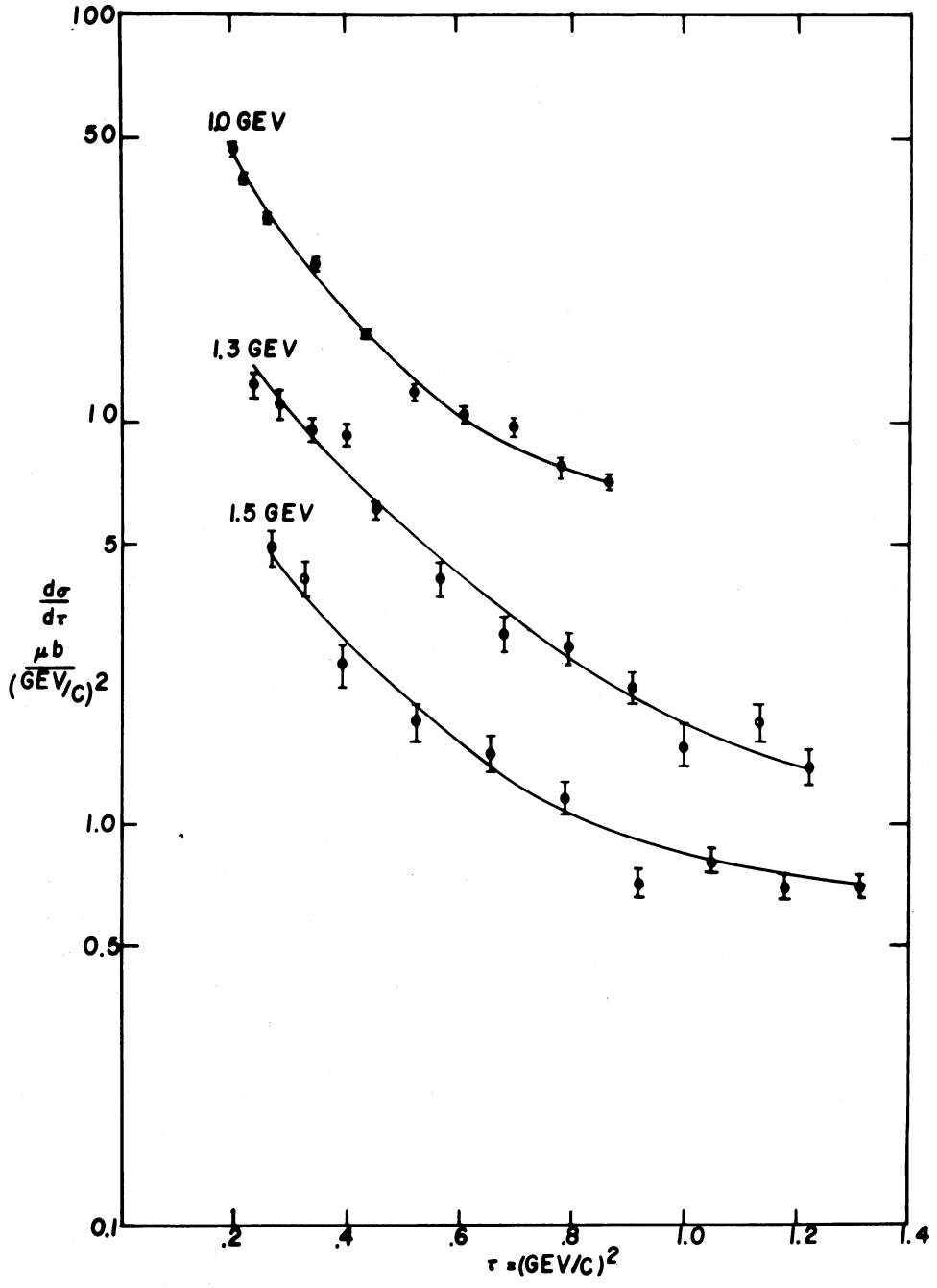

Fig. 27. Exponential fit to cross sections at 1.0, 1.3, and 1.5 GeV.

IX. CONCLUSIONS

The data of this experiment agreed well with the point of the differential cross section obtained by Bayukov et al.[14] at 1.0 GeV. At present, there are no other published data in the few GeV range with which to compare the backward proton-deuteron elastic differential cross sections obtained in this experiment. The 2.0 GeV small angle data of Kirillova et al.[15] described a strict exponential trend for four-momentum transfers below 0.13 $(GeV/c)^2$. The experiment observed a shoulderlike departure of the forward differential cross section from the original slope of the diffraction peak as the four-momentum increased above 0.44 $(GeV/c)^2$.

The backward scattering of protons by deuterons has received reasonable interpretation by assuming that one-neutron exchange is the dominant process. The slope of the observed backward peak was predicted by the one-nucleon Feynman diagram using the proton-neutron-deuteron vertex function of Blankenbecler, Goldberger, and Halpern,[16] but the predicted magnitude exceeded that of the observed peak by a factor of 5.00 at 1.0 GeV incident proton kinetic energy. The use of various form factors reduced the magnitude considerably and also adversely affected the shape of the cross section. The form factors were the Fourier transforms of the deuteron wave function in coordinate space, and their original purpose was to obtain an accurate representation of the high momentum components of the deuteron. The form factors suggested by the regular Hulthén wave function, the Hulthén wave function with a hard core and the Moravcsik analytic fit to the Gartenhaus wave function were presented in this work, and each of the form factors was shown to decrease the agreement of the theoretical differential cross section with the experimental data. Apparently, the high momentum components of the deuteron are somewhat larger than previously suspected. A consideration of absorption in the initial and final state interactions may lead to a modest reduction of the theoretical magnitude and to a possible change in the shape. However, due to the lack of proton-deuteron phase shift data in this energy range, the usual methods of computing the absorption cannot be applied. Calculation of the phase shifts from the scant forward data was considered, but the application of the resulting absorption factors to a partial wave expansion of the backward scattering amplitudes could not be justified. Ross and Shaw[77] have pointed out that the suppression of the differential cross sections due to absorption may differ greatly in the forward and backward directions.

The backward differential cross sections were also analyzed within the framework of three-body formalisms. The problem was formulated in the method of Amado,[39] and the zeroth iteration (the one-nucleon exchange diagram) was found to exhibit the closest agreement with the available data. Since this method utilized the low energy parameters of the effective range theory, a nonrelativistic propagator was used. The difference in the predicted dif-

ferential cross sections between using a relativistic propagator and a non-relativistic propagator is shown in Fig. 28. The relativistic propagator predicts a slightly steeper slope, which more closely fits the experimental data. The predictions of the three-body method may be improved by solving a completely relativistic set of Faddeev equations.

The shoulderlike departure of the data in this experiment at 2.0 GeV from the forward diffraction peak has been interpreted by extending the high energy approximation of Franco and Glauber[66] to higher momentum transfers. Consideration of single-scattering only does not given a satisfactory interpretation of the data above four-momentum transfers of 0.5 $(GeV/c)^2$; however, inclusion of double-scattering interactions is observed to account for the change in slope of the differential cross section. The magnitude and slope of the experimental data for four-momentum transfers above 0.5 $(GeV/c)^2$ are determined quite accurately as manifestitations of the incident proton being successively scattered by both constituents of the deuteron. Due to interference between single- and double-scattering, a dip occurred in the predicted differential cross section which has no apparent justification in the experimental data. The depth of the dip has been shown to be sensitive to the sign and magnitude of the real parts of the scattering amplitudes. The large uncertainty of the ratio of the real part of the proton-neutron scattering amplitude to the imaginary part of the scattering amplitude, $\alpha_n = 0.2 \pm 0.4$, determined by Kirillova et al.[15] and the predictions of the high energy approximation allow one to assert that α_n is negative as is the case for proton-proton elastic scattering at 2.0 GeV.

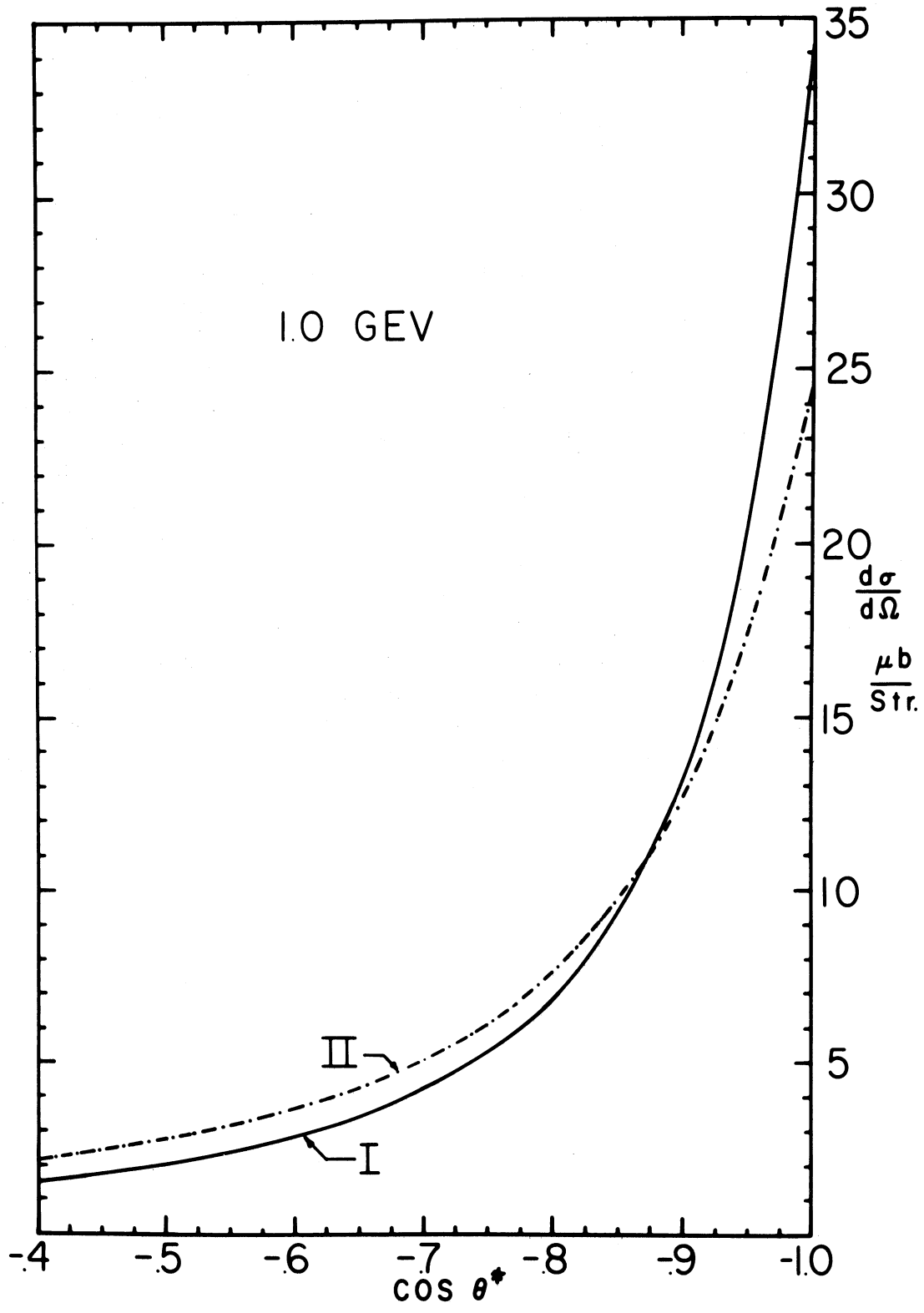

Fig. 28. The effects of relativistic and nonrelativistic propagators at 1.0 GeV. (I) Using relativistic propagator; (II) using nonrelativistic propagator.

APPENDIX A

EVALUATION OF MATRIX ELEMENT

The square of the matrix element with sums over the proton and deuteron spins is evaluated. In Chapter II, the matrix element was expressed by

$$M = u(p_1)^T \bar{\Gamma}_2 \frac{1}{i\not{n} + m + i\epsilon} \Gamma_1 \bar{u}(p_2)^T$$

Then

$$|M^2| = M^\dagger M = \frac{1}{(n^2 + m^2)^2} \left[\bar{u}(p_2)^T\right]^\dagger \Gamma_1^\dagger (-i\not{n} + m)^\dagger \Gamma_2 \left[u(p_1)^T\right]^\dagger$$

$$u(p_1)^T \Gamma_2 (-i\not{n} + m) \Gamma_1 u(p_2)^T$$

The expressions for Γ_1 and Γ_2 are given in Chapter II. Using the identity

$$\sum_{\substack{\text{prot.}\\ \text{spins}}} \left|\bar{u}(p_2)\, \gamma_4 u(p_1)\right|^2 = \text{tr}\left[\gamma_4 \frac{(\not{p}_1 + m)}{2m} \gamma_4 \frac{(\not{p}_2 + m)}{2m}\right]$$

and summing over the proton spins yields

$$\sum_{\substack{\text{deut.}\\ \text{spins}}} \sum_{\substack{\text{prot.}\\ \text{spins}}} M^\dagger M = \sum_{\substack{\text{deut.}\\ \text{spins}}} \frac{1}{(n^2 + m^2)^2} \frac{1}{(2m)^2} \frac{1}{(2\sqrt{2}\, M_d)^4}$$

$$\text{tr}\Big[(\gamma \cdot \xi_1)(M_d - i\not{d}_1)(-i\not{n} + m)(M_d - i\not{d}_2)(\gamma \cdot \xi_2)(i\not{p}_1 + m)$$

$$(\gamma \cdot \xi_2)(M_d - i\not{d}_2)(-i\not{n} + m)(M_d - i\not{d}_2)(\gamma \cdot \xi_1)(i\not{p}_2 + m)\Big] .$$

The deuteron spins are summed over using the identities

$$\sum_{\substack{\text{deut.}\\ \text{spins}}} (p \cdot \xi)(n \cdot \xi) = p \cdot n + \frac{(p \cdot d)(n \cdot d)}{M_d^2}$$

and $\not{p}\not{n} + \not{n}\not{p} = 2\, p \cdot n$ for any four vectors p and n. The matrix element then assumes the form

$$\frac{1}{6}\sum |M|^2 = \frac{3}{128}\,(2mM_d - p_1 \cdot d_2)^2\,\left(\frac{1}{mM_d^2}\right)\,\frac{1}{(n^2 + m^2)^2}$$

$$\left(\frac{4\pi N}{m}\right)^4 \left[F(\kappa)\right]^4 K$$

where

$$K = \Big[m^2 M_d^2 - m^2 d_1 \cdot d_2 - n^2 d_1 \cdot d_2 - mM_d n \cdot (d_1 + d_2)$$

$$+ 2n \cdot d_1\, n \cdot d_2 - M_d^2\, n \cdot n\Big] \quad .$$

APPENDIX B

DEUTERON WAVE FUNCTIONS

This appendix lists the various deuteron wave functions used in present theoretical work. A basic requirement of the wave functions is that they adequately determine the static properties of the deuteron. If α is the same as defined in Chapter II with $u(r)$ as the S-state wave function and $w(r)$ as the D-state wave function, the non-relativistic deuteron problem with a tensor force consists in solving the coupled differential equations:

$$\frac{d^2u(r)}{dr^2} - \left[\alpha^2 - v_c(r)\right] u(r) + 2\sqrt{2}\, v_T(r)\, w(r) = 0$$

$$\frac{d^2w(r)}{dr^2} - \left[\alpha^2 + \frac{6}{r^2} - v_c(r) + 2v_T(r)\right] w(r) + 2\sqrt{2}\, v_T(r)u(r) = 0$$

safisfying the conditions that $\int_0^\infty \left[u^2(r) + w^2(r)\right] dr = 1$ and the wave functions go to zero as r goes to zero or infinity. The $v_c(r)$ is the central potential and the $v_T(r)$ is the tensor potential comprising a total potential,

$$V(r) = -m \left[v_c(r) + S_{12}v_T(r)\right]$$

where $\hbar = 1$. Once the wave functions $u(r)$ and $w(r)$ are determined, the electric quadrupole moment may be calculated by

$$Q = \frac{1}{\sqrt{50}} \int_0^\infty r^2 \left[u(r)w(r) - \frac{w^2(r)}{\sqrt{8}}\right] dr \quad .$$

Since the electric quadrupole moment is known to be positive, the $u(r)$ and $w(r)$ must have the same sign. If the proton magnetic moment μ_p and the neutron magnetic moment μ_n are known, the deuteron magnetic moment is given by

$$\mu_d = \mu_p + \mu_n - \frac{3}{2}\left(\mu_p + \mu_n - \frac{1}{2}\right) \int_0^\infty w^2(r)dr \quad .$$

The following deuteron wave functions are frequently used in practice.

1. Hulthén wave function[28]:

(a) Regular wave function

$$u(r) = N(e^{-ar} - e^{\beta r})$$

$$\alpha = 0.232\ f^{-1}, \quad \beta = 5.18\ \alpha$$

(b) Wave function with radius r_c hard core

$$u(r) = N\, e^{-\alpha r}\left[1 - e^{-\beta(r-r_c)}\right]$$

$$w(r) = N\xi e^{-\alpha r}\left[1 - e^{-\gamma(r-r_c)}\right]^n \left[1 + \frac{3(1 - e^{-\gamma r})}{\alpha r} + \frac{3(1 - e^{-\gamma r})^2}{\alpha^2 r^2}\right]$$

where all positive n are allowed for $r_c \neq 0$ and ξ and γ are determined to fit Q, μ_d and other properties of the deutron.

2. Gartenhaus wave function[30]:

A numerical tabulation for the deuteron wave function was computed by Gartenhaus using a cutoff Yukawa theory. Moravcsik obtained analytic fits to the tabulation in the form:

$$u(r) = N(e^{-\alpha r} - e^{-dr})(1 - e^{-cr})(1 - e^{-gr})$$

$$w(r) = \begin{cases} 0.658\ r^3 & \text{for } 0 < r < 0.63f \\ 2.34 r^3 e^{-2r} & \text{for } 0.63 < r < 2.10f \\ 0.147 e^{-0.256r} + 0.810 e^{-0.577r} & \text{for } 2.10 < r < +\infty \end{cases}$$

where $c = 6.853\alpha$, $d = 8.190\alpha$, $g = 10.776\alpha$.

3. Hamada-Johnston wave function[78]:

The deuteron wave function with a hard core of 0.343f was tabulated by Hamada and Johnston, who assumed a potential with central, tensor, linear LS and quadratic LS terms. The long range quadratic LS potential was added to decrease the magnitude of the $^3D_2$ phase shift at high energies. An analytic fit to the Hamada-Johnston wave function without the hard core has been constructed by McGee.[79] The S- and D-state wave functions are of the form

$$u(r) = N(e^{-\alpha r} + \sum_{j=1}^{4} C_j e^{-\epsilon_j r})$$

$$w(r) = \rho N \left[\alpha r h_2(i\alpha r) + \sum_{j=1}^{5} D_j \eta_j r h_2(i\eta_i r)\right]$$

where h_2 (iy) is the spherical Hankel function and the values of C_j, ϵ_j, D_j, and η_j are given in the following table:

	u(r)		w(r)	
j	C_j	ϵ_j	D_j	η_j
1	-.6361	5.732α	-20.34	4.833α
2	- 6.6150	12.844α	-36.60	10.447α
3	15.216	17.331α	-123.02	14.506α
4	- 8.9651	19.643α	305.11	16.868α
5			-126.16	21.154α

4. Gaussian wave function:

A convenient analytical form of the deuteron is the simple Gaussian. By using a variational method to minimize the energy for the deuteron ground state, Verde[80] obtained the form

$$u(r) = \left(\frac{2\beta^2}{\pi}\right)^{3/4} re^{-\beta^2 r^2}$$

where $\beta = 1.3367\alpha$

5. Christian-Gammel wave function:

The deuteron wave function has been fit to a sum of Gaussians by Christian and Gammel.[81] They obtained a wave function of the form

$$u(r) = 0.02133r\, e^{-0.03r^2} + 0.08582r\, e^{-0.16r^2} + 0.18115r\, e^{-0.76r^2}$$

The above are the most commonly used analytical forms of the deuteron wave function. There also exists many deuteron wave functions in tabular form only which many researchers use in numerical calculations.

BIBLIOGRAPHY

1. Murphy, G. M., and Johnston, H., Phys. Rev. 45, 500 (1934).

2. Estermann, I., and Stern, O., Nature 132, 169 (1933); Nature 133, 911 (1934).

3. Widmett, T. F., Phys. Rev. 91, 499 (1953).

4. Kellogg, J.M.B., Rabi, I. I., and Ramsey, N. F., Jr., Phys. Rev. 57, 677 (1940).

5. Kolsky, H. G., Phipp, T. E., Jr., and Ramsey, N. F., Jr., Phys. Rev. 87, 395 (1952).

6. Schwinger, J., Phys. Rev. 55, 235 (1939).

7. Cassels, J. M., Stafford, C. H., and Pickavance, T. G., Nature 168, 556 (1951).

8. Kuroda, K., Michalowicz, A., and Poulet, M., Phys. Letters 13, 67 (1964).

9. Stern, M. O., and Bloom, A. L., Phys. Rev. 83, 178 (1951).

10. Schamberger, R. D., Phys. Rev. 83, 1276 (1951).

11. Chamberlain, O., and Clark, P. D., Phys. Rev. 102, 473 (1956).

12. Crewe, A. V., Ledley, B., Lillethem, E., Marcowitz, S., and Pondrom, L. G., Phys. Rev. 114, 1361 (1959).

13. Leksin, G. A., Zh. Eksperim. i. teor. Fiz. 32, 440 (1956). (English transl.: Soviet Phys.-JETP 5, 371, 1957.)

14. Bayukov, Yu. D., Vorobev, D. S., Leksin, G. A., Federov, V. B., and Khovansky, V. C., Dubna preprint (to be published).

15. Kirillova, L. F., Nikitin, V. A., Pantuev, V. S., Shafranova, M. G., Strunov, L. N., Khachaturyan, M. N., Khristov, L. G., Korbel, A., Rob, L., Damyanov, S., Zlateva, A., Zlatanov, Z., Iordanov, V., Kanazirski, Kh., Markov, P., Rodorov, T., Chernev, Kh., Dalkhazhav, N., and Tuvdendorzh, T., Zh. Yadern, Fiz. 1, 533 (1965). (English transl.: Soviet Phys.-Nucl. Phys. 1, 379, 1965); and ZhETF Pis'ma 3, 15 (1966). (English transl.: Soviet Phys.-JETP Letters 3, 8, 1966.)

16. Blankenbecler, R., Goldgerger, M. L., and Halpern, F. R., Nucl. Phys. 12, 629 (1959).

17. Perl, M. L., Jones, L. W., and Ting, C. C., Phys. Rev. 132, 1273 (1963).

18. Heinz, R. M., Overseth, O. E., and Ross, M. H., Bull. Am. Phys. Soc. 10, 19 (1965).

19. Heinz, R. M., Thesis, University of Michigan, 1964 (unpublished).

20. Mathews, J., and Deo, B., Phys. Rev. 143, 1340 (1966).

21. Cook, V., Cork, B., Holley, W. R., and Perl, M. L., Phys. Rev. 130, 762 (1963).

22. Bernstein, J., Phys. Rev. 129, 2323 (1963).

23. Nearing, J., Phys. Rev. 132, 2323 (1963).

24. Goldberger, M. L., Nambu, Y., and Oehme, R., Ann. Phys. 2, 266 (1957).

25. Gourdin, M. Le Bellac, J., Renard, F. M., Tran Thanh Van, V., Nuovo Cimento 37, 524 (1965).

26. Rarita, W., and Schwinger, J., Phys. Rev. 59, 436 (1941).

27. Chew, G. F., and Goldberger, M. L., Phys. Rev. 77, 470 (1950).

28. Hulthén, L., and Sugawara, M., Handbuch der Physik XXXIX, 1, Springer-Verlag, Berlin, Göttingen, Heidelberg, 1957.

29. Blankenbecler, R., and Cook, L. F., Jr., Phys. Rev. 119, 1745 (1960).

30. Gartenhaus, S., Phys. Rev. 100, 900 (1956).

31. Moravcsik, M. J., Nucl. Phys. 7, 113 (1958).

32. Schweber, S. S., An Introduction to Relativistic Quantum Field Theory (Row, Peterson and Company, 1961).

33. Bjorken, J. D., and Drell, S. D., Relativistic Quantum Mechanics (McGraw-Hill Book Company, 1964).

34. Jauch, J. M., Helv. Phys. Acta 31, 661 (1958).

35. Lippmann, B. A., and Schwinger, J., Phys. Rev. 79, 469 (1950).

36. Faddeev, L. D., Zh. Eksperim. i. Teor. Fiz. 39, 1459 (1960). (English transl.: Soviet Phys.-JETP 12, 1014, 1961.)

37. Omnes, R. L., Phys. Rev. 134, B1358 (1964).

38. Mitra, A. N., Nucl. Phys. 32, 529 (1962).

39. Amado, R. D., Phys. Rev. 132, 485 (1963).

40. Weinberg, S., Phys. Rev. 133, B232 (1964).

41. Vaughn, M., Aaron, R., Amado, R. D., Phys. Rev. 124, 1258 (1961).

42. Aaron, R., Amado, R. D., and Yam, Y. Y., Phys. Rev. 140, B1291 (1965).

43. Courant, R., and Hilbert, D., Methods of Mathematical Physics (Interscience Publishers, Inc., 1961), p. 134.

44. Yam, Y. Y., Thesis, University of Pennsylvania, 1965 (unpublished).

45. Lovelace, C., Phys. Rev. 135, B1225 (1964).

46. Kohn, W., Rev. Mod. Phys. 26, 292 (1954).

47. Dunford, N., and Schwartz, J. T., Linear Operators (Interscience Publishers, Inc., 1958).

48. Coleman, E., Heinz, R. B., Overseth, O. E., and Pellett, D. E., Phys. Rev. Letters 16, 761 (1966).

49. Perl, M. L., Lee, Y. Y., and Marquit, E., Phys. Rev. 138, B707 (1965).

50. Orear, J., Rubinstein, R., Scarl, D. B., White, D. H., Krisch, A. D., Frisken, W. R., Read, A. L., and Ruderman, H., Phys. Rev. Letters 15, 309 (1965).

51. Coffin, C., Dikmen, N., Ettlinger, L., Meyer, D., Saulys, A., Terwilliger, and Williams, D., Phys. Rev. Letters 15, 838 (1965).

52. Foley, K. J., Lindenbaum, S. J., Love, W. A., Ozaki, S., Russell, J. J., and Yuan, L.C.L., Phys. Rev. Letters 11, 503 (1963).

53. Barge, D., Chu, W., Leipuner, L., Crittenden, R., Martin, H. H., Ayer, F., Marshall, L., Li, A. C., Kernan, W., and Stevenson, M. L., Phys. Rev. Letters 13, 69 (1964).

54. Aachen-Berlin-Birmingham-Bonn-Hamburg-London-München collaboration, Phys. Rev. 138, B897 (1965).

55. Sonderegger, P., Kirz, J., Guisan, O., Falk-Vairant, P., Bruneton, C., Borgeaud, P., Stirling, A. V., Caverzasio, C., Guillaud, J. P., Yvert, M., and Amblard, B., Phys. Rev. Letters 20, 75 (1966).

56. Kreisler, M. N., Martin, F., Perl, M. L., Longo, M. J., and Powell, S. T., private communication.

57. Simmons, L. M., Phys. Rev. Letters 12, 229 (1964).

58. Kowalski, K. L., and Feldman, D., Phys. Rev. 130, 276 (1963).

59. Fulton, T., and Schwed, P., Phys. Rev. 115, 973 (1959).

60. Chew, G. F., and Goldberger, M. L., Phys. Rev. 87, 778 (1952).

61. Ashkin, J., and Wick, G. C., Phys. Rev. 85, 686 (1952).

62. Chew, G. F., and Wick, G. C., Phys. Rev. 85, 636 (1952).

63. Chew, G. F., Phys. Rev. 74, 809 (1948).

64. Barge, D., Thesis, Rensselaer Polytechnic Institute, 1960 (unpublished).

65. Everett, A., Phys. Rev. 126, 831 (1962).

66. Franco, V., Glauber, R. J., Phys. Rev. 142, 1195 (1966).

67. Bennett, G. W., Cosmotron Internal Report No. GWB-2, 1962 (unpublished).

68. Sugarman, R., Merritt, F. C., and Higginbotham, W. A., Nanosecond Counter Circuit Manual, Brookhaven National Laboratory Report BNL 711(T-248), 1962 (unpublished).

69. Cumming, J. B., Poskanzer, A. M., and Hudis, J., Phys. Rev. Letters 6, 484 (1961).

70. Poskanzer, A. M., Remsberg, L. P., Katcoff, S., and Cumming, J. B., Phys. Rev. 133, B1507 (1964).

71. Cummings, J. B., Friedlander, G., and Swartz, C. E., Phys. Rev. 111, 1386 (1958).

72. Horwitz, N., and Murray, J. J., Phys. Rev. 117, 1361 (1960).

73. Bekker, B. I., Pantuev, V. S., Sviridov, B. A., and Khachaturyan, M. N., Zh, Eksperim. i. Teor. Fiz. 45, 1260L (1963). (English transl.: Soviet Phys.-JETP 18, 872L, 1964.)

74. Cumming, J. B., Friedlander, G., and Katcoff, S., Phys. Rev. 125, 2078 (1962).

75. Cumming, J. B., Hudis, J., Poskanzer, A. M., and Kaufman, S., Phys. Rev. 128, 2392 (1962).

76. Chen, F. F., Leavitt, C. P., and Shapiro, A. M., Phys. Rev. 103, 211 (1956).

77. Ross, M. H., and Shaw, G. L., Phys. Rev. Letters 12, 627 (1964).

78. Hamada, T., and Johnston, I. D., Nucl. Phys. 34, 382 (1962).

79. McGee, I., private communication.

80. Verde, M., Helv. Phys. Acta 22, 339 (1949).

81. Christian, R. S., and Gammel, J. L., Phys. Rev. 91, 100 (1958).

82. Söding, P., Phys. Letters 8, 285, (1964)

83. Carter, A. A., and Bugg, D. V. Phys. Letters 20, 203 (1966)

ACKNOWLEDGMENTS

I am grateful to Professor Oliver E. Overseth for his inspiring guidance during the course of this work. As a research physicist, teacher, and friend, he has made my doctoral studies a very satisfying experience.

I would like to thank my colleagues Dr. Richard M. Heinz and David E. Pellett for their indispensable assistance during the experiment.

Professor Lawrence M. Jones deserves my deepest appreciation for many helpful discussions; and I wish to thank Dr. Ying-Yeung Yam for interesting conversations on the theoretical aspects of proton-deuteron scattering.

Unclassified
Security Classification

DOCUMENT CONTROL DATA - R&D

(Security classification of title, body of abstract and indexing annotation must be entered when the overall report is classified)

1. ORIGINATING ACTIVITY *(Corporate author)*
The University of Michigan
Department of Physics
Ann Arbor, Michigan

2a. REPORT SECURITY CLASSIFICATION
Unclassified

2b. GROUP

3. REPORT TITLE

PROTON-DEUTERON ELASTIC SCATTERING AT HIGH MOMENTUM TRANSFERS

4. DESCRIPTIVE NOTES *(Type of report and inclusive dates)*
Technical Report No. 25

5. AUTHOR(S) *(Last name, first name, initial)*

Coleman, Ernest

6. REPORT DATE	7a. TOTAL NO. OF PAGES	7b. NO. OF REFS
July 1966	85	81

8a. CONTRACT OR GRANT NO.	9a. ORIGINATOR'S REPORT NUMBER(S)
Nonr-1224(23)	03106-25-T
b. PROJECT NO. NR-022-274	
c.	9b. OTHER REPORT NO(S) *(Any other numbers that may be assigned this report)* Technical Report No. 25
d.	

10. AVAILABILITY/LIMITATION NOTICES

Distribution of this document is unlimited.

11. SUPPLEMENTARY NOTES	12. SPONSORING MILITARY ACTIVITY
	Department of the Navy Office of Naval Research Washington, D. C.

13. ABSTRACT

An experimental and theoretical investigation of proton-deuteron elastic scattering at high momentum transfers is presented. The differential cross sections for backward elastic scattering at incident proton kinetic energies of 1.0, 1.3, and 1.5 GeV have been measured for four-momentum transfer squared (-t) from 2.6 to 5.0 $(GeV/c)^2$, which corresponds to cosine of center-of-mass proton scattering angles ($\cos \theta^*$) from -0.5 to -0.9. A backward peak is observed, and the slope and magnitude of the peak have been determined. At 2.0 GeV for forward elastic differential cross section has been measured for -t from 0.44 to 1.54 $(GeV/c)^2$ or $\cos \theta^*$ from 0.875 to 0.565. A shoulderlike departure from the forward diffraction peak was observed.

The one-nucleon exchange peripheral model has been successful in interpreting the backward peak. Calculations based on modern three-body quantum mechanical formalisms for the three-nucleon system supporting a two-body bound state also suggest the one-nucleon exchange process as the dominant mechanism. The measured forward differential cross section has been explained by the importance of double-scattering of the incident proton at higher momentum transfers. A negative value for the ratio of the real part to the imaginary part of the neutron-proton elastic scattering amplitude at 2.0 GeV is shown to yield maximum agreement with the experimental data.

DD FORM 1 JAN 64 1473

Unclassified
Security Classification

14. KEY WORDS	LINK A		LINK B		LINK C	
	ROLE	WT	ROLE	WT	ROLE	WT

INSTRUCTIONS

1. ORIGINATING ACTIVITY: Enter the name and address of the contractor, subcontractor, grantee, Department of Defense activity or other organization *(corporate author)* issuing the report.

2*a*. REPORT SECURITY CLASSIFICATION: Enter the overall security classification of the report. Indicate whether "Restricted Data" is included. Marking is to be in accordance with appropriate security regulations.

2*b*. GROUP: Automatic downgrading is specified in DoD Directive 5200.10 and Armed Forces Industrial Manual. Enter the group number. Also, when applicable, show that optional markings have been used for Group 3 and Group 4 as authorized.

3. REPORT TITLE: Enter the complete report title in all capital letters. Titles in all cases should be unclassified. If a meaningful title cannot be selected without classification, show title classification in all capitals in parenthesis immediately following the title.

4. DESCRIPTIVE NOTES: If appropriate, enter the type of report, e.g., interim, progress, summary, annual, or final. Give the inclusive dates when a specific reporting period is covered.

5. AUTHOR(S): Enter the name(s) of author(s) as shown on or in the report. Enter last name, first name, middle initial. If military, show rank and branch of service. The name of the principal author is an absolute minimum requirement.

6. REPORT DATE: Enter the date of the report as day, month, year; or month, year. If more than one date appears on the report, use date of publication.

7*a*. TOTAL NUMBER OF PAGES: The total page count should follow normal pagination procedures, i.e., enter the number of pages containing information.

7*b*. NUMBER OF REFERENCES: Enter the total number of references cited in the report.

8*a*. CONTRACT OR GRANT NUMBER: If appropriate, enter the applicable number of the contract or grant under which the report was written.

8*b*, 8c, & 8*d*. PROJECT NUMBER: Enter the appropriate military department identification, such as project number, subproject number, system numbers, task number, etc.

9*a*. ORIGINATOR'S REPORT NUMBER(S): Enter the official report number by which the document will be identified and controlled by the originating activity. This number must be unique to this report.

9*b*. OTHER REPORT NUMBER(S): If the report has been assigned any other repcrt numbers *(either by the originator or by the sponsor)*, also enter this number(s).

10. AVAILABILITY/LIMITATION NOTICES: Enter any limitations on further dissemination of the report, other than those imposed by security classification, using standard statements such as:

(1) "Qualified requesters may obtain copies of this report from DDC."

(2) "Foreign announcement and dissemination of this report by DDC is not authorized."

(3) "U. S. Government agencies may obtain copies of this report directly from DDC. Other qualified DDC users shall request through _____."

(4) "U. S. military agencies may obtain copies of this report directly from DDC. Other qualified users shall request through _____."

(5) "All distribution of this report is controlled. Qualified DDC users shall request through _____."

If the report has been furnished to the Office of Technical Services, Department of Commerce, for sale to the public, indicate this fact and enter the price, if known.

11. SUPPLEMENTARY NOTES: Use for additional explanatory notes.

12. SPONSORING MILITARY ACTIVITY: Enter the name of the departmental project office or laboratory sponsoring *(paying for)* the research and development. Include address.

13. ABSTRACT: Enter an abstract giving a brief and factual summary of the document indicative of the report, even though it may also appear elsewhere in the body of the technical report. If additional space is required, a continuation sheet shall be attached.

It is highly desirable that the abstract of classified reports be unclassified. Each paragraph of the abstract shall end with an indication of the military security classification of the information in the paragraph, represented as *(TS), (S), (C), or (U)*.

There is no limitation on the length of the abstract. However, the suggested length is from 150 to 225 words.

14. KEY WORDS: Key words are technically meaningful terms or short phrases that characterize a report and may be used as index entries for cataloging the report. Key words must be selected so that no security classification is required. Identifiers, such as equipment model designation, trade name, military project code name, geographic location, may be used as key words but will be followed by an indication of technical context. The assignment of links, rules, and weights is optional.